ANALYSIS OF SEPIC DC/DC CONVERTER USING PERTURB & OBSERVE ALGORITHM FOR PHOTOVOLTAIC CHARGE CONTROLLER

WAN MUHAMMAD FIRDAUS BIN WAN SULAIMAN

Thesis submitted in fulfillment of the requirements for the award of the degree of Master of Engineering in Electrical

Faculty of Electrical and Electronics Engineering
UNIVERSITI MALAYSIA PAHANG

APRIL 2015

UNIVERSITI MALAYSIA PAHANG

Author's full name : Wan Muhammad Firdaus Bin Wan Sulaiman

Date of birth : 25th September 1983

Title : Analysis of SEPIC DC/DC Converter Using Perturb & Observe Algorithm for Photovoltaic Charge Controller

Academic Session : Semester 1 2014/2015

I declare that this thesis is classified as:

☐ **CONFIDENTIAL** (Contains confidential information under the Official Secret Act1972)*

☐ **RESTRICTED** (Contains restricted information as specified by the organization where research was done)*

√ **OPEN ACCESS** I agree that my thesis to be published as an online open access (Full text)

I acknowledge that Universiti Malaysia Pahang reserves the right as follows:

1. The Thesis is the Property of University Malaysia Pahang
2. The Library of University Malaysia Pahang has the right to make copies for the purpose of research only.
3. The Library has the right to make copies of the thesis for academic exchange.

Certified by:

(Student's Signature)	(Signature of Supervisor)
830925-07-5067	Dr.Hamdan Bin Daniyal
New IC/Passport Number	Name of Supervisor
Date: 26 April 2015	Date : 26 April 2015

SUPERVISOR'S DECLARATION

I hereby declare that I have checked this thesis and in my opinion, this thesis is adequate in terms of scope and quality for the award of the degree of Master of Engineering in Electrical.

Signature :

Name of Supervisor : Dr Hamdan Bin Daniyal

Position : Senior Lecturer

Date : 26 April 2015

STUDENT'S DECLARATION

I hereby declare that the work in this thesis is my own except for quotations and summaries which have been duly acknowledged. The thesis has not been accepted for any degree and is not concurrently submitted for award of other degree.

Signature :
Name : WAN MUHAMMAD FIRDAUS BIN WAN SULAIMAN
ID Number : MEE11005
Date : 26 APRIL 2015

Every challenging work needs self efforts as well as guidance, especially those who are close to our hearts. Alhamdulillah praise to Allah, that gives me a good health to finish this thesis. My humble effort, of course, I dedicated this thesis to my sweet and loving parents, parents in-law and wife whose affection, love, encouragement and prayers of day and night make me able to get such success and honor; along with the hardworking, patience and respected supervisor, Dr Hamdan Bin Daniyal.

ACKNOWLEDGEMENTS

In the name of Allah, the Most Gracious and the Most Merciful Alhamdulillah, all praises to Allah for the strengths and His blessing in completing this thesis. Special appreciation goes to my supervisor, Dr Hamdan Bin Daniyal, for his supervision and constant support. His invaluable help of constructive comments and suggestions throughout the experiment and thesis works have contributed to the success of this research.

I would like to also express my appreciation to my labmate, Bakri bin Hassan, and Mohd Shafie Bin Bakar for their help throughout the experiment for this thesis. My acknowledgement also goes to all the technicians and office staffs of the Department of Electrical & Electronics Engineering for their co-operations during this study.

Last but not least, I reserved my acknowledgement to my parents and parents in-law for their sacrifice, love and encouragement in order to finish this study. I am also grateful for my wife and lovely daughter for their sacrifice, patience and understanding that really matters in order to make this thesis possible. No words could describe my appreciation for their support and faith towards me to attain my goals.

ABSTRACT

The solar energy is one of the renewable energy sources that plays an important part in our daily life nowadays. The solar energy harvesting system usually consists of solar panels and inverters. The inverter consists of many subsystems; solar charge controller is one of them. As the name suggests, solar charge controller plays a crucial role in harvesting maximum energy from the sun's irradiation. This thesis focuses on solar charge controller area; which presents theoretical studies on the photovoltaic (PV) module characteristics and Maximum Power Point Tracking (MPPT) capability. This study uses real irradiation data to analyze the PV module characteristics and the MPPT algorithm in MATLAB. The simulations in PSIM software is to verify the Single Ended Primary Inductor Converter (SEPIC) circuit with Perturb & Observe (P&O) MPPT algorithm method. This simulation provides an information on the charge controller capability to produce an output power as close as the input power on the changement of the solar irradiation intensity. This simulation provides an information on how the P&O algorithm reacts to the changement of solar irradiation and how long it took for this MPPT to track the Maximum Power Point (MPP). The SEPIC hardware analysis is likely to be the determination of the losses in the SEPIC circuit at certain working frequency parameters and component selections. This experiment also contributes to the knowledge on the switching and conduction losses, where in reality depending on many parameters. On the ideal SEPIC circuit (lossless converter), the efficiency can reach as high as 98% at maximum solar irradiation. By comparison, given the same components with the same value, the experimental SEPIC circuit can obtain an efficiency of only 77%.

ABSTRAK

Tenaga solar adalah salah satu sumber tenaga boleh diperbaharui yang memainkan peranan penting dalam kehidupan seharian kita pada masa kini. Sistem pengusahasilan tenaga solar ini biasanya terdiri daripada panel solar dan penyongsang. Penyongsang ini terdiri daripada banyak sistem kecil di mana pengawal caj solar adalah salah satu daripadanya. Seperti namanya, pengawal caj solar memainkan peranan penting dalam pengusahasilan tenaga maksimum dari sinaran matahari. Tesis ini memberi tumpuan kepada pengawal caj solar; yang mana akan membentangkan kajian secara teori kepada ciri-ciri modul PV dan keupayaan Pengesan Titik Kuasa Maksimum (MPPT). Kajian ini menggunakan data penyinaran sebenar untuk menganalisis ciri-ciri modul PV dan algoritma MPPT dalam MATLAB. Simulasi di PSIM adalah untuk pengesahan litar SEPIC dengan menggunakan kaedah MPPT yang dipilih. Simulasi ini memberi maklumat mengenai keupayaan pengesanan MPPT dari segi masa dan juga keamatan sinaran matahari. Analisis tentang perkakasan SEPIC menjadi penentu dalam kehilangankuasa dalam litar SEPIC pada frekuensi dan pilihan komponentertentu. Eksperimen ini memberi beberapa keputusan yang tidak dijangka dari segi nilai kehilangan kuasa. Ia juga menyumbang kepada pengetahuan tentang jangkaan dalam kehilangan kuasa semasa pensuisan dan konduksi yang pada hakikatnya bergantung kepada banyak parameter.

TABLE OF CONTENTS

LIST OF TABLES

LIST OF FIGURES

LIST OF SYMBOLS

k	Boltzmann constant (1.3806503 × 10^{-23}J/K)
M	Conversion ratio
D	Duty cycle
n	Diode ideality factor
I_0	Reverse saturation current of the diode
q	Electron charge (1.60217646 × 10^{-19}C)
T	Cell temperature in Kelvin = (273+25)
α	Temperature coefficient of short circuit current (%/˚C)
G	Irradiance (W/m^2)
f_{sw}	Switching frequency (kHz)
P_m	Maximum power
V_{mp}	Voltage at maximum power point
I_{mp}	Current at maximum power point
V_{oc}	Open circuit voltage
I_{sc}	Short circuit voltage
R_s	Series resistance
C_s	Coupling capacitor
$V_{th(min)}$	MOSFET minimum threshold voltage
V_D	Diode forward voltage drop
I_L	Inductors current
R_{DSon}	MOSFET drain-source resistance
Q_{GD}	MOSFET gate-drain charge
DCR	DC resistance
Q_{rr}	Diode reverse recovery charge
V_{cf}	Voltage across diode during turn off condition

LIST OF ABBREVIATIONS

BJT	Bipolar Junction Transistor
CCM	Continuous conduction mode
DC	Direct current
ESR	Electrostatic charge resistance
IGBT	Insulated Gate Bipolar Transistors
IncCond	Incremental Conductance
I-V curve	Current versus Voltage curve
kWp	Kilowatt peak
MOSFET	Metal Oxide Silicon Field Effect Transistors
MPP	Maximum Power Point
MPPT	Maximum Power Point Tracking
NREL	National Renewable Energy Laboratory
PV	Photovoltaic
P-V curve	Power versus voltage curve
PWM	Pulse-width modulation
P&O	Perturb and Observe
RMS	Root Mean Square
SCRs	Silicon-Controlled Rectifiers
SEPIC	Single Ended Primary Inductor Converter
SMPS	Switch Mode Power Supplies
STC	Standard Test Condition

CHAPTER 1

INTRODUCTION

1.1 OVERVIEW

Over the past few years, there was plenty speculation of fuel price hikes, a world energy crisis and concerns of global warming. The increasing demand of energy and the growing concern about the environment has sparked enormous interest in the utilization of renewable energy. For the time being, renewable energy represents only 7 % of the global energy consumed and it will slightly increase as the need for the global energy increased (Bose, 2010). One of the alternative energy sources that are recently flourishingis the sun, mainly because it is free, sustainable, environmental friendly and maintenance free.

The sun's energy, which is converted to solar electricity, or photovoltaic (PV), is likely being one of our major energy sources in the near future. PV is energy from the sun, which the light is converted directly into electricity without creating any air or water pollution. It consists of silicon, which going through a doping process to produce positive and negative type semiconductor materials. When light enters the cell, some of the photons from the light are absorbed by the semiconductor atoms, freeing electrons from the cell’s negative layer to flow through an external circuit and back into the positive layer. The main electrical characteristics of a PV cell or module are summarized in the relationship between the current and voltage. The solar radiation that is absorbed by the cell controls the current (I), while the increases in the temperature of the solar cell reduce its voltage (V). A single PV cell is basically a direct current (DC) source, where the current is determined by the area of the cell and the amount of exposed solar irradiation. One of the examples of the PV module structure is as shown in Figure 1.1.

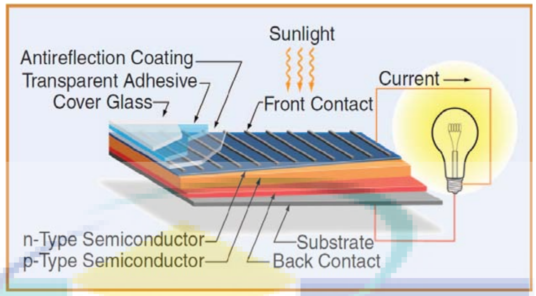

Figure 1.1: PV Module construction

Source: Kroposki, Margolis et al. 2009

There was a long list to show a chronological history of solar PV, but it is important to know that in 1839, French scientist, Edmond Becquerel, discovered the photovoltaic effect while experimenting with an electrolytic cell made up of two metal electrodes placed in an electricity-conducting solution; the electricity-generation increased when exposed to light. In 1876, William Adams, a British physicist, discovered a material of photovoltaic which is selenium with his student, Richard Day. They, altogether, then made it to solid cells with 1 % – 2 % efficiency. And in 2008, scientists at the U.S. Department of Energy's National Renewable Energy Laboratory (NREL) have achieved a new world record in solar cell efficiency. They managed to get a photovoltaic device have 40.8 % of efficiency. The achievement and evolution in PV industry are really outstanding and exceptional. The PV system is gaining an important as a renewable source due to advantages such as the absence of fuel cost, little maintenance and no noise and wear due to the absence of moving parts. Even though solar energy constitutes a very small percentage of our energy system today, the size of the resource is enormous which we can state that the earth receives more energy from the sun in one hour than the global population uses in an entire year (Kroposki, Margolis et al., 2009).

Although the PV system has many advantages, there are still two major disadvantages to the use of photovoltaic systems; the high installation cost and the lower energy conversion efficiency. Efficiency is the main component in solar PV technology as the solar energy that disappears without converting to electrical energy is considered a loss. As PV installation averagely at a cost of around RM5000/kWp (Ali, 2013), thus every power that loss during the process are costly. The relatively high cost of photovoltaic power systems has required system designers to maximize efficiency wherever possible. Even modest gains in overall efficiency can result in significant savings in the cost of operating the power system. Compared to the cost of electrical energy available from conventional sources the cost of energy from photovoltaic is still fairly high so it is important that the maximum available amount of energy be extracted from the solar array. To maximize the power output of the PV system, a DC/DC converter with an appropriate Maximum Power Point Tracking (MPPT) algorithm is commonly employed within a controller device named Solar Charge Controller. Together, the DC/DC converter and MPPT algorithm control the terminal voltage of the PV system at optimal values in various solar radiation conditions, where at a certain weather condition; the output power of a PV panel depends on the terminal voltage of the system. Figure 1.2 shows the PV system block diagram that works to ensure the PV module operation point always at the MPP.

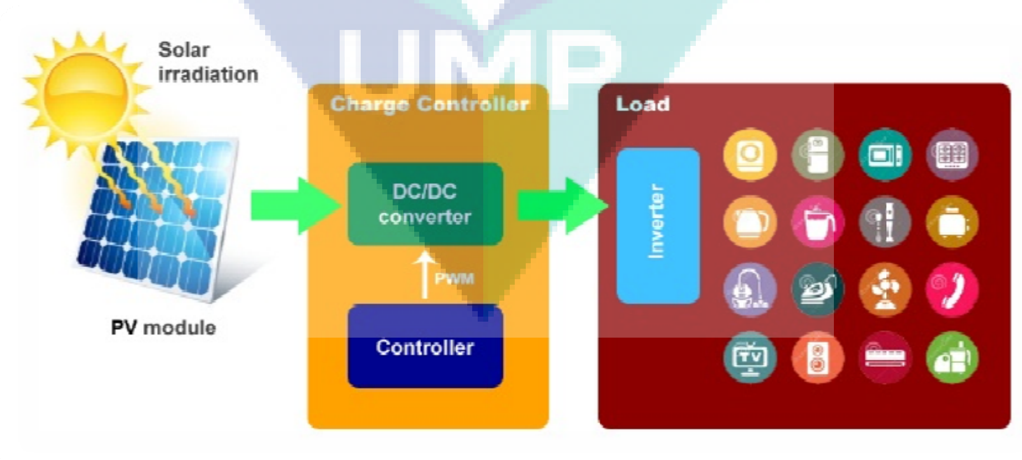

Figure 1.2: PV system block diagram from charge controller's perspective

1.2 PROBLEM STATEMENT

In this thesis, the solar charge controller is being studied in term of efficiency and performance. Questions have been raised about the efficiency where it is actively discussed as one of the main issue which is causing either by MPPT algorithm or DC/DC converter topology (J.M. Enrique, 2006; Esram and Chapman, 2007; A. Dolara, 2009; Patarau, Daraban et al., 2011). Research on the converter efficiency arises in many scopes, but the one that should be concerned of, is the design of the converter itself (Kimball, Flowers et al., 2004). There are increasing concern that apart from the PV system, there are also a need for analysis on DC/DC converters' efficiency in a wind farm technology (Prabhakar, Bollinger et al., 2008) which triggered that the efficiency issue of the DC/DC converters needs to be taken into consideration for the designers regardless on which applications it will be used. While there has been considerable research on the efficiency analysis of DC/DC converter, only certain studies have proposed a new method of DC/DC to improve the converter efficiency (Kim, Lee et al., 2013; Kawaguchi, Yamaguchi et al., 2008; Al-Saffar, Ismail et al., 2008). One major issue arose that the converters used for photovoltaic applications had a common reliability issues, which is a failed electrolytic capacitor used in filters (Lahyani, Venet et al., 1998). Thus, it is important for the designers not only to maximize the extracted energy, but also to ensure that the converter does not require failure prone components like large capacitors. Previous studies of Martin A. Green (2013) on PV module, the efficiency of conversion of the incident radiation to electrical energy in the PV cell is low and could be as high as 24.1 % for thin film type module at Standard Test Condition, STC.

1.3 OBJECTIVES

The objectives of this study are:

1. To develop a model of PV module in computer simulation based on varying solar irradiation at a specific geographical location.
2. To realize a charge controller in computer simulation; consists of PV module, SEPIC DC/DC converter and control system.
3. To analyze the efficiency and the losses of a SEPIC DC/DC converter via practical experiment.

1.4 SCOPE AND LIMITATIONS

To achieve the objectives, this study is conducted on a best efforts basis. Like all other studies, this study is focused at a specific scope and is bounded by limitations. It should be noted that the study covers the overall study of solar charge controller; from the solar irradiance, solar panel, DC/DC converter and its controller. The inverter is not part of the study, and will be looked at as a load from the solar charge controller's perspective.

Objective 1:
Geographical and time scope: The context of the study is based on data logged from the UMP's weather station at Pekan, Pahang. The data spans for over the period of one year and three months; from Jan 2011 to March 2012.
Lab resource limitation: The model of PV is based on a readily available PV panel during the study, the Mitsubishi PV-TE125MF5N.

Objective 2:
For Objective 2, a thorough literature study is conducted, mainly on choosing the appropriate DC/DC converter topology and the suitable control algorithm. This is explained in detail in Chapter 2. At the end of the literature review, the study narrowed to focus on SEPIC DC/DC converter and Perturb & Observe (P&O) algorithm, hence the title of the thesis. A simulation is conducted to achieve Objective 2, where the SEPIC with P&O system is tested using the cloudiest and the sunniest data set from the Objective 1 study.

Objective 3:

Objective 3 is about the efficiency and the losses of SEPIC DC/DC converter. To achieve this objective, a SEPIC DC/DC converter is constructed with the same parameters and same component sizing as in Objective 2. As for the controller, open-loop control is sufficient for efficiency analysis, where an Arduino board is used as the controller. The limitation of the Arduino board applied to the study, especially on the switching frequencies, where the maximum possible is 62.3 kHz. The converter is normally operate at swiching frequency higher than 50 kHz (Burmester, Rayudu et al., 2013).

1.5 OVERVIEW OF THE THESIS

This study has been divided into two parts. The first part deals with the simulation of solar charge controller while the second part deals with the DC/DC converter efficiency analysis experiment. The charge controller has a DC/DC converter that using a Single Ended Primary Inductor Converter (SEPIC) topology. This study includes a simulation of the PV module and SEPIC circuit model in MATLAB and PSIM respectively, plus a hardware testing for the SEPIC. The PV module used is the modules that available in the Fakulti Kejuruteraan Elektrik & Elektronik, Universiti Malaysia Pahang, which is Mitsubishi PV-TE125MF5N. This thesis is organized in five chapters. Chapter 1 is a brief introduction of Renewable Energy as a whole and specifically on the use of the PV system with the concern over its price compare to efficiency. In Chapter 2, literatures that relevant to the issue are presented along with the reviews of various books, journals and articles. The literatures focused on the PV cell characteristics, MPPT algorithm (P&O) and DC/DC converter (SEPIC). Chapter 3 presents the methodology of the study. This chapter includes simulation procedures and component selection for experimental purposes which involve some calculations. Chapter 4 is relate or a continuation of Chapter 3 where the results that obtained from simulation and experiment are presented and discussed. Graphs and figures are included to be observed and discussed. In the last chapter (Chapter 5), the study is concluded and summarized based on the methodology used and the results obtained. Moreover, further works that can be conducted are also recommended.

CHAPTER 2

LITERATURE REVIEW

2.1 INTRODUCTION

French physicist, Edmund Becquerel, discovered the first photovoltaic effect when he illuminated a metal electrode in an electrolytic solution back in 1839. Then, William Adams, a British physicist, discovered a material of photovoltaic which is selenium thirty-seven years later with his student, Richard Day. They, altogether then made it to solid cells with 1 % – 2 % efficiency (Masters, 2004). The PV timeline evolution is as per attached in APPENDIX B which is prepared by United States Department of Energy. PV systems are comprised of photovoltaic cells, devices that convert light energy directly into electricity. The word photovoltaic comes from “photo,” meaning light, and “voltaic,” which refers to producing electricity. Therefore, the photovoltaic process is producing electricity directly from sunlight (S.E.C.O, 1997).

The uses of solar energy become more demanding year by year. PV based installation demand has grown consistently by 20 %–25 % per annum over the past 20 years (Carrasco, Franquelo et al., 2006). Today, the production of PV cells is following an exponential growth curve since technological advancement of the late ‘80s that has started to rapidly improve efficiency.

Despite its rapid growth, there remain several challenges that hinder the widespread use of PV power systems. The main limitation is the high cost of the module. It is difficult to ignore that the cost is basically determined by the economics of scale of a certain country, supply-demand, price of basic material and the cell manufacturing processes (Taheri, Salam et al., 2010). To ensure that the installation of

PV is effective, there is a need to ensure that the power output of the PV modules should be at its optimum. Several attempts have been made to overcome the problem, where one evidence suggests that this can be achieved by employing a specific circuit, famously known as Maximum Power Point Tracker (MPPT) (Rebei, Gammoudi et al., 2014; Zanotti, dos Santos et al., 2013; Durgadevi, Arulselvi et al., 2011; Coelho, Concer et al., 2009) . Therefore, an efficient PV module requires the MPPT to assured that the maximum power is delivered at the operation point, where the magnitudes of the PV generator and load circuit resistances are equal as shown in Figure 2.1.

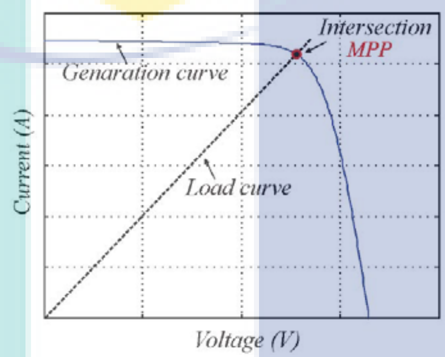

Figure 2.1: Load and generation curves intersection

Source: (Coelho, Concer et al. 2009)

2.2 PHOTOVOLTAIC

Photovoltaic (PV) is a method of generating electrical power by converting solar radiation into direct current electricity using semiconductors that exhibit the photovoltaic effect. Photovoltaic power generation employs solar panels composed of a number of solar cells containing a photovoltaic material. Mainstream materials presently used for photovoltaic include mono-crystalline silicon, poly-crystalline silicon, amorphous silicon, cadmium telluride and copper indium gallium selenide/sulfide. Due to the increased demand for renewable energy sources, the manufacturing of solar cells and photovoltaic arrays has advanced considerably in recent years.

2.2.1 Photovoltaic Cell

PV cells convert sunlight directly into electricity without creating any air or water pollution. PV cells are made of at least two layers of semiconductor material. One layer has a positive charge, the other negative. When light enters the cell, some of the photons from the light are absorbed by the semiconductor atoms, freeing electrons from the cell's negative layer to flow through an external circuit and back into the positive layer. This flow of electrons produces electric current (S.E.C.O, 1997). The main electrical characteristics of a PV cell or module are summarized in the relationship between the current and voltage. The solar radiation that is absorbed by the cell controls the current (I), while the increases in the temperature of the solar cell reduce its voltage (V).

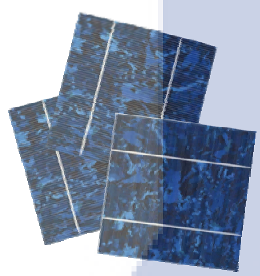

Figure 2.2: Photovoltaic cells

Source: (MITSUBISHI 2007)

A single PV cell is basically a direct current (DC) source, where the current is determined by the area of the cell and the amount of exposed solar irradiation. The voltage of an individual silicon cell is in the order of 0.5 V. Therefore, the cells have to be connected in series to constitute a module with reasonable voltage levels.

2.2.2 Photovoltaic Module

PV modules (the type of mono and poly-crystalline) consist of PV cells that connected in series by two wires and normally attached in a series of 36 or 72. The amount of available light falling on these solar cells affects the production of electric current. The temperature of the cell affects its voltage and the larger the cell, the more current it will produce. There are various types (Mono-crystalline, Poly-crystalline and Amorphous) and sizes (typically sized from 60 W to 170 W) of PV module that available in the PV market worldwide.

The reason to connect the cells in series is to provide a suitable voltage for battery charging as well as storage (non grid-tied system). Furthermore, it was also needed for the use of DC/DC converters in the solar charge controller system which required a specific voltage. Typical PV module use 36 solar cells connected in series and will have a total voltage of around 16 V (36 x 0.5 V) and this is why the individual solar PV cells which make up a solar module have a standard size (156 mm x 156 mm) (Yingli, 2013; KYOCERA, 2011; MITSUBISHI, 2007). There are also available modules with 30, 54, 60 and 72 cells connection. A 60 cells module will operate at a higher voltage than the 54 cells module which allows them to overcome the reduction in output voltage when the modules are operating at high temperatures. Figure 2.3 shows the different of form *I-V* curve under different type of cell connections.

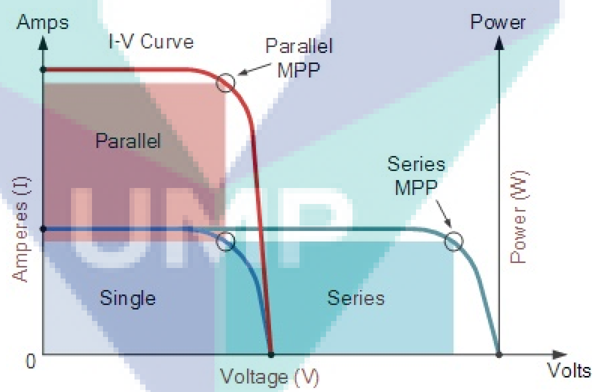

Figure 2.3: *I-V* curve for various types of PV cell connections

Source: (Articles 2013)

There are three main panel types come from the three different forms of crystalline materials. In 2012, mono-crystalline module and poly-crystalline module are the most modules sold globally, approximately 93 % of all modules type while

Amorphous silicon module is approximately only 4.2 % sold globally (EvoEnergy, 2012).

2.2.3 The *I-V* Curve and Maximum Power Point

The *I-V* curve is a characteristic of any PV module which consists of the PV module current and voltage on its x-axis and y-axis respectively. A PV module can produce the power at an operating point, anywhere on the *I-V* curve where the coordinates of the operating point are the operating voltage and current. There is a unique point near the knee of the *I-V* curve, called a maximum power point (MPP), at which the module operates with the maximum efficiency and produces the maximum output power. The rectangle area as in Figure 2.4 is equal to the output power which is a product of voltage and current.

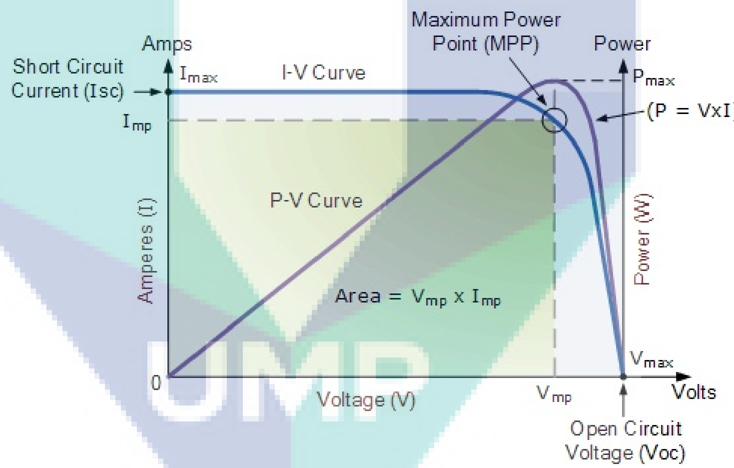

Figure 2.4: *I-V* and *P-V* curve of a typical PV module working under Standard Test Condition (STC)

Source: (Articles 2013)

2.3 MAXIMUM POWER POINT TRACKING

Dang (1990), from California Polytechnic State University, Pomona was the first person that made an attempt to study MPPT on his research. The maximum power point tracker (MPPT) is now prevalent in grid-tied PV power systems and is becoming more popular in stand-alone systems. MPPT plays an important role in photovoltaic (PV) power systems because they maximize the power output from a PV system for a given set of conditions, and therefore maximize the array efficiency (Abdelmoula, Moughamir et al., 2014; Durgadevi, Arulselvi et al., 2011). MPPT's found and maintain operation at the maximum power point, using an MPPT algorithm. Nowadays, this algorithm is executed using a microcontroller that used the PV current and voltage data to control the duty cycle that applied to the DC/DC converter circuit. There are many researches done on tracking the MPP with the entire algorithm proposed (Burmester, Rayudu et al., 2013; Muoka, Haque et al., 2012; Hohm and Ropp, 2000) but there is lack of source on which algorithm is appropriate for a suitable topology of a DC/DC converter. However, one particular algorithm, the perturb and observe (P&O) method, claimed by many in the literature to be inferior to others, continues to be by far the most widely used method in commercial PV MPPT (Charfi and Chaabene, 2014; Byunggyu, Gwonjong et al., 2011; Kazmi, Goto et al. 2009; Femia, Petrone et al., 2004; Hohm and Ropp, 2000).

2.3.1 Perturb & Observe Algorithm

The P&O algorithm is a simple method for MPPT. The algorithm is an iteration based approach to MPPT (Elgendy, Zahawi et al., 2012; Salas, Olías et al., 2006). A flowchart of the method can be seen in Figure 2.5. The first step in this algorithm is to sense the current, I_k and voltage, V_k coming out of the PV panel and these values is used to calculate the output power, P_k of the panel. The algorithm then compares the present output power with the power from the previous iteration that has been stored in memory. If the algorithm is just in the first iteration the current power will be compared against some constant, k placed in the algorithm during programming. The system compares the difference between the present power and the previous power against a predefined constant. This constant is placed within the algorithm to ensure that when the method has found the MPP on the PV panel, the duty cycle will remain constant until any condition changes large enough to change the location of the MPP. If this step is not included the algorithm would constantly change the duty cycle, causing the operating point of the panel to move back and forth across the MPP. The movement across the MPP is an unwanted oscillation that can be disruptive to power flow and could also cause unwanted loss from not having the operating point right over the MPP at all times.

The next step in the algorithm is determining whether the current power, P_k is greater than or less than the previous power, P_{k-1}. The answer to this tells the algorithm which branch of the flowchart to take next. No matter which direction the algorithm takes, the next step is to compare the voltage in the current, $V_{in(k)}$ and the voltage in the previous, $V_{in(k-1)}$ iterations. The voltage comparison tells the algorithm which side of the MPP the operating point is at thereby allowing the algorithm to adjust the duty cycle in the right direction, either a positive or a negative addition to the current duty cycle. The final step of the method is to actually change the duty cycle being output to the converter, and wait for the converter to stabilize before starting the process all over again.

The main advantage of choosing the P&O as an algorithm is easier and simple to implement and its low computational method. However, there are some limitations that cannot be ignored such like the oscillations around the MPP in steady state operation and slow response speed. But, these limitations can be reduced by optimizing the sampling rate depends on the converters' dynamic (Kollimalla and Mishra, 2014; Sharma and Purohit, 2012; Femia, Petrone et al., 2004; Liu and Lopes, 2004).

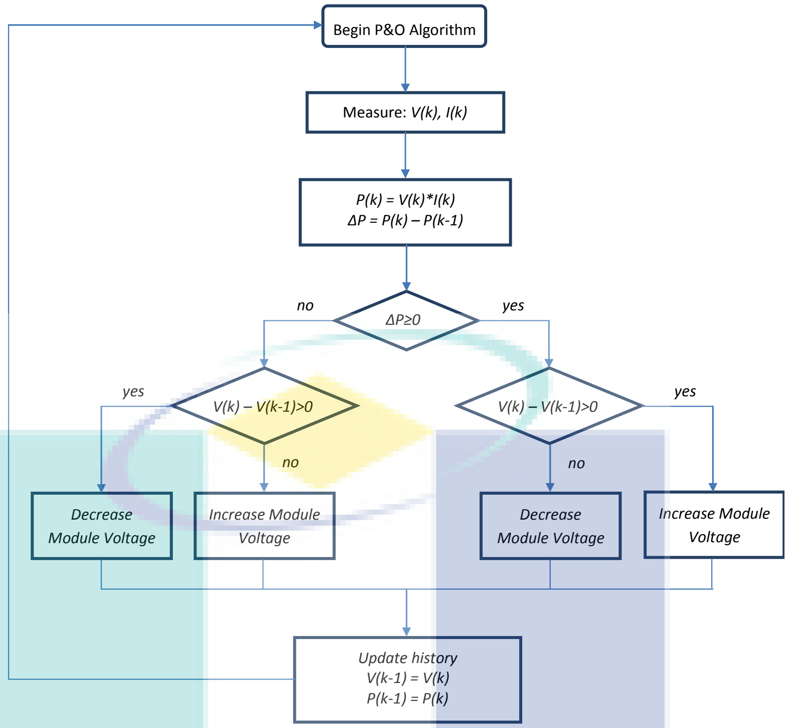

Figure 2.5: P&O algorithm flowchart

2.3.2 Incremental Conductance Algorithm

Apart from P&O, the incremental conductance method (IncCond) also regards as another popular algorithm. This algorithm was introduced to improve any problems occurred from the P&O algorithm (Jerin, 2014; Hussein, Muta et al., 1995). The algorithm works on the fact that the slope of the *P-V* curve is equal to zero at the MPP. The left hand side of the MPP, the power is increasing with the voltage and its decreasing on the right of MPP. This can be written as the following equation:

at MPP $$\frac{dP}{dV} = 0 \tag{2.1}$$

left of the MPP $$\frac{dP}{dV} > 0 \tag{2.2}$$

right of the MPP $$\frac{dP}{dV} < 0 \tag{2.3}$$

These equations can be written in terms of the current and voltage by:

$$\frac{dP}{dV} = \frac{d(I.V)}{dV} = I + V\frac{dI}{dV} \tag{2.4}$$

Hence, this algorithm shows that the only information needed to determine the relative location of the MPP is only by measuring the incremental and instantaneous module conductance, *dI/dV* and *I/V* respectively.

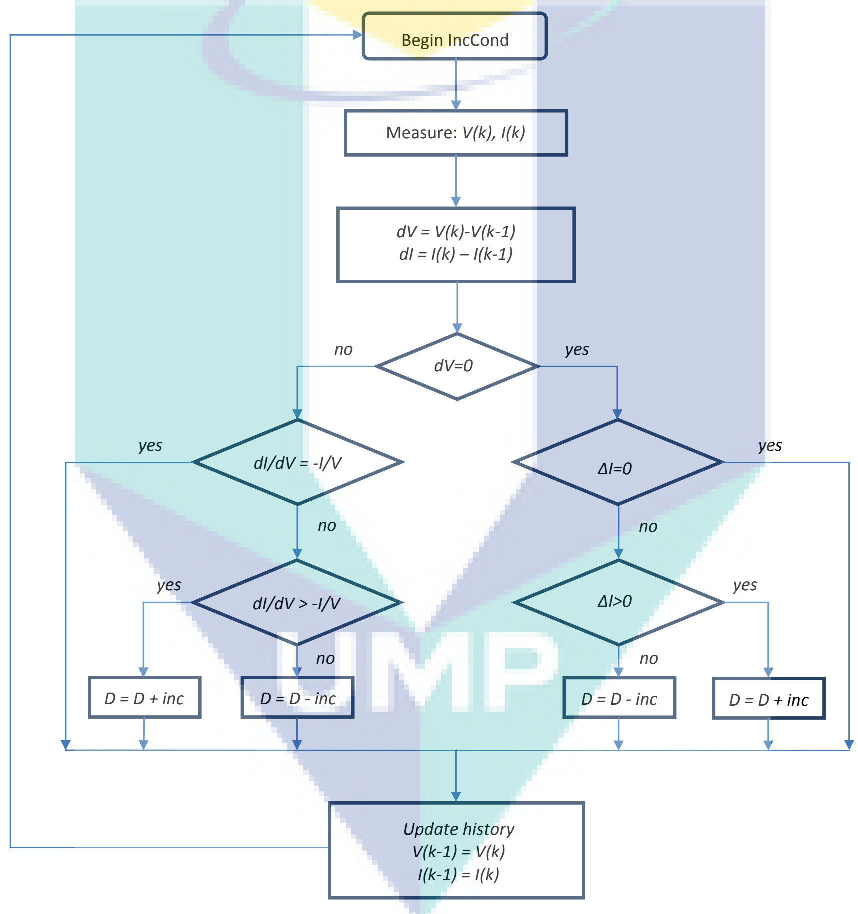

Figure 2.6: IncCond algorithm flowchart

As the list of algorithms keeps on increasing, its complexity and cost of implementation also keeps on increasing. This is the reason why the P&O method is chosen, due to its simplicity and also by its low computational demand.

2.4 DC/DC CONVERTER

The purpose of a DC/DC converter is to supply a regulated DC output voltage to a variable-load resistance from a fluctuating DC input voltage. In many cases the DC input voltage is obtained by rectifying a line voltage that is changing in magnitude.The output voltage in DC/DC converters is generally controlled using a switching concept. Early DC/DC converters were known as choppers with Silicon-Controlled Rectifiers (SCRs) used as the switching mechanisms. Modern DC/DC converters classified as Switch Mode Power Supplies (SMPS) employ Insulated Gate Bipolar Transistors (IGBTs) and Metal Oxide Silicon Field Effect Transistors (MOSFETs). In solar photovoltaic application, DC/DC converters work in conjunction with MPPT to control through a strategy that allows imposing the photovoltaic module operation point on the maximum power point (MPP) or close to it.The generated power exhibits a nonlinear *I-V* characteristic and its maximum power point (MPP) vary with solar irradiation and temperature. Therefore, an intermediate DC/DC converter is necessary to adjust the voltage and current levels, and matches the PV source to the load (Hemalatha, Hariprasad et al., 2014; Kashyap, Ahmadi et al., 2013; Alghuwainem , Coelho, dos Santos et al., 2012; Salameh and Taylor, 1990).

Basic switching converters such as Buck, Boost, Buck-boost and SEPIC converter have been widely applied. These types of converters are known as non-isolated topologies where they do not have isolation transformers. The Buck topology is a step-down converter where the output voltage is stepped down to lower than the input voltage. The converter circuit diagram is shown as in Figure 2.7. In PV application, the converter is implemented with the MPPT algorithms to make sure that the load voltage is lower than PV module output voltage.

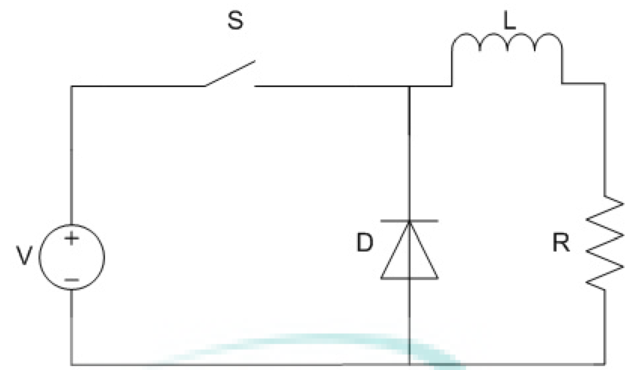

Figure 2.7: Buck converter circuit

The conversion ratio for Buck converter can be described as:

$$M = \frac{V_{out}}{V_{in}} = D \tag{2.5}$$

The Boost topology is the one commonly used converter in a PV system as illustrates in Figure 2.8.

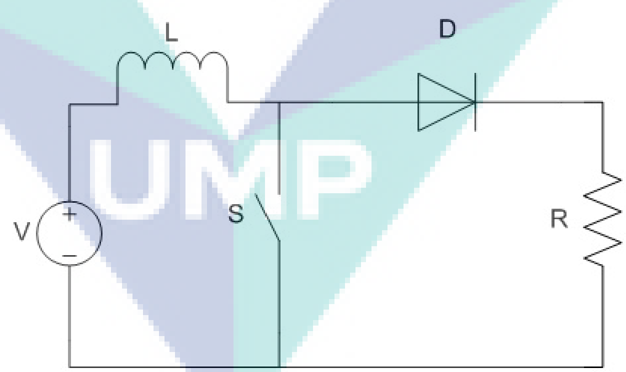

Figure 2.8: Boost converter circuit

The Boost topology is a step-up converter where the output voltage is stepped up to higher than the input voltage. The Boost converter can operate in MPPT circuit as long as the voltage required by the load is larger than the PV module voltage. The primary advantage of Boost converter compared to the Buck converter is when it operated in Continuous Conduction Mode (CCM), it draws a smooth current from the

PV array by applying a small capacitor at the array terminals compared to the Buck converter which requires a big capacitor to smooth the current array.The conversion ratio for Buck converter can be described as:

$$M = \frac{V_{out}}{V_{in}} = \frac{1}{1-D} \tag{2.6}$$

In a PV system that using batteries, the PV module MPP is higher than the charging voltage of the batteries. At this point, a Buck converter can well operate at the MPP. The problem arises when the MPP dropped below the charging voltage of the battery in the case when there is a low irradiance condition. This is the case where a Buck-Boost converter is needed when the boost capability can step up the MPP higher than the battery charging voltage and at the same time increasing the efficiency. The Buck-Boost circuit is shown in Figure 2.9 while its conversion ratio can be written as:

$$M = \frac{V_{out}}{V_{in}} = \frac{D}{D-1} \tag{2.7}$$

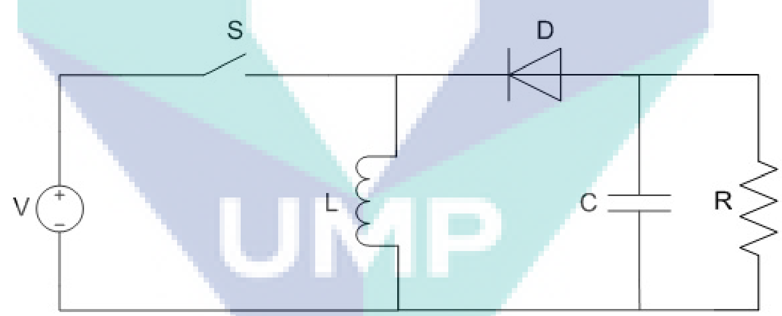

Figure 2.9: Buck-Boost converter circuit

Although the Boost converter is very popular among them, however, SEPIC converter have been regarded the better choice because its benefits that include buck-boost conversion function without polarity reversal and low ripple input current (Chiang, Hsin-Jang et al., 2009). Conventional hard-switching converters were presenting large switching losses, which decrease the converter efficiency. The main reason of choosing SEPIC is because it can easily adapt to any PV output voltage and also any battery input where it provides a positive regulated output voltage from an input voltage that varies from above to below the output voltage.

2.4.1 SEPIC Topology

The single-ended primary-inductance converter (SEPIC) is a DC/DC converter topology that widely used in battery-powered systems. Figure 2.10 shows a simple circuit diagram of a SEPIC converter, consisting of an input capacitor, C_{in}; an output capacitor, C_{out}; coupled inductors *L1* and *L2*; an AC coupling capacitor, C_s; a power FET, *Q1*; and a diode, *D1*.

Figure 2.11 and Figure 2.12 shows the SEPIC operation in continuous conduction mode (CCM) with *Q1* is ON and OFF, respectively. To understand the voltages at the various circuit nodes, it is important to analyze the circuit in the DC condition when *Q1* is off and not switching. During steady-state CCM, pulse-width modulation (PWM) operation, and neglecting ripple voltage, capacitor C_s is charged to the input voltage, V_{IN}. Knowing this, we can easily determine the voltages as shown in Figure 2.10.

When *Q1* is off, the voltage across *L2*is equal to V_{OUT}. Since C_{in} is charged to V_{IN}, the voltage across *Q1* when *Q1* is off is $V_{IN} + V_{OUT}$, so the voltage across *L1* is V_{OUT}. When *Q1* is on, capacitor *Cs*, charged to V_{IN}, is connected in parallel with *L2*, so the voltage across *L2* is $-V_{IN}$. The currents flowing through various circuit components are shown in Figure 2.13. When *Q1* is on, the energy from the input and from C_S is stored in *L1* and *L2*, respectively. When *Q1* turns off, *L1*'s current continues to flow through *Cs* and *D1*, and into C_{out} and the load. Both C_{out} and *Cs* get recharged so that they can continuously providing the current to the load and to *L2*, respectively, during the next half switching cycle when *Q1* is on again.

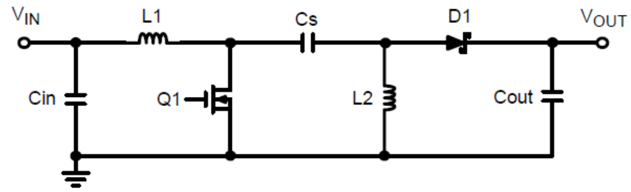

Figure 2.10: SEPIC Topology

Source: (Zhang 2013)

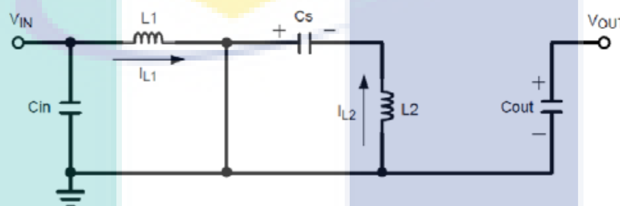

Figure 2.11: SEPIC Converter Current Flow during Q1 On-Time

Source: (Zhang 2013)

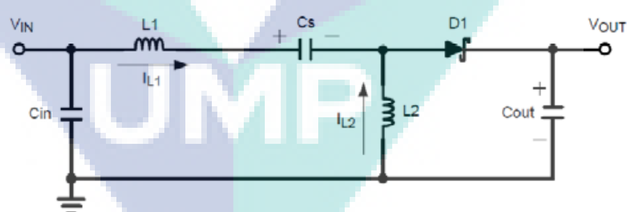

Figure 2.12: SEPIC Converter Current Flow during Q1 Off-Time

Source: (Zhang 2013)

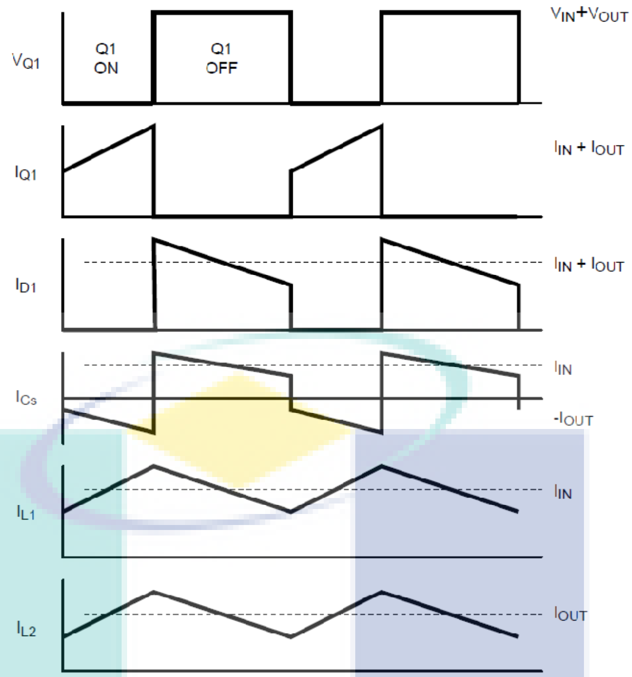

Figure 2.13: SEPIC Converter Switching Waveforms

Source: (Zhang 2013)

The SEPIC is known for its capability of providing a wide range of output voltage from lower than to greater than the input voltage without having to invert the polarity. The conversion ratio, M is defined as:

$$M = \frac{V_{out}}{V_{in}} = \left(\frac{D}{1-D}\right) \tag{2.8}$$

If $D < 0.5$, the output voltage will be lower than the input voltage. When $D > 0.5$, the output voltage will be greater than the input voltage. Figure 2.14 shows SEPIC conversion ratio, M, versus duty cycle, D. The conversion ratio heading to the infinite value as the duty cycle value is approaching 1.

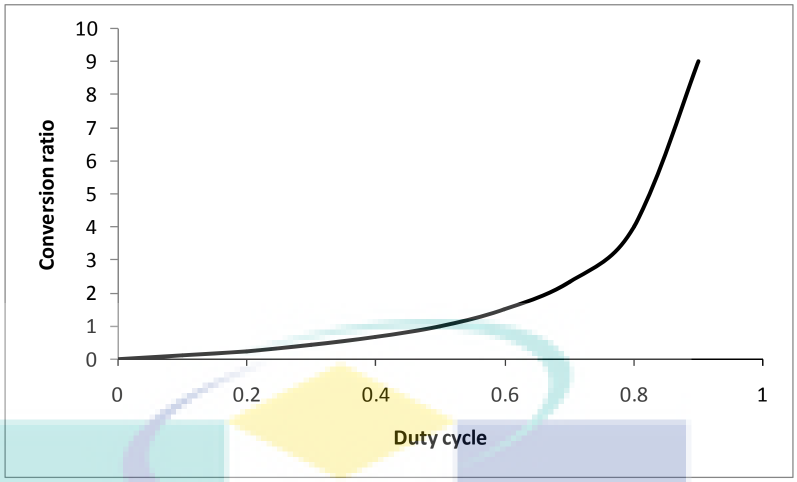

Figure 2.14: SEPIC conversion ratio

2.5 EFFICIENCY ANALYSIS OF DC/DC CONVERTER

The ideal DC-DC converter delivers 100 % efficiency; in practice, efficiencies of 70 % to 95 % are typically obtained while boosting, reducing, or inverting supply voltages. Resistance in the power source is one of the most important factors that can limit efficiency. The DC/DC converter efficiency became an important issue in the power electronics field. Each design and topology became more critical for its designers to implement. In the renewable energy environment, the sources fluctuate depending to the availability of the energy sources which make the energy storage and consumption become important. Researchers and designers have tried on many aspects to outcome this issue based on the implementation of the converters and topology used. For example, (Zhiguo, Fan et al., 2005) analyzed about the power losses which considers the different loss mechanisms. The analysis also can be considered in term of regulation ability, power ratings and also switch stresses (Junjian, Yeates et al., 2013). Apart from the power losses, there are also an efficiency analysis regarding power characteristics in DC/DC converter by decreasing the overall power dissipation and current demand (Volkan Kursun, 2002).

2.6 SUMMARY

This chapter explains about the history and construction of a PV; from a PV cell to PV module and the characteristics of the *I-V* curve. In this chapter, there is a brief explanation on solar charge controller construction. The charge controller that consists of MPPT algorithm and DC/DC converter, where two types of MPP algorithm and four types of DC/DC converter topology were presented. The final review in this chapter focused on the efficiency analysis of the DC/DC converter. The P&O algorithm is chosen because of its simplicity to implement into the system. Then the DC/DC converter topologies are explained together with the brief explanation focused on SEPIC operation. Meanwhile, SEPIC is chosen because of its capability of step-up and step-down the output voltage without having to invert the polarity. The combination of P&O algorithm and SEPIC which is also known as charge controller will be analyzed in this study.

CHAPTER 3

METHODOLOGY

3.1 INTRODUCTION

In this chapter, the study is divided into two sections of the Solar Charge Controller. The first section is concentrating on the controller part while the second section is focused on the power circuit. In the first section, it begins with the data collection for solar irradiation in Pekan, Pahang. Then, a modeling of a PV cell using an equivalent electrical circuit followed by testing P&O algorithm is realized in MATLAB. In the second section, a SEPIC circuit is designed and simulates using PSIM and finish with the experiment that will focus on the circuit efficiency and loss analysis.

The experiment is conducted without having any continuity with the simulation that previously done. The circuit used the same parameters in the simulation, but with different input and testing parameters. On the other hand, the experiment is running only in the open loop circuit compared to the simulation which is tested in close loop circuit. The sampling frequency selection is determined only to suit the charge controller performance under rapid changing solar irradiation. During hardware experiment, the PWM signal is delivered by the Arduino UNO board at two frequencies tested; 7.8 kHz and 62.3 kHz. The methodology block diagram is as shown in Figure 3.1. The block diagram illustrates the three methods use in this research in accordance with the research objective. The first block labelled by MATLAB correspond to the first objective. The second block that labelled by PSIM correspond to the second objective while the third objective represent by the red rectangle on the far right corner of the diagram.

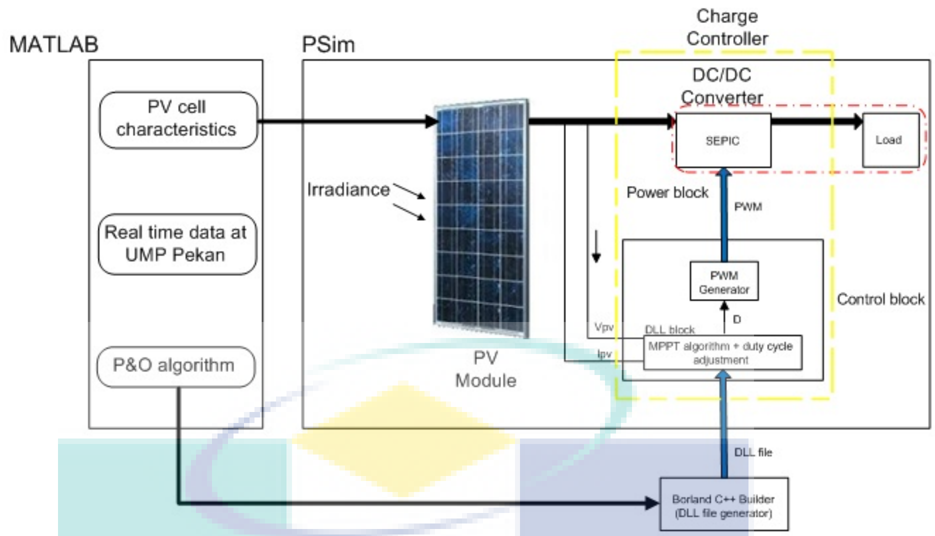

Figure 3.1: Methodology block diagram

3.2 MODELING THE PV MODULE IN MATLAB

First of all, solar irradiation data are collected from the UMP weather station for simulation purpose. Two criteria of data are collected, which consists of the sunniest and the cloudiest day in the UMP for the period from January 2011 to March 2012. The cloudiest day along that period was on 28 December 2011 and the sunniest day is on 19 March 2012. From 24-hours solar irradiation data, only 12-hours data picked from 0700 hours to 1900 hours. This is to neglected all zero irradiation data that occur nearly from 1900 hours until 0700 hours. All the data are logged using WeatherLink which is a comprehensive software to store, display and analyze all accumulated weather data and, if required, to run a live weather reporting website as in Figure 3.2. The collected data will be compiled and plotted in the MATLAB editor shown in APPENDIX A. This data will then used to evaluate the P&O algorithm later.

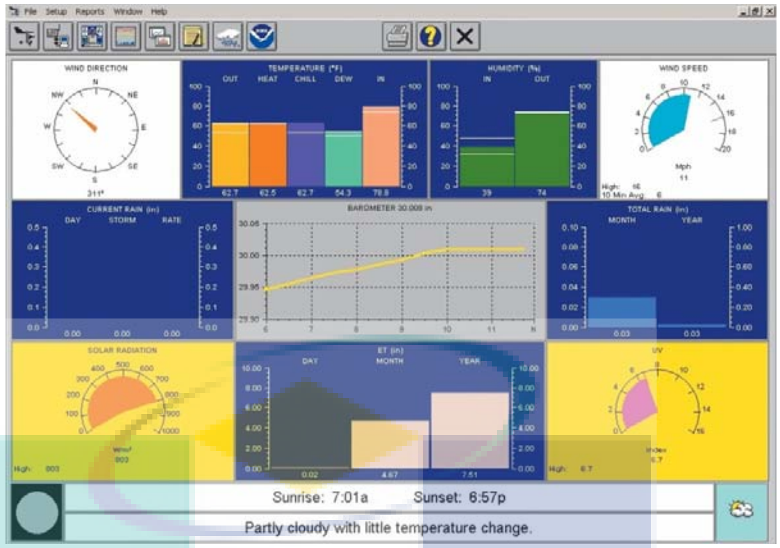

Figure 3.2: WeatherLink software interface

As for modeling purpose, The PV module, Mitsubishi PV-TE125MF5N is 36 polycrystalline silicon solar cells in series which able to provide 125 W of maximum power (MITSUBISHI, 2007) is selected. The specifications of the module are shown in Table 3.1. The model was evaluated using MATLAB using the equations shown in this section. The current, *I*, is then evaluated using three variable parameters, voltage, irradiation, and temperature. If one of the input variables is a vector, the output variable (current) is also a vector.

Table 3.1: Electrical specification of PV_125MF5N module

	PV-TE125MF5N	
Parameter	**Variable**	**Value**
Maximum Power	P_m	125 W
Maximum Power Voltage	V_{mp}	21.8 V
Maximum Power Current	I_{mp}	7.9 A
Open-circuit Voltage	V_{oc}	17.3 V
Short-circuit Current	I_{sc}	7.23 A

The simplest equivalent circuit of a solar cell is a current source in parallel with a diode as previously studied by (Chapin, Fuller et al., 1954). It consists of a current source (I_{sc}), a diode (D), and a series resistance (R_s). As the effect of shunt resistance

(R_{sh}) is very small in a single module, thus it is neglected (Walker, 2000). To make the circuit a better model, it will also include temperature effects on the short-circuit current (I_{sc}) and the reverse saturation current of the diode (I_0). It uses a single diode with the diode ideality factor (n) set to achieve the best *I-V* curve match. The equivalent circuit of PV cell is shown in Figure 3.3 below.

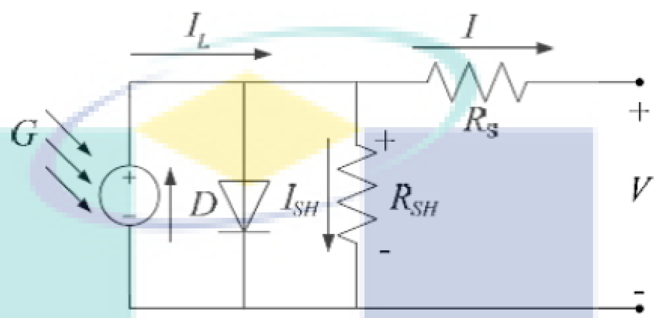

Figure 3.3: Equivalent electrical circuit of a PV cell

Adapted from : (Chiang, Hsin-Jang et al. 2009)

As presented by Chapin, Fuller et al. (1954), the current-voltage relationship of the PV cell is described as following equation:

$$I = I_{sc} - I_o\left[e^q\left(\frac{V + I.R_s}{nkT}\right) - 1\right] \tag{3.1}$$

where:

I is the cell / module current,

$I_0$is the reverse saturation of the diode,

k is the Boltzmann constant ($1.3806503 \times 10^{-23}$ J/K),

q is the electron charge ($1.60217646 \times 10^{-19}$ C),

n is the diode ideality factor,

V is the cell voltage {(module voltage) ÷ (number of cells in series)},

T is the cell temperature in Kelvin = (273+25);

The short-circuit current (I_{sc}) was first calculated at a given cell temperature (T):

$$I_{sc}|_T = I_{sc}|_{T_{ref}}.\left[1 + a\left(T - T_{ref}\right)\right] \tag{3.2}$$

where, I_{sc} at T_{ref} is given in the datasheet (measured under irradiance of 1000 W/m^2), T_{ref} is the reference temperature of PV cell in Kelvin (K), usually 298 K (25 ˚C); α is the temperature coefficient of I_{sc} in percent change per degree temperature also given in the datasheet.

The short-circuit current (I_{sc}) is proportional to the amount of irradiance. I_{sc} at a given irradiance (G) is:

$$I_{sc}\Big|G = \left(\frac{G}{G_0}\right) I_{sc}\Big|\, G_0 \tag{3.3}$$

$G_o$is the nominal value of irradiance, which are normally 1 kW/m^2.

The reverse saturation current of the diode (I_0) at the reference temperature (T_{ref}) is given below with the diode ideality factor added:

$$I_0 = \frac{I_{sc}}{\left(e^{qV_{oc}/nkT} - 1\right)} \tag{3.4}$$

The reverse saturation current (I_0) is temperature dependent and the I_0at a given temperature (T) is calculated by the following equation:

$$I_0|_T = I_o|_{T_{ref}}.\left(\frac{T}{T_{ref}}\right)^{\frac{3}{n}}.e^{\frac{-q.E_g}{nk}\left(\frac{1}{T}-\frac{1}{T_{ref}}\right)} \tag{3.5}$$

The diode ideality factor (n) must be estimated because its value is unknown. The estimation value must be between one and two where, $n = 1$ (for ideal diode) is used for instance, until more accurate value can be estimated during simulation. The effect of the varying diode ideality factor is shown as in Figure 3.4.

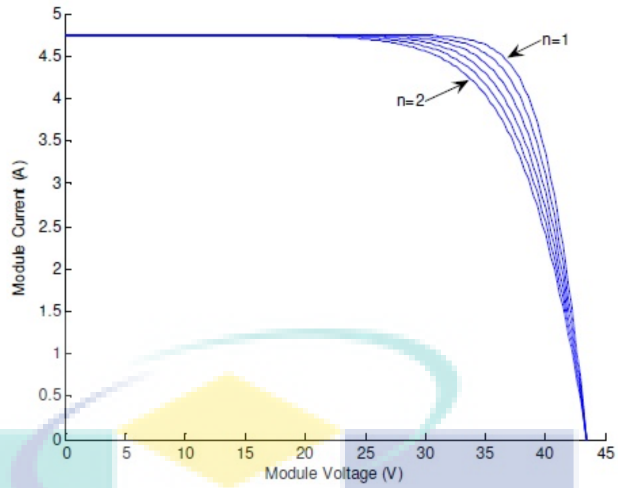

Figure 3.4: Effect of diode ideality factor on *I*-*V* curve

Source: (Oi 2005)

The series resistance (R_s) of the PV module has a large impact on the slope of the *I*-*V* curve near the open-circuit voltage (V_{oc}), therefore, the value of R_s is calculated by evaluating the slope of the *I*-*V* curve at the V_{oc}. The equation for R_s was derived by:

$$R_s = -\frac{dI}{dV} - \frac{nkT/q}{I_0 . e^{q(\frac{V+I.R_S}{nkT})}} \tag{3.6}$$

and for open circuit voltage when, $V = V_{oc}$ (I=0), then:

$$R_s = -\frac{dV}{dI}|V_{oc} - \frac{nkT/q}{I_0 . e^{\frac{qV_{oc}}{nkT}}} \tag{3.7}$$

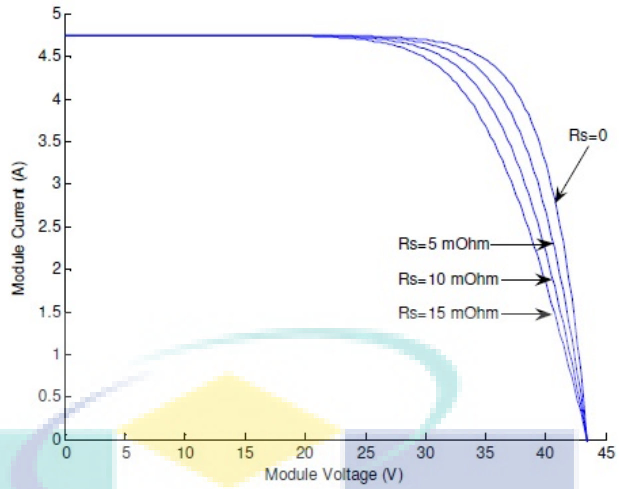

Figure 3.5: Effect of series resistance on *I*-*V* curve

Source: (Oi 2005)

Hence, the Eq.(3.1) could be solved with the known R_s value. This model however is complex because the solution of current is recursive by inclusion of a series resistance in the model (Walker, 2000). Therefore, the Newton-Raphson method was used for rapid convergence of the answer as described below:

$$x_{n+1} = x_n - \frac{f(x_n)}{f'(x_n)} \tag{3.8}$$

where, $f'(x)$ is the derivative of the function, $f(x) = 0$, x_n is a present value and x_{n+1} is a next value.

The function then rewrites in Eq.(3.1) that gives:

$$f(I) = I_{sc} - I - I_0 \left[e^{q\left(\frac{V+I.R_S}{nkT}\right)} - 1 \right] = 0 \tag{3.9}$$

Eq. (3.9) then put into Eq.(3.8) that gives output current that is computed iteratively as:

$$I_{n+1} = I_n - \frac{I_{sc} - I_n - I_0[e^{q\left(\frac{V+I_n.R_S}{nkT}\right)} - 1}{-1 - I_0\left(\frac{q.R_S}{nkT}\right)e^{q\left(\frac{V+I_n.R_S}{nkT}\right)}} \tag{3.10}$$

The constants and equations, then presented in MATLAB where the module operating current, I_a, is evaluated using three variable parameters, voltage, irradiation, and temperature. Finally, the modeled PV module function is integrated with the P&O tracking algorithm file editor showed in APPENDIX A and used the solar irradiation data that logged earlier to simulate the outcome of the system during the sunniest and cloudiest day on the selected days.

3.3 SEPIC PSIM SIMULATION

PSIM is one of simulation tools that designed specifically for power electronics and motor drives usage. This simulation tool provides a schematic capture interface while the simulation results viewed using waveform viewer called Simview. Due to its simplicity and capability, it was chosen as a simulation tool for the SEPIC circuit. The circuit is designed based on the block diagram as in Figure 3.6. The components sizing and selection for SEPIC is predetermines using the calculation shown in sub-section 3.3.2. The converter parameters are shown as in Table 3.2.The circuit will be simulated in two conditions. The first is an open loop simulation and the other one is a close loop simulation which using a DLL block in the setup. The close loop simulation is intended to test P&O algorithm along with SEPIC at varying solar irradiation where the DLL block works as the controller for the circuit.

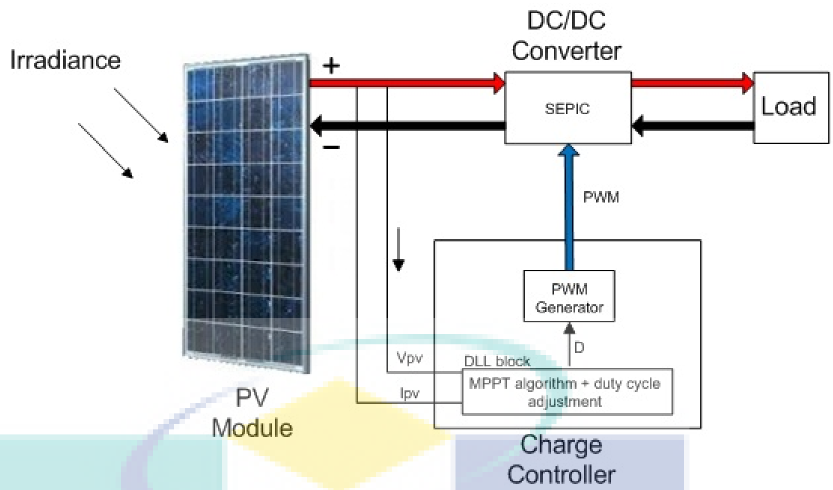

Figure 3.6: Block diagram of the designed system

3.3.1 PSIM Solar Module (Physical Model) Setup

There are two types of solar module in PSIM simulation tools; physical model and functional model. The functional model is the one that needs only few basic parameters which are the open-circuit voltage, open-circuit current, maximum power voltage and maximum power current. It cannot provide inputs that have a variation of solar irradiance and temperature. Hence, users could opt for the physical model type. The physical model solar module needs three steps in order to obtain the model parameters which are:

(i) use the information from the datasheet;

(ii) make an initial guess of certain parameters such as diode ideality factor;

(iii) obtain the *I-V* and *P-V* curves, and also MPP. Then compare with datasheet for different operating conditions, and fine tune the parameters.

As most of the parameters have already defined during modeling the solar module in MATLAB, the setup becomes easier. All the parameters needed are filling in the box as shown in Figure 3.8. The software will then generate the *I-V* and *P-V* curve of this particular module, and calculate the maximum power, maximum voltage and maximum current. The block for solar module (physical model) is as shown in Figure 3.7.

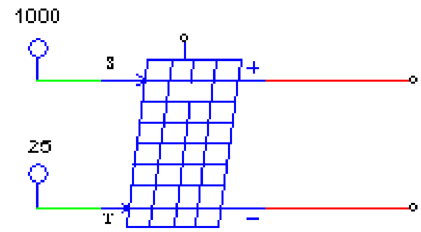

Figure 3.7: Solar module (physical model) block with 1000 W/m^2 irradiance and 25 ^{o}C temperature input

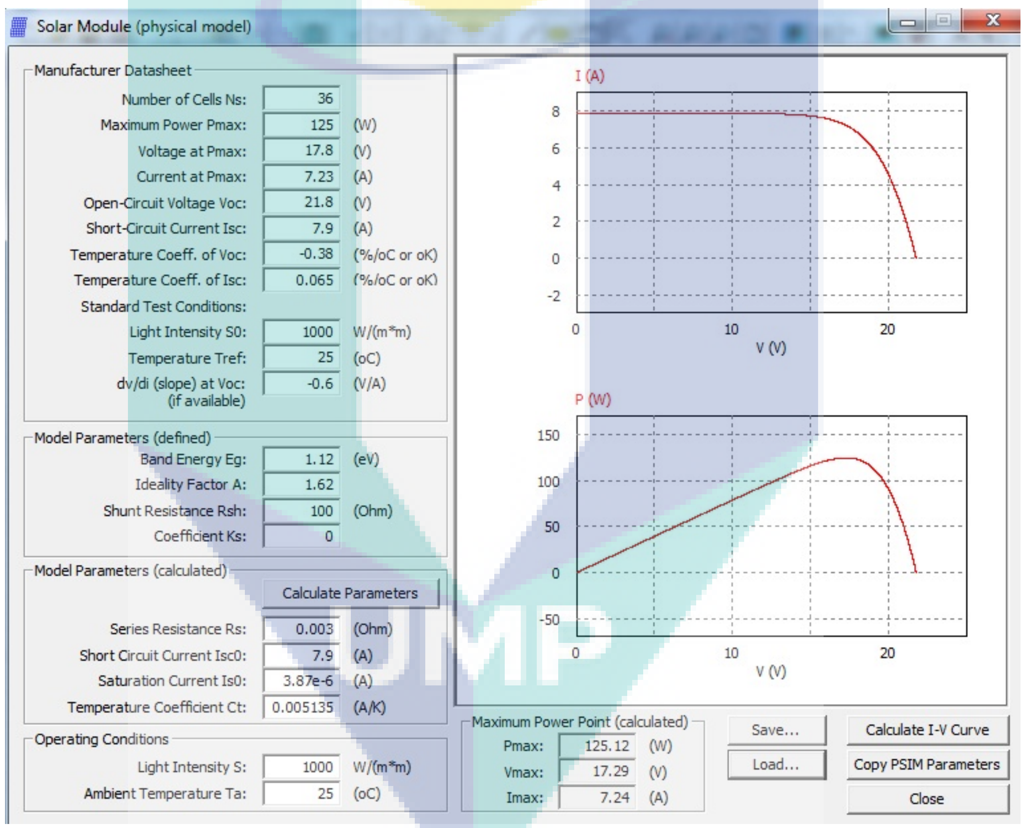

Figure 3.8: PSIM solar module parameters setup

3.3.2 SEPIC Components Sizing and Selection

The component sizing and selection was determined based on these following equations by considering the parameters in Table 3.2.

Table 3.2: Design specifications and parameters for SEPIC

Components Parameter	SEPIC DC/DC Converter	
	Variable	**Value/Model name**
Input Voltage	V_{in}	5 V- 25 V
Input Current	I_{in}	0-8 A
Outptut Voltage	V_{out}	8 V-35 V
Outptut Current	I_{out}	0-9 A
Switching Frequency	f_{sw}	50 kHz
Maximum Outptut Power	P_{max}	125 W
Duty cycle	D	0.3 – 0.7

a) Duty cycle consideration

Duty cycle is given by Eq. (3.11) for a SEPIC converter operating in a continuous conduction mode (CCM).

$$D_{max} = \frac{V_{out} + V_D}{V_{in(min)} + V_{out} + V_D} = \frac{13.5 + 0.4}{5 + 13.5 + 0.4} D_{max} \tag{3.11}$$

$$= 0.74 D_{min} = \frac{V_{out} + V_D}{V_{in(max)} + V_{out} + V_D}$$

$$= \frac{13.5 + 0.4}{25 + 13.5 + 0.4} D_{min} = 0.36$$

where V_D is the forward voltage drop of the diode *D1*.

b) Inductor

The ripple current flowing in equal value inductors *L1* and *L2* is given by:

$$\Delta I_L = I_{in} * 40\% = I_{out} * \frac{V_{out}}{V_{in(min)}} * 40\% \Delta I_L \tag{3.12}$$

$$= 4.5 * \frac{13.5}{5} * 0.4 = 4.86\ A$$

where the 40% is the value to allow the peak-to-peak ripple current of the maximum input current at the minimum input voltage. Hence, the inductor value calculated by:

$$L1 = L2 = L = \frac{V_{in(min)}}{\Delta I_L * f_{sw}} * D_{max} \qquad (3.13)$$
$$= \frac{5}{4.86 * 50^3} * 0.74 = 15.2\ \mu H$$

where f_{sw} is the switching frequency.

The inductors peak current then calculated by:

$$I_{L1(peak)} = I_{out} * \frac{V_{out} + V_D}{V_{in(min)}} * \left(1 + \frac{40\%}{2}\right) I_{L1(peak)} \qquad (3.14)$$
$$= 4.5 * \frac{13.5 + 0.4}{5} * \left(1 + \frac{0.4}{2}\right) = 15A$$

$$I_{L2(peak)} = I_{out} * \left(1 + \frac{40\%}{2}\right) I_{L2(peak)} \qquad (3.15)$$
$$= 4.5 * \left(1 + \frac{0.4}{2}\right) = 5.4A$$

c) Power MOSFET

There are a few important parameters to consider when choosing the MOSFET. Those parameters are the minimum threshold voltage, $V_{th(min)}$, the on-resistance, R_{DSon}, gate-drain charge, Q_{GD}, and the maximum drain to source voltage, $V_{DS(max)}$. The MOSFET's gate to source voltage, V_{GS} value should be used based on the gate drive voltage.
The peak current of the MOSFET is calculated by:

$$I_{Q1(peak)} = I_{L1(peak)} + I_{L2(peak)} I_{Q1(peak)} \qquad (3.16)$$
$$= 15 + 5.4 = 20.4\ A$$

and the RMS current through the switch is:

$$I_{Q1(rms)} = I_{out}\sqrt{\frac{(V_{out}+V_{in}+V_D)*(V_{out}+V_D)}{V_{in(min)}^{\ 2}}} I_{Q1(rms)} \tag{3.17}$$

$$= 4.5\sqrt{\frac{(13.5+5+0.4)*(13.5+0.4)}{5^2}} I_{Q1(rms)}$$

$$= 3.24\,A$$

d) Diode

The diode peak current is as the same as the MOSFET's, $I_{Q1(peak)}$. The diode selection is to ensure that it can withstand the minimum peak reverse voltage base on this calculation:

$$V_{RD1} = V_{in(max)} + V_{out(max)} V_{RD1} = 25 + 35 \tag{3.18}$$

$$= 60\,V$$

The diode average current is equal to output current, so we can say that the power dissipation of the diode is equal to:

$$P_D = I_{RD(avg)} * V_D P_D = 4.5 * 0.4 = 1.8\,W \tag{3.19}$$

e) Coupling capacitor

The selection of coupling capacitor, C_s is depends on the RMS current given by:

$$I_{C_{s(rms)}} = I_{out} * \sqrt{\frac{V_{out}+V_D}{V_{in(min)}}} I_{C_{s(rms)}} \tag{3.20}$$

$$= 4.5 * \sqrt{\frac{13.5+0.4}{5}} = 7.5\,A$$

where the peak-to-peak ripple voltage on C_s that assuming no ESR is:

$$\Delta V_{C_s} = \frac{I_{out} * D_{max}}{C_s * f_{sw}} \Delta V_{C_s} = \frac{4.5 * 0.74}{47^{-6} * 50^3} = 1.42\ V \tag{3.21}$$

f) Output capacitor

The output capacitor, C_{out} must have the capability to handle the maximum RMS current because the output current is supplied by the output capacitor when the switch, Q_1 is turned on. The RMS current in the output capacitor described as:

$$I_{C_{out(rms)}} = I_{out} * \sqrt{\frac{V_{out} + V_D}{V_{in(min)}}} I_{C_{out(rms)}} \tag{3.22}$$

$$= 4.5 * \sqrt{\frac{13.5 + 0.4}{5}} = 7.5\ A$$

ESR and bulk capacitance of the C_{out} directly control the output ripple. The first assumption is V_{ripple} = 2 % of the output voltage, V_{out}. Then, by assuming half of the ripple is caused by the ESR and the other half by the capacitance amount, it will be described as:

$$ESR \leq \left(\frac{V_{ripple} * 0.5}{I_{L1(peak)} + I_{L2(peak)}}\right) ESR \tag{3.23}$$

$$\leq \left(\frac{0.02 * 13.5 * 0.5}{15 + 5.4}\right) = 6.6\ m\Omega$$

and

$$C_{out} \geq \left(\frac{I_{out} * D_{max}}{V_{ripple} * 0.5 * f_{sw}}\right) C_{out} \tag{3.24}$$

$$\geq \left(\frac{4.5 * 0.74}{0.02 * 13.5 * 0.5 * 50^3}\right) = 493.3\ \mu F$$

g) Input capacitor

The input capacitor, C_{in} should be capable of handling the RMS current. A 10µF or higher value with a good quality capacitor would prevent impedance interactions with the input supply. The RMS current in the C_{in} is given by:

$$I_{C_{in(rms)}} = \frac{\Delta I_L}{\sqrt{12}} I_{C_{in(rms)}} = \frac{4.86}{\sqrt{12}} = 1.4\ A \tag{3.25}$$

An open loop SEPIC is designed in PSIM as in Figure 3.9 and the close loop circuit is as in Figure 3.10. It is based on the Table 3.3 after the consideration on the component sizing calculation. In addition, the circuit also includes an inductor, *L3*, which act as a filter.

Table 3.3: SEPIC components

Components Parameter	SEPIC DC/DC Converter	
	Variable	**Value/Model name**
Input Capacitor	C_{in}	47 µF
AC Coupling Capacitor	C_s	47 µF
Output Capacitor	C_{out}	1000 µF
Coupled Inductor 1	L_1	47 µH
Coupled Inductor 2	L_2	47 µH
Filtered Inductor	L_3	1 mH
Power MOSFET	Q_1	IRF540N
Diode	D_1	30CPF12
Resistive load	R_L	9 Ω

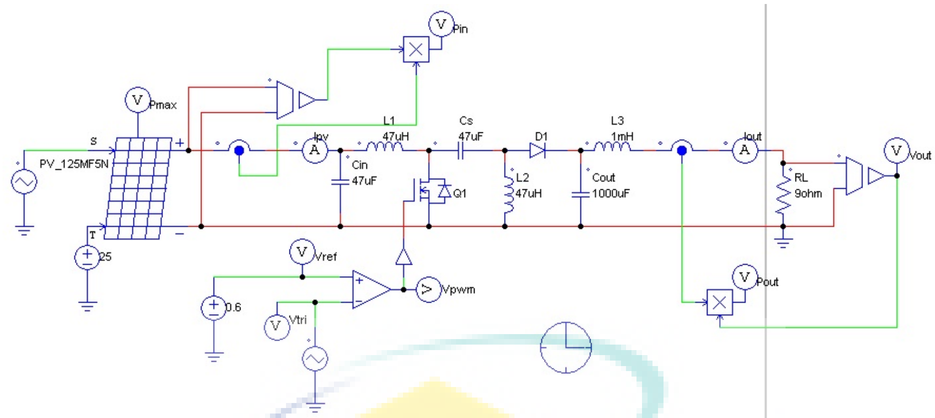

Figure 3.9: SEPIC open loop circuit

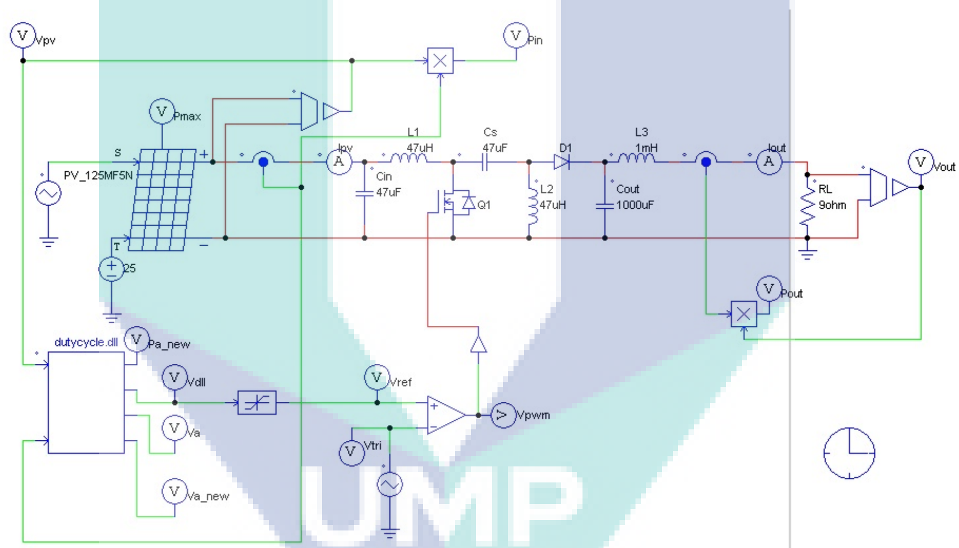

Figure 3.10: SEPIC close loop circuit

3.4 SEPIC LOSS ANALYSIS

The hardware implementation is focused on the analysis of the SEPIC efficiency and losses. The efficiency is affected by various types of losses involved in SEPIC.There will be two major losses from two switching components to be focused during the experiment; the switching loss and conduction loss of power MOSFET and diode. These losses contribute to the biggest percentage of the circuit efficiency. Since the hardware implementation is focused on the efficiency issue of SEPIC, only the open loop system is developed. On top of the parameters in Table 3.3, additional parameters needed for practical experiment are shown in Table 3.4.

Table 3.4: Hardware testing parameters

	PV-TE125MF5N	
Parameter	**Variable**	**Value**
Input Voltage	V_{in}	10 V
Switching frequency	f_{sw}	7.8 kHz & 62.3 kHz
Duty cycle	D	0.3 – 0.7
Load resistance	R_L	9 Ω

The circuit will be tested at different frequencies and duty cycles in order to measure losses that occur at different parameters. The frequency selected is based on the capability of the Arduino UNO board that delivered the PWM to the MOSFET. The 62.3 kHz frequency is the maximum frequency that can be set by the Arduino UNO board while the 7.8 kHz frequency is selected randomly from the Arduino UNO timer setting. The duty cycle range selected from 0.3 to 0.7 as the circuit operated at its best around it (Oi, 2005; Geir Opdahl, 2010). The duty cycle value will be adjusted by 0.2 per step along the experiment.

3.4.1 SEPIC losses

In general, power loss is the sum of the two types of losses in the converter, which are switching and conduction. Conduction losses usually dominate at higher output loads; whereas switching losses remain relatively fixed and dominate atlower output loads. However, in SEPIC, there are certain losses apart from the two which came from those passive components. The list of losses in SEPIC can be described as:

a) Capacitor loss

The capacitor losses are comprised of the losses from the coupling capacitor, C_s and output capacitor, C_{out}. The input capacitor, C_{in} didn't give too much impact in overall capacitor losses, hence it is neglected.

The capacitor losses then can be described as:

$$P_C = P_{C_s} + P_{C_{out}} \tag{3.26}$$

$$P_{C_s} = (I_{out}^2 * R_{esr} * D) + I_{out}^2 * \left(\frac{D^2}{1-D}\right) * R_{esr} \tag{3.27}$$

and

$$PC_{out} = \left(\frac{I_{out}^2 * R_{esr}}{2}\right) \tag{3.28}$$

b) Inductor loss

The inductor power loss is defined as:

$$P_{Ind} = P_{core} + P_{DCR} \tag{3.29}$$

Core loss, P_{core} is often provided directly from manufacturers. But there exists the formula that can be used to calculate the core loss for a ferrite core:

$$P_{core(mW)} = K_1 * f^x * B^y * V_e \tag{3.30}$$

where:

K_1= Constant for core material,

f = Frequency in kHz,

B =Peak flux density in kGauss,

x = Frequency exponent,

y = Flux density exponent,

V_e=Effective core volume (cm^3);

By entering the K_1 coefficient, the frequency and flux density exponents, which are unique to each core material, the core loss can be calculated.

Meanwhile, the wire loss caused by DC resistance is defined by:

$$P_{DCR(W)} = I_{rms}^2 * DCR \tag{3.31}$$

where:

I_{rms} is the rms value of the peak current applied to the inductor and DCR is the dc resistance of the inductor. The inductor loss is assumed to be 0.5 % of the output power (Sekiya, 2011).

c) Diode loss

There are two losses can be calculated at the diode, there are diode conduction loss and switching loss. The diode conduction loss can be described as:

$$P_{D(cond)} = V_D * I_D \tag{3.32}$$

where:

V_D is the forward voltage across the diode and I_D is the current flow through the diode. The diode switching loss however, calculated by:

$$P_{D(sw)} = f_{sw} * (V_{cf} + V_{out}) * Q_{rr} \tag{3.33}$$

where:

f_{sw} is the switching frequency, V_{cf} is the voltage across the diode when it is turned off, and Q_{rr} is the diode reverse recovery charge.

d) MOSFET loss

The MOSFET, which in particular also a semiconductor device as similar to the diode, also has two types of losses which are the conduction loss and switching loss. The MOSFET conduction loss is given by:

$$P_{Q1} = I_{on(rms)}^2 * R_{dson} \tag{3.34}$$

where:

I_{on} is the drain current when the MOSFET is on, and R_{DSon} is the drain-source resistance of the MOSFET.

The MOSFET switching loss then can be separated to two losses, switch on loss and switch off loss. The two switching losses then calculated as:

$$P_{Q1(sw_{on})} = \left(\frac{f_{sw} * V_{dsoff} * I_{on(rms)} * T_{on}}{2}\right) \tag{3.35}$$

$$P_{Q1(sw_{off})} = \left(\frac{f_{sw} * V_{dsoff} * I_{on(rms)} * T_{off}}{2}\right) \tag{3.36}$$

Hence, the total switching loss can be described as:

$$P_{Q1(sw)} = P_{Q1(sw_{on})} + P_{Q1(sw_{off})} \tag{3.37}$$

where:

V_{dsoff} is the drain-to-source voltage when the MOSFET is off, T_{on} is the time to turn the MOSFET on, and T_{off} is the time to turn the MOSFET off.

Figure 3.11 shows the connection between SEPIC and the Tektronix TPS 2024B oscilloscope for loss measurements. The clearer figure on the probe connection is illustrated in Figure 3.12 for MOSFET loss measurement and Figure 3.13 for diode loss measurement.

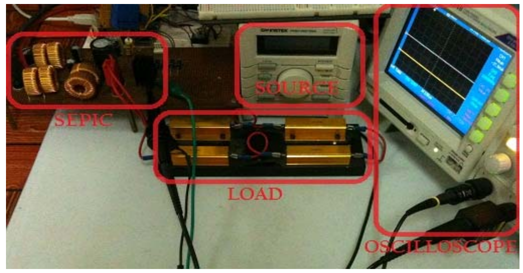

Figure 3.11: The experimental setup

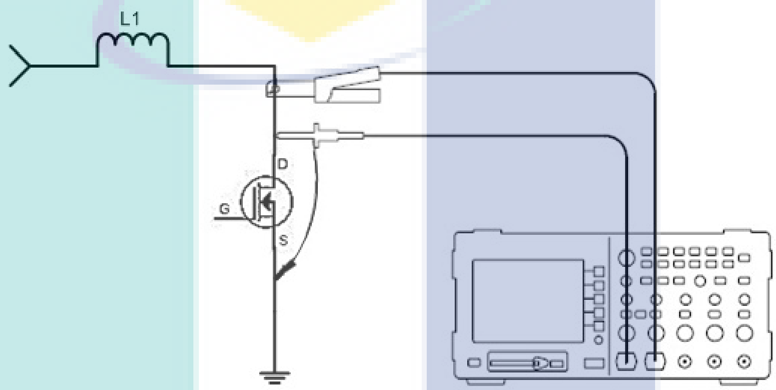

Figure 3.12:MOSFET losses measurement connection in the SEPIC circuit

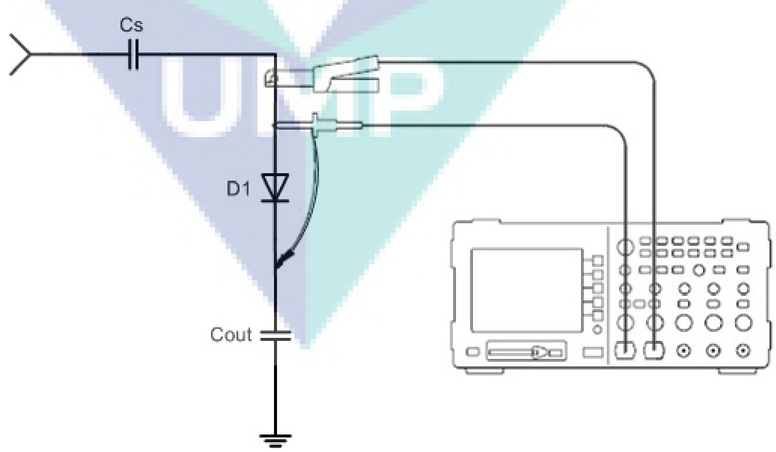

Figure 3.13: Diode losses measurement connection in the SEPIC circuit

3.5 SUMMARY

This chapter has briefly explained about the methodology used in the project started with the solar irradiance data collection in Universiti Malaysia Pahang, Pekan Campus and its implementation in MATLAB. Then, the modeling of PV module in MATLAB based on the manufacturer's datasheet and the equation from solar cell equivalent electrical circuit. This simulation is purposely to acquire data from the selected module that using P&O algorithms as a controller. The temperature is set fixed at nominal 25 ^{o}C where only the irradiation changing. The next sub-chapter explained on the circuit setup in PSIM simulation tools which started from the solar module (physical model) setup, to SEPIC design based on the SEPIC components sizing calculation. In this simulation, the charge controller is tested using two types of input, which are constant and varied. This purpose is to test the performance of the charge controller under rapid changing of solar irradiation. Lastly, the type of losses that occurred in SEPIC for the efficiency analysis experiment has been presented.

CHAPTER 4

RESULTS AND DISCUSSIONS

4.1 INTRODUCTION

Simulations and experiments results are presented and discussed in this chapter. The outcome of each simulation (MATLAB & PSIM) along with the experiment is observed and analyzed. The result will discuss on the solar irradiation at the selected area (Universiti Malaysia Pahang, Pekan campus), the *I-V* and *P-V* curve of the modeled module to the effect of varying densities of solar irradiation and temperature.

In the power section, the PSIM simulation shows various results from open loop and close loop circuit to discuss about. The experimental results will be discussed around the losses occurred (which in particular focused on the two switching devices, MOSFET and Diode) and also the overall efficiency.

4.2 MATLAB PV MODELING SIMULATION

4.2.1 Real Solar Irradiation Data Collection

The first result obtains are the data collection on the solar irradiance on the particular day selected as in sub-section 3.2. The data showed the two most contrary weather conditions along the selection period. The cloudiest day selected fall on 28 December 2011 and the sunniest day fall on 19 March 2012. The data plotted using the script as in APPENDIX A came out with the result as in Figure 4.1 on the sunniest day and Figure 4.2 on the cloudiest day.

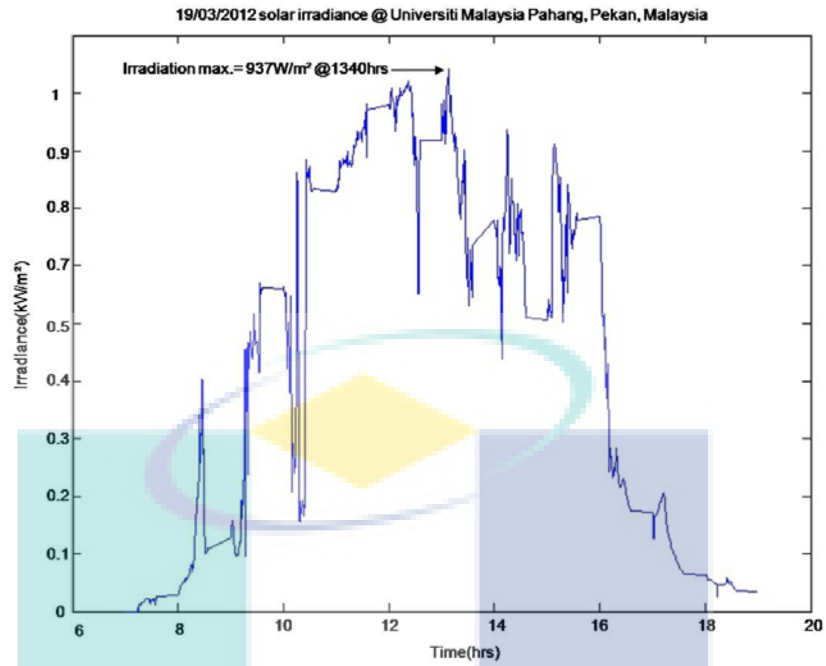

Figure 4.1: Solar irradiance during sunniest day on 19 March 2012 at Universiti Malaysia Pahang, Pekan Campus

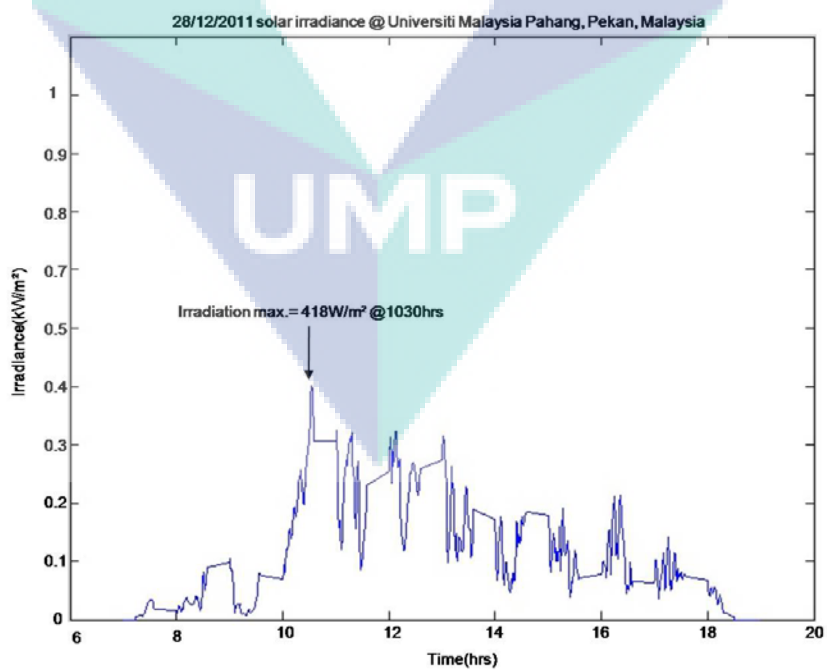

Figure 4.2: Solar irradiance during cloudiest day on 28 December 2011 at Universiti Malaysia Pahang, Pekan Campus

The findings of the simulations is obvious that there were differing on the maximum irradiance between the two conditions. Figure 4.1 shows that the maximum irradiance on the sunniest day was 937 W/m² at 1340 hours, whereas on the cloudiest day, it was 418 W/m² at 1030 hours as shown in Figure 4.2. The result shows that the discrepancy of maximum output power between the two weather conditions is about 44.6 %. It is apparent from these figures that the PV output power should drop around the discrepancy percentage during cloudy days or more precisely, during the monsoon season.

4.2.2 Modeling of PV Module in MATLAB

The following simulation results show the PV-TE125MF5N module *I-V* and *P-V* curves with the variations of temperature and solar irradiation that modeled in MATLAB. There are four different characteristics that represent each variation of temperature and five different characteristics that represent the variation of solar irradiation.

Figure 4.3 shows the variations of temperature clearly affected the *I-V* characteristics of the module. The simulation indicates that the hotter the temperature, the lesser the voltage produced by the module. As shown in Figure 4.3, the percentage of voltage that varied every 25 ^{o}C of temperature is about 8.3 %. On the other hand, the module current slightly increase as the temperature rising. It can be seen that the current varied about 1.3% on each 25 ^{o}C of temperature variation.

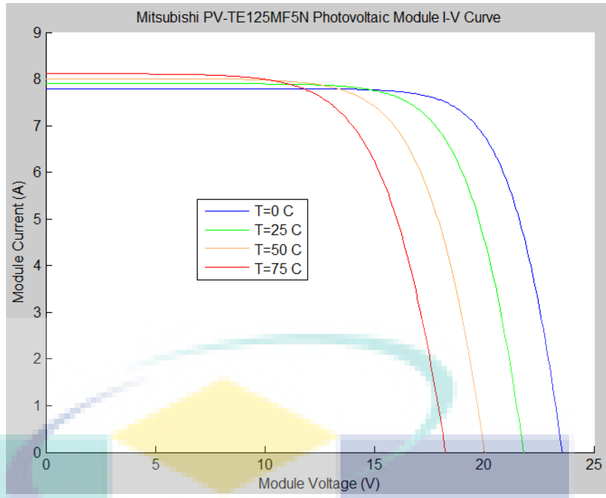

Figure 4.3: *I-V* characteristics of PV module with variations of temperature

Contrary to the result in Figure 4.3, the variations of solar irradiation have a big impact on the PV current as illustrated in Figure 4.4. It is further observed that the current increase with the increasing of solar intensity, thereby increasing the power output of the solar cell. Another observation shows that at every 200 W/m^2 variation of the intensity, the module current varies about 20.2 %, but at the same time the module voltage varies in non constant rate. Figure 4.4 illustrates that at 200 W/m^2, the PV module voltage ideally produced of 19 V compares to the highest intensity at 21.8 V.

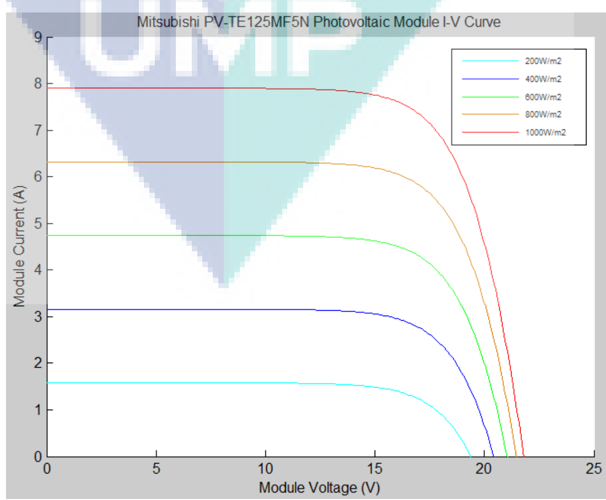

Figure 4.4: *I-V* characteristics of PV module with variations of solar irradiation

The PV module *P-V* curve shows that the module performs better at lower temperature. Furthermore, it can achieve maximum power that is above its nominal power rating as seen in Figure 4.5. The voltage varies constantly at 8.3 % every 25 ^{o}C of temperature variations. Interestingly, this shows that PV module works better in cooler climates with higher solar intensity.

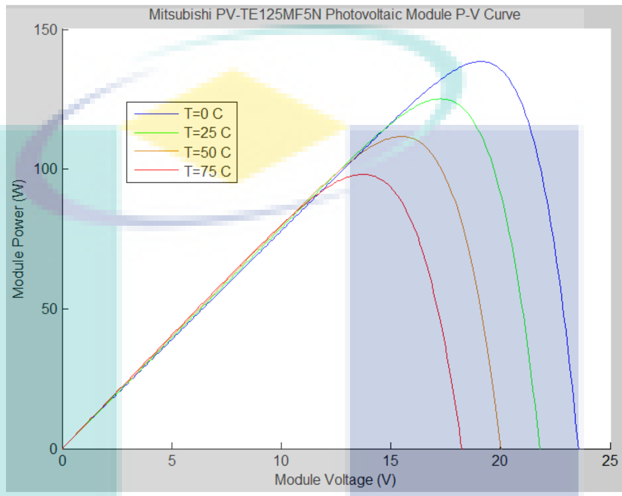

Figure 4.5: *P-V* characteristics of PV module with variations of temperature

Meanwhile, the variations of solar irradiation play a vital role in the module overall performance as seen in Figure 4.6. The result shows that as the intensity decreased, the module output power decreased at a rate of 20 % every 200 W/m^2 of intensity variation.

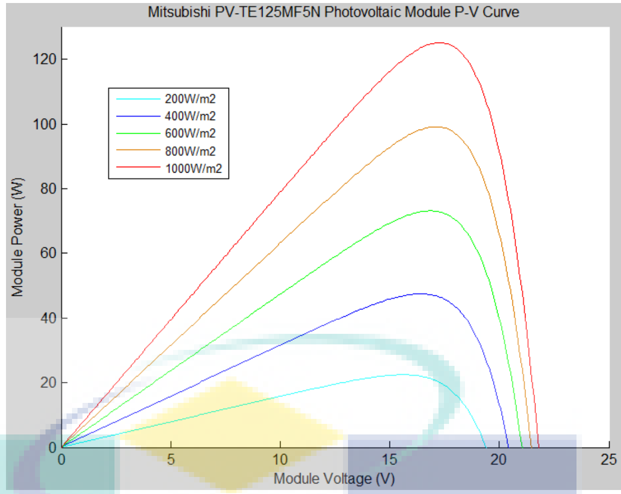

Figure 4.6: *P-V* characteristics of PV module with variations of solar irradiation

4.2.3 P&O MPPT Simulation in MATLAB Based on PV Module Characteristics and Solar Irradiation Data Collection

The MPP location in the *I–V* plane is not known precisely and always changes depending on the solar irradiance and temperature. Therefore, it needs to be located. The MPP can be located by a tracking algorithm. The following simulation results show the module performance on the two days selected by using the P&O tracking algorithm. During the cloudy day, the irradiance level changes rapidly because of passing clouds and it will affect the performance of MPP tracking. Figure 4.7 shows the trace of PV operating points in green point while the red star point represents an MPP at each *P-V* curve. It is apparent in Figure 4.7 that the tracking points are farther the MPP at some point due to the rapidly changing of irradiance level. Further observed on the cloudy day simulation shows that the module can produce a power of 45.4 W at maximum. This value represents only 36.3 % of the module maximum power rating as tabulated in Table 4.1.

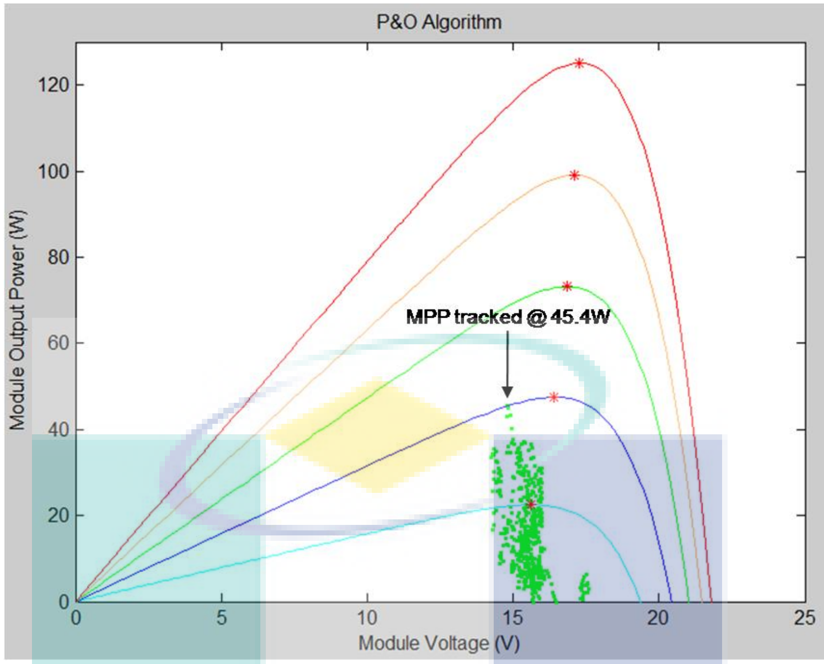

Figure 4.7: P&O MPP tracking on 28 December 2011 at Universiti Malaysia Pahang, Pekan Campus using PV- TE125MF5N module

Meanwhile, on the sunniest day, the result seems more impressive because of more constant irradiation without irradiance level that change too gradually since there is less cloud influence. It is obvious that the MPP tracking performance is better than on the cloudiest day as shown in Figure 4.8 where, the trace of a PV operating point is more concentrated around the MPP without too much deviation. Without doubt, the tracking algorithm works better above 400 W/m^2 intensity of solar irradiance. It is relatively clear that during this condition, the module produced the output power of 117.6 W using P&O MPPT algorithm which is 94 % of its maximum power rating of 125 W as tabulated in Table 4.3.

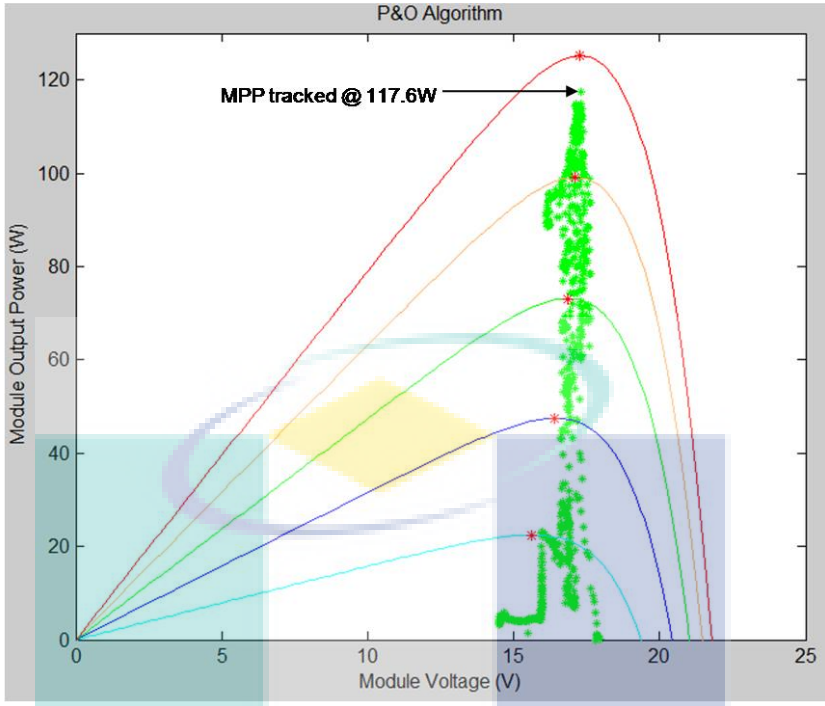

Figure 4.8: P&O MPP tracking on 19 March 2012 at Universiti Malaysia Pahang, Pekan Campus using PV- TE125MF5N module.

Table 4.1: MITSUBISHI PV-TE125MF5N module output power during cloudiest day

Parameter	PV-TE125MF5N module		
	$P_{max(nominal)}$	P_{mpp} (P&O)	Percentage
Cloudiest day, 28 December 2011	125 W	45.4 W	36.3 %

Table 4.2: MITSUBISHI PV-TE125MF5N module output power during sunniest day

Parameter	PV-TE125MF5N module		
	$P_{max(nominal)}$	P_{mpp} (P&O)	Percentage
Sunniest day, 19 March 2012	125 W	117.6 W	94 %

4.3 PSIM CONVERTER CIRCUIT SIMULATION

The PSIM simulation result provides the PV output power at close-loop circuit condition under constant and rapidly changing solar irradiation. Since the goal of open loop simulation is only for proper component sizing guidance, the open loop result is not discussed here. Due to its ideal component characteristic, the open loop SEPIC simulation is a lossless converter with 100 % efficiency.

4.3.1 SEPIC Close-loop Simulation under Constant Solar Irradiation

The first three data, simulate the circuit where the intensity of solar irradiation is set at 200 W/m^2, 600 W/m^2 and 1000 W/m^2 respectively. By referring to Figure 4.9, at the intensity equal to 200 W/m^2, the output power is certainly weaker than the PV input power. While the input power, P_{in} is equal to19.6 W, the output power, P_{out} is equal to18.8 W which is about 96 % of the maximum power that it could achieve as tabulated in Table 4.3.

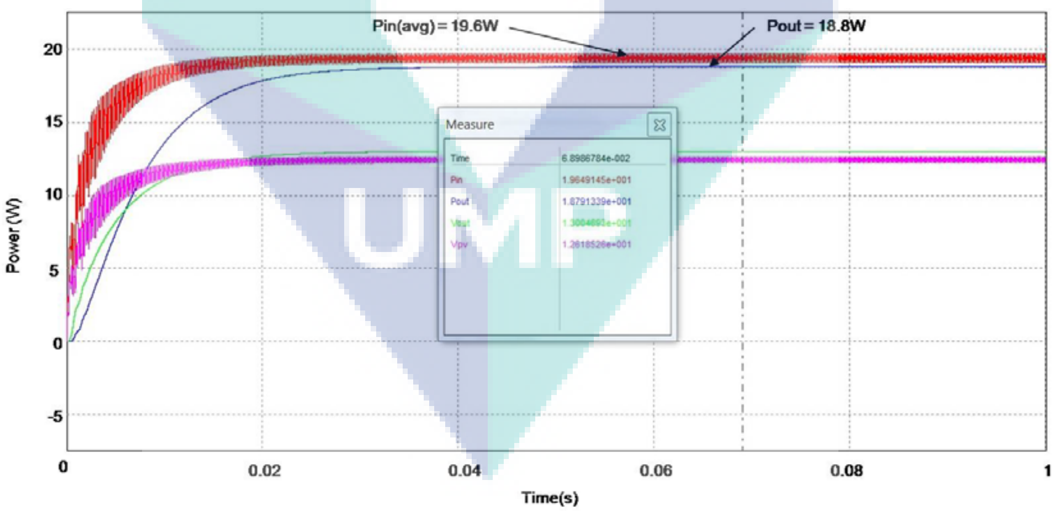

Figure 4.9: Power and voltage at 200 W/m^2 irradiation

As illustrated in Figure 4.10, the maximum power that the PV module can achieve at intensity equal to 600 W/m^2 is 72.4 W. By then, the maximum power that draws from the circuit is as high as 71.5W which gives about 98.8 % of maximum power it could achieve which also been tabulated in Table 4.3. Figure 4.11 shows that at the maximum intensity of 1000 W/m^2, the simulated module achieved as high power as it can produce according to its manufacturer's datasheet which is 125 W. The simulated output power, P_{out} however, produced an output power of around 123.4 W which have a discrepancy of 1.3 % of the maximum power as tabulated in Table 4.3. At this point, it is obvious that the close loop circuit gives an average efficiency of 98 % where it undeniably shows a good tracking capability under constant solar irradiation.

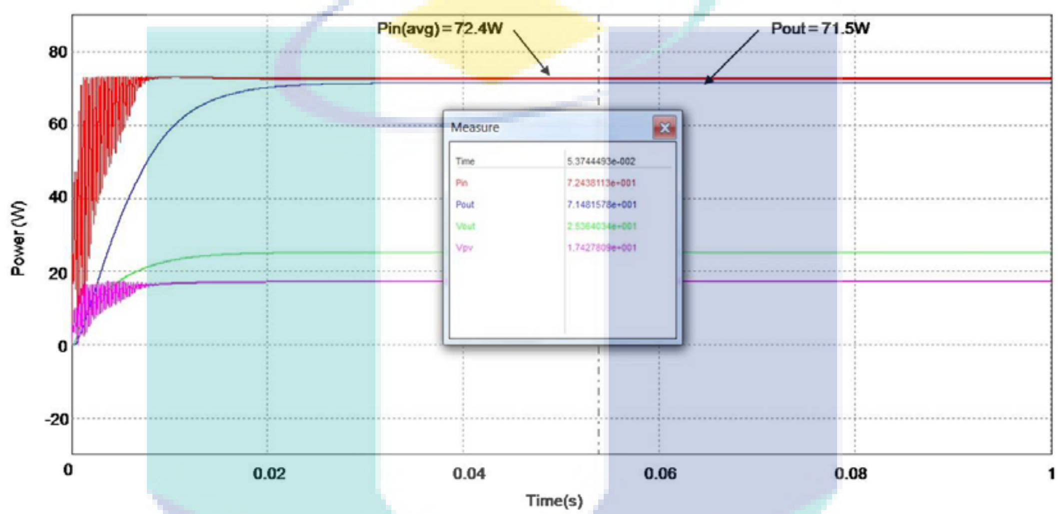

Figure 4.10: Power and voltage at 600 W/m^2 irradiation

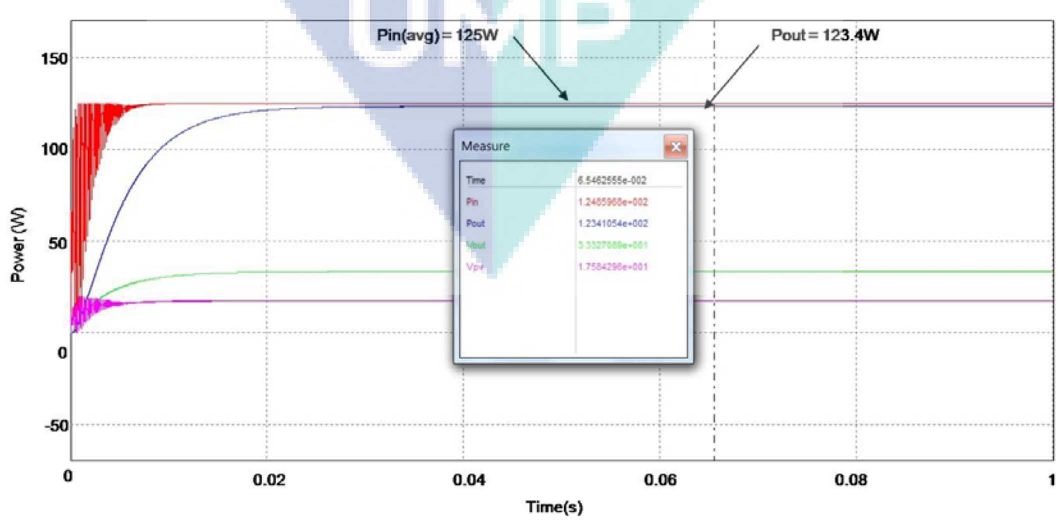

Figure 4.11: Power and voltage at 1000 W/m^2 irradiation

Table 4.3: PV-TE125MF5N module output power on three different constant solar irradiation

Solar Irradiance	PV-TE125MF5N		
	P_{in}	P_{out}	Discrepency
200 W/m^2	19.6 W	18.8 W	4 %
600 W/m^2	72.4 W	71.5 W	6 %
1000 W/m^2	125 W	123.4 W	1.3 %

4.3.2 SEPIC Close-loop Simulation under Varying Solar Irradiation

Under varying solar irradiation, this simulation used the square and triangle signal as an input. This is to show the tracking capability of the P&O algorithm under rapidly changing irradiation condition by using two different sampling frequencies; 10 Hz and 50 Hz.

At 10 Hz sampling rate, it is obvious that the P&O MPP is lagging about 4ms from the input and unable to track to the maximum power. Figure 4.12 illustrates that the tracker could only achieve a maximum power of only 117 W which gives the efficiency of 93.6 %.

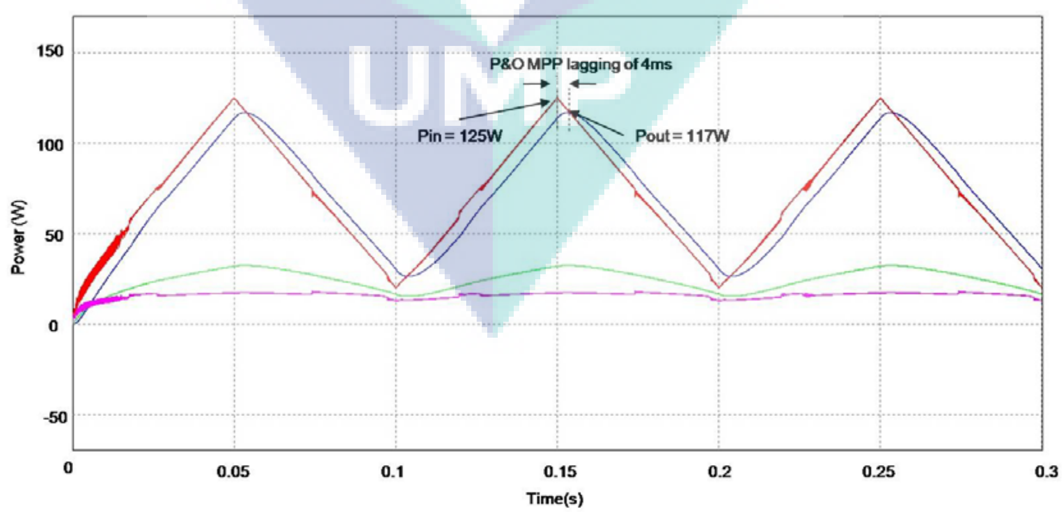

Figure 4.12: Output power at 10 Hz sampling rate using a triangle input signal

While at 50 Hz sampling rate as in Figure 4.13, the tracker is certainly unable to track at rapidly changing solar irradiation where further observation confirmed that the tracker is only able to track until 94.8 W before changing its tracking path. Another interesting finding is that the tracker definitely needed a time to stabilize before the changing of solar irradiation as shown in Figure 4.14.

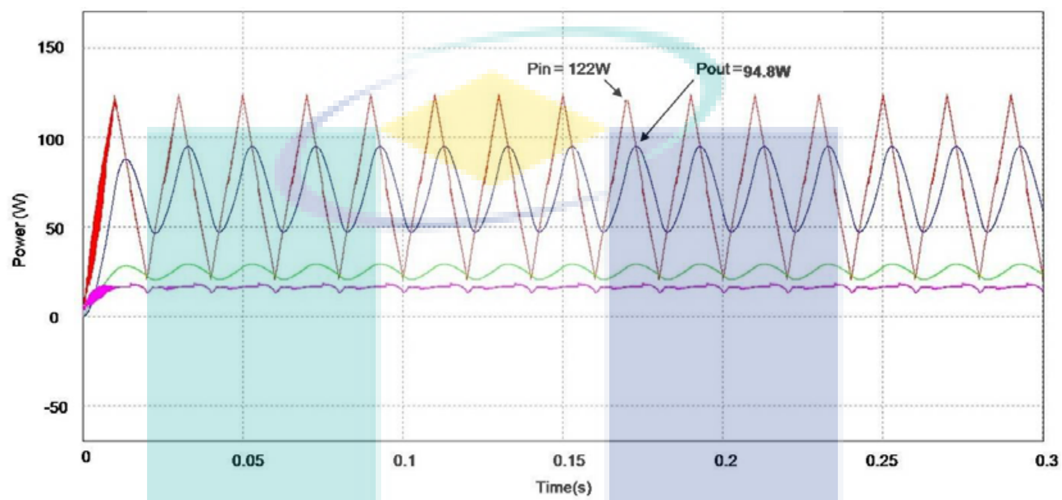

Figure 4.13: Output power at 50 Hz sampling rate using a triangle input signal

As Figure 4.14 illustrates, the tracker undoubtedly needs at least 32 ms in order to track to the MPP with the solar irradiation changing from 200 W/m^2 to 1000 W/m^2. The simulation proves that any fast changing in solar irradiation under 32 ms will affect the capability of the tracker.

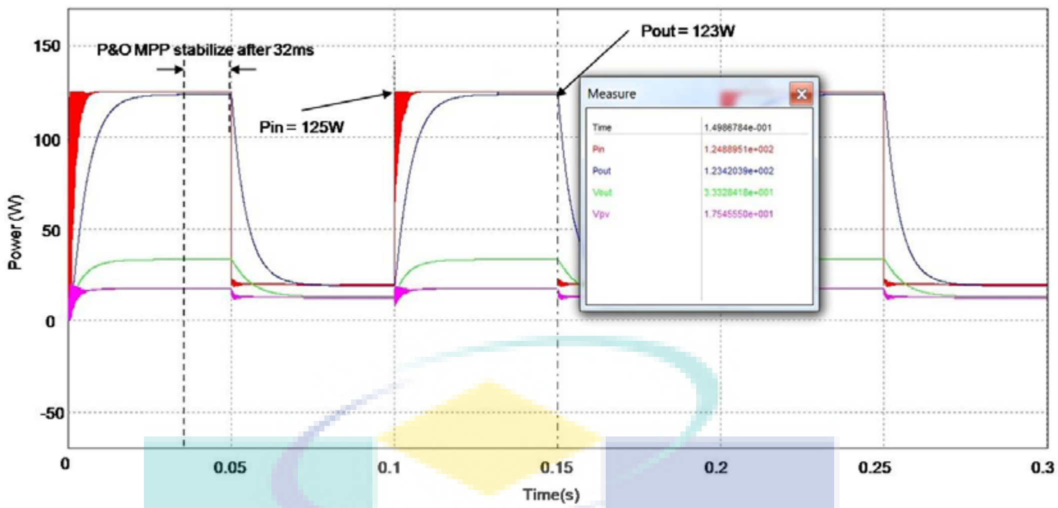

Figure 4.14: Output power at 10 Hz sampling rate using a square input signal

Prior to the previous findings, Figure 4.15 clearly shows that the tracker is not able to track the MPP over 30 Hz of irradiation changing frequency. It is apparent that at 50 Hz sampling rate frequency using a square wave input signal, at every 20 ms of the solar irradiation changing from 200 W/m^2 to 1000 W/m^2, it can track up to 111 W at maximum before decreasing. The results of this simulation clearly show that the P&O algorithm works fine under constant solar irradiation, but unable to track an MPP under rapidly changing solar irradiation below than 32 ms. All the simulation results then summarized in Table 4.4.

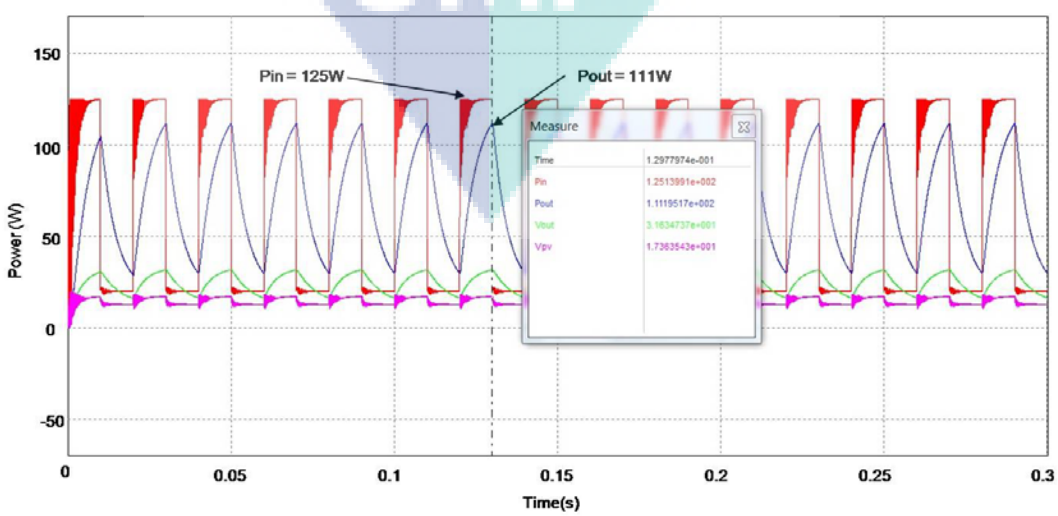

Figure 4.15: Output power at 50 Hz sampling rate using a square input signal

Table 4.4: PV-TE125MF5N module output power on two different input irradiation and different frequency

PV-TE125MF5N				
Input signal	**Frequency**	**P_{in}**	**P_{out}**	**Efficiency**
Triangle	10 Hz	125 W	117 W	93.6 %
Triangle	50 Hz	125 W	94.8 W	75.8 %
Square	10 Hz	125 W	123 W	98.4 %
Square	50 Hz	125 W	111 W	88.8 %

4.4 SEPIC HARDWARE ANALYSIS

The hardware analysis consists of the measurement and calculation of losses and efficiency. The loss analysis focused on the two switching components in the circuit which are MOSFET and diode. These two components contribute to the major losses in the circuit. The experiment is carried out using the parameters mentioned in sub-section 3.4 and divided into four groups of measurements and calculations.

4.4.1 Diode loss measurement and calculation

The diode loss measurement is taken in two different frequencies for analysis. The switching frequency, f_{sw} is set at 7.8 kHz and 62.3 kHz. The total diode loss consists of diode conduction loss and diode switching loss. The measurement losses then compared to the calculation losses for both conduction and switching loss. The diode conduction loss and the diode switching loss calculation were as in Equation (3.32) and Equation (3.33) respectively.

As Figure 4.16 illustrates, the circuit has a huge diode conduction loss at f_{sw} = 7.8 kHz. However, on the observation at f_{sw} = 62.3 kHz shows that the diode conduction loss was not even exceed 1W. Further analysis shows the discrepancy between the two frequencies is from as low as 1.7W at the lowest duty cycle to as high as 9.7 W at the highest duty cycle while the discrepancy between the two methods are very marginal with 0.08 W at lower frequency and 0.03 W at higher frequency. These results are undeniable as the diode current at f_{sw} = 7.8 kHz is higher than at f_{sw}= 62.3 kHz.

Obviously, in accordance with the Equation (3.32), it is expected that the value of the frequency doesn't have much influence in diode conduction loss calculation and measurement.

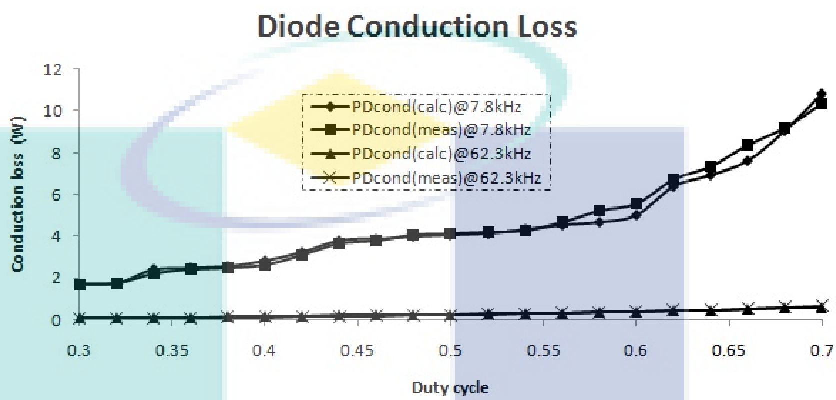

Figure 4.16: Diode conduction loss

What is to be an unlikely figure in Figure 4.17 is that there are more losses at f_{sw}= 7.8 kHz. Presumably, the switching loss is having frequency as one of its calculation parameters, but the output voltage, V_{out} and the voltage across the diode when it is turned off, V_{cf} play a huge part in the diode switching loss determination. It is however clear that there are no significant differences of the average loss between the two frequencies which is only 0.55 W. Further analysis shows the discrepancy between the two measurements at both frequencies is 0.02 W and 0.04 W respectively. It is proven that the diode loss is inversely proportional to the switching frequency.

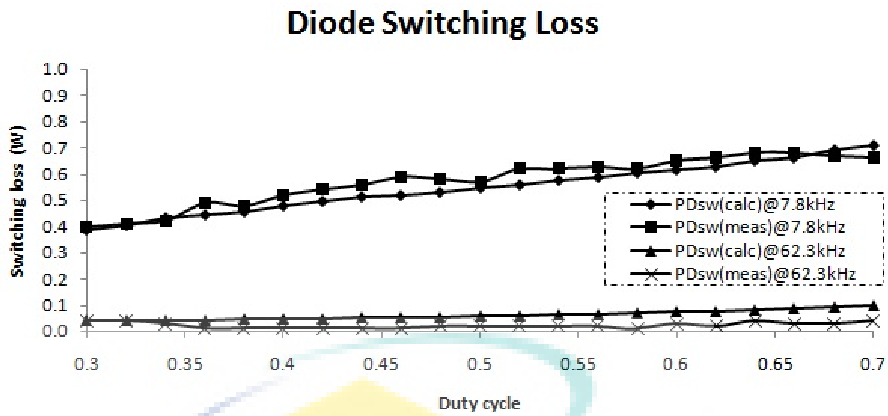

Figure 4.17: Diode switching loss

4.4.2 MOSFET loss measurement and calculation

The MOSFET loss measurement parameter is to measure the voltage drain-to-source, V_{DS}, the drain current, I_D; while the turn-on, T_{on} and turn-off, T_{off} time of the MOSFET measurement data will be used as the calculation parameters as in Equation (3.34), Equation (3.35) and Equation (3.36). The voltage drain-to-source, V_{DS} and the drain current, I_D were used to measure the MOSFET conduction and switching losses. The rated $R_{DS(on)}$ for MOSFET IRF540N is 44 mΩ maximum which varies depending on the value of V_{GS}. The MOSFET conduction loss data is calculated by assuming the $R_{DS(on)}$ value are the same at all duty cycle. As written in (PowerSemiconductorDevice, 2011), MOSFET has a relatively higher conduction loss and lower switching loss compare to Bipolar Junction Transistor, BJT. At lower frequency, the MOSFET tend to have more losses on conduction compare at the higher frequency.

Figure 4.18 illustrates the MOSFET conduction loss on two different frequency setting and two different type of measurement. From the observation, at f_{sw}= 62.3 kHz, the conduction loss between the two measurements are obviously looking similar. It is somewhat not necessarily having a big margin between the two methods that happened at f_{sw} = 7.8 kHz. It is inevitable due to the higher amount of the drain current, I_D at this frequency and the value of the $R_{DS(on)}$ decreasing which contribute to higher loss value. On top of that, it is apparent that the value of $R_{DS(on)}$ is varying in the measurement method compared to the calculation which the $R_{DS(on)}$ value is constant at all duty cycle calculation. It is concluded that the average discrepancy between the two methods is 0.86 W at lower frequency and 0.35 W at higher frequency. The results bring altogether that the average loss margin between the two frequencies is 1.56 W.

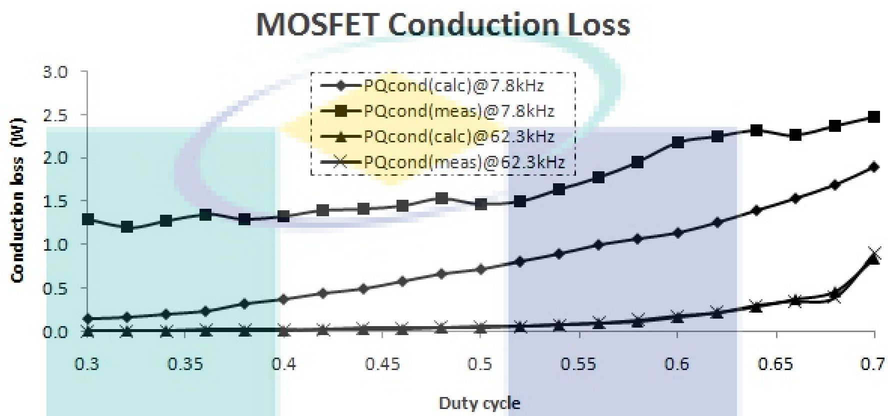

Figure 4.18: MOSFET conduction loss

In contrary to its conduction loss, the MOSFET switching loss shows that there are more losses at higher frequency, but only happens after 0.52 duty cycle as in Figure 4.19. Starting from this point, the loss increase significantly from 2.16 W to 10.5 W with an average of 0.82 W increment per 0.02 duty cycle step. The experiment definitely shows that the MOSFET gate are allowing the possibly high amount of current to flow through its channel at the stated duty cycle. With the addition of the frequency value that relatively higher than the other one, it is expected to have a result as illustrated in Figure 4.19**:** MOSFET switching loss. The findings from the experiment gives that the average discrepancy between the two methods are 0.86 W or 31 % at f_{sw} = 7.8 kHz and 0.35 W or 12.5 % at f_{sw} = 62.3 kHz. Although the losses is higher than at f_{sw} = 62.3 kHz, the discrepancy between the two methods is lower. This finding somehow is probably to be contrary to the article published in (PowerSemiconductorDevice, 2011) on the MOSFET loss characteristics compared to BJT. The least from this experiment somehow clearly proves that the MOSFET conduction loss is inversely proportional to swiching frequency.

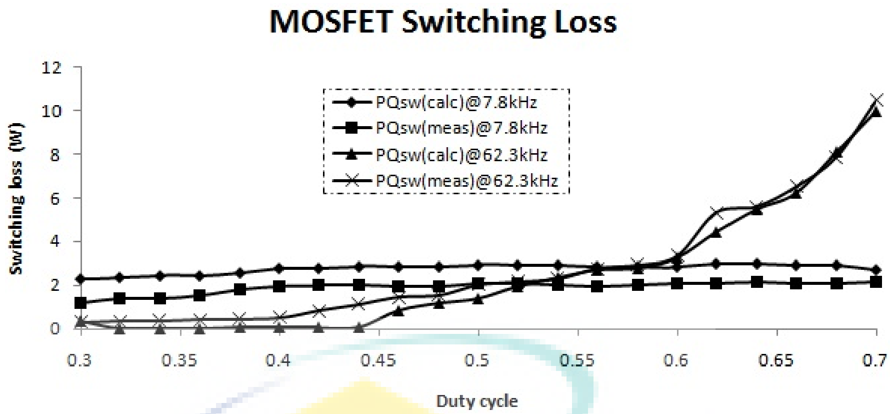

Figure 4.19: MOSFET switching loss

4.4.3 Circuit efficiency calculation

The circuit efficiency calculation is based on the circuit input and output power. The measured input and output power for f_{sw} = 7.8 kHz and 62.3 kHz are shown in Figure 4.20 and Figure 4.21 respectively.

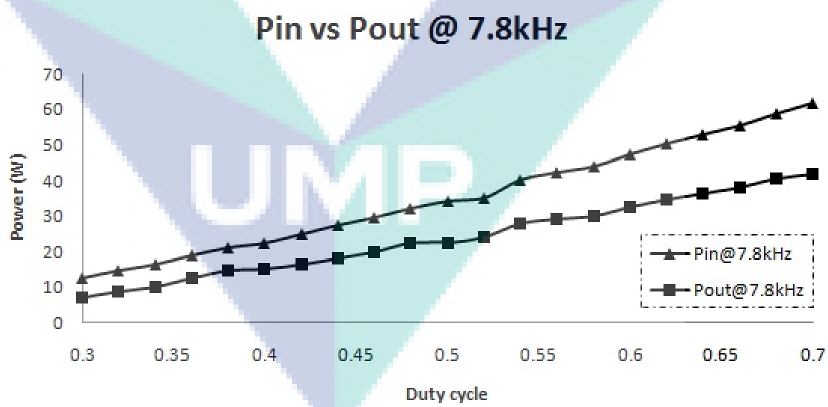

Figure 4.20: Power to power comparison at 7.8 kHz

The input power and output power graph at f_{sw} = 7.8 kHz is obviously proportional to the duty cycle. As the duty cycle value increasing, the gap between the two lines also increases. It is in fact that current value increasing as the duty cycle increase. The smallest loss was 5.51 W at the lowest duty cycle and the biggest loss was

20 W at the highest duty cycle, which is definitely contributed by the diode conduction losses. The observation in Figure 4.21 shows that the output power looks as similar to the input power. Referring to a lower frequency result, there is no doubt that the gap increase as the duty cycle increases, but not as linear as in the previous result. Further analysis on the result shows the variation looks more exponential with the lowest loss was 0.5 W at the lowest duty cycle and the highest loss was 15 W at the highest duty cycle which is undoubtedly contributing by the MOSFET switching losses.

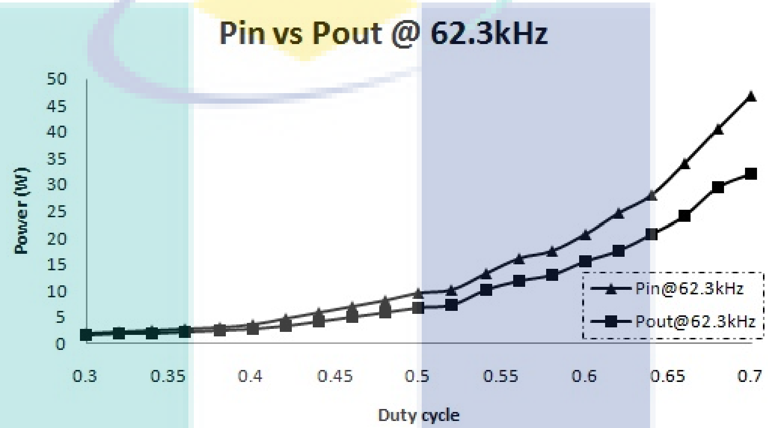

Figure 4.21: Power to power comparison at 62.3 kHz

It is conclusive that the circuit has a greater output power at f_{sw} = 7.8 kHz compared to the one at f_{sw} = 62.3 kHz as illustrated in Figure 4.22 and Figure 4.23. It is however admitted that the loss at f_{sw} = 7.8 kHz is greater which contribute to the low efficiency of the circuit as shown in the efficiency graph in Figure 4.24. The average losses caused by the diode and the MOSFET at f_{sw} = 7.8 kHz of this circuit is 8.82 W or 77.3 % of the average total circuit loss which is 11.41 W. Meanwhile, Figure 4.23 illustrates the average losses caused by the diode and the MOSFET at f_{sw} = 62.3 kHz for this circuit is 3.23 W compared to the average total circuit loss which is 4.04 W which is nearly 80 % of the total circuit loss. The experiment, without question, produced an expected result where the two switching elements contribute to a major loss of overall circuit losses. It is somehow unlikely that the amount of losses at f_{sw} = 7.8 kHz are more than the losses at f_{sw} = 62.3 kHz.

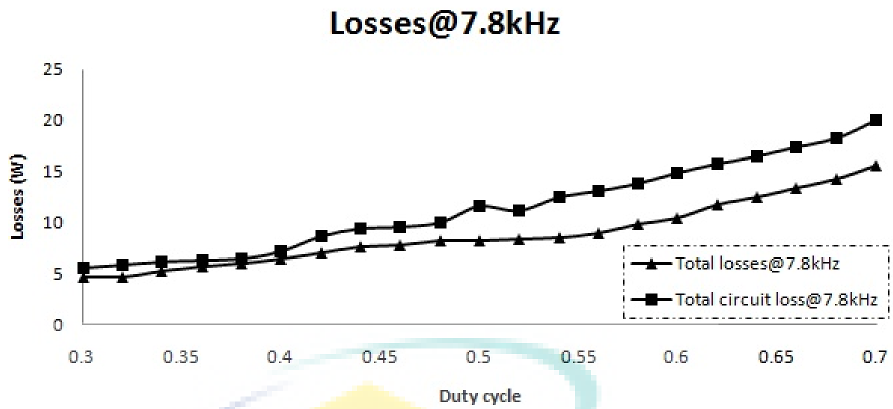

Figure 4.22: Total losses at frequency = 7.8 kHz

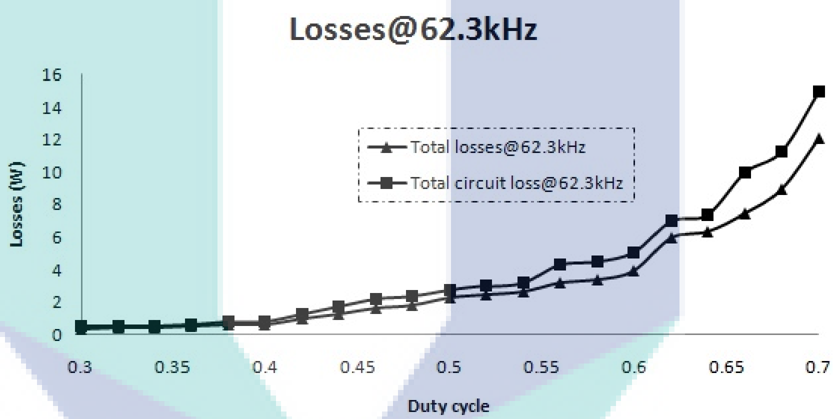

Figure 4.23: Total losses at frequency = 62.3 kHz

It is however definitely that the reason why there are more losses at lower frequency and vice-versa had previously proved and discussed in sub-section 4.4.1 and 4.4.2. Prior to the amount of losses, the circuit have an average efficiency of 66.9 % at f_{sw} = 7.8 kHz and 73.3 % at f_{sw} = 62.3 kHz as illustrated in Figure 4.24.

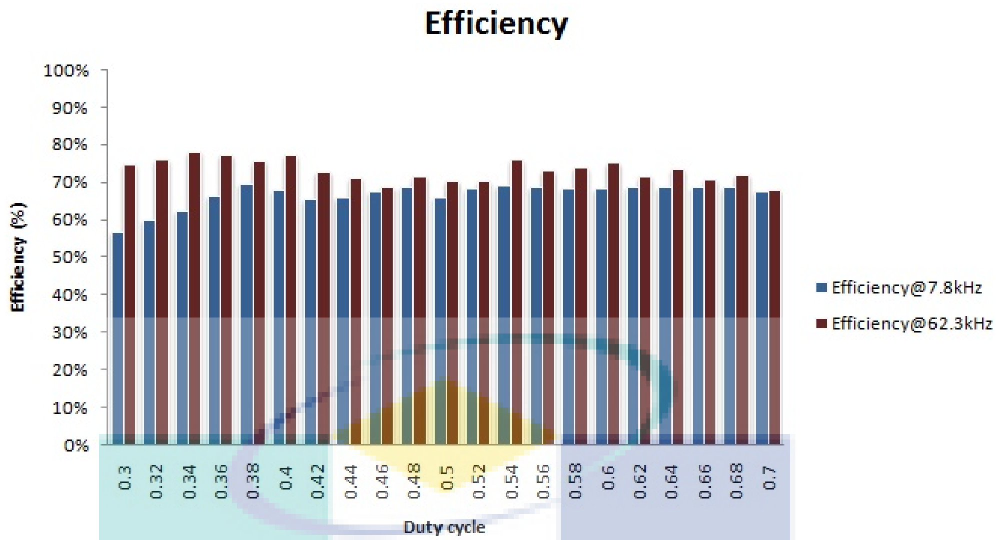

Figure 4.24: Circuit efficiency

The overall results of the experiment are presented in Figure 4.25 and Figure 4.26 respectively for both frequencies tested. As discussed earlier, the diode loss dominated the total losses at f_{sw}= 7.8 kHz. In contrary, it is clear that the diode loss is just a small amount of losses at f_{sw}= 62.3 kHz, which is dominated by the MOSFET loss.

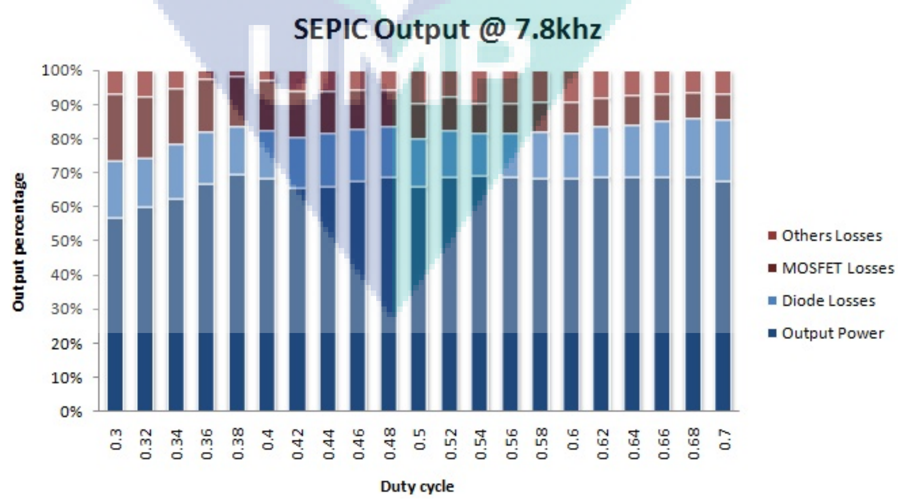

Figure 4.25: SEPIC loss distribution chart with output power at frequency = 7.8 kHz

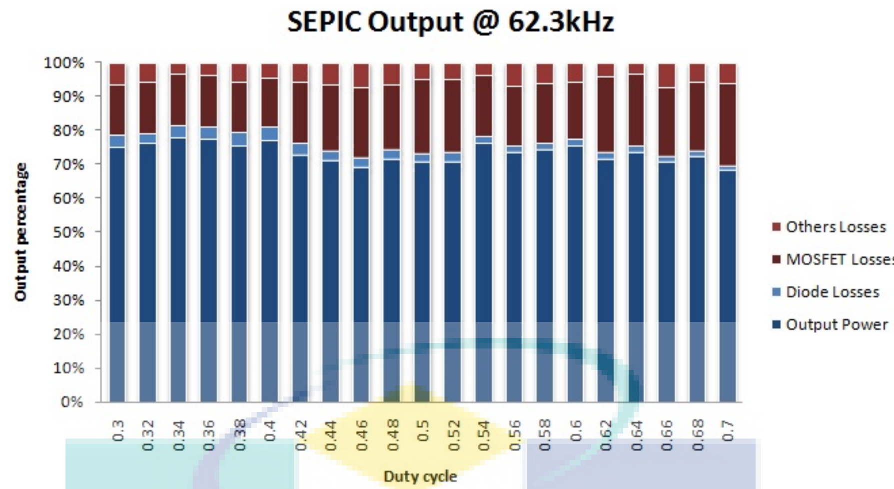

Figure 4.26: SEPIC losses distribution chart with output power at frequency = 62.3 kHz

4.5 SUMMARY

This chapter has shown and interpreted results of various types of experiment. There are three main discussions involved from the results obtained which are from the MATLAB PV modeling simulation, PSIM converter circuit simulation and SEPIC hardware analysis. Under the MATLAB simulation, it is certain that the MPPT P&O algorithm works fine during sunny days. The algorithm creates an oscillation around the MPP during cloudy days. This is proved during the PSIM converter simulation that by using this algorithm, the tracker unable to cope with the rapidly changing irradiation as it needs at least 32ms in order for the algorithm to track the MPP. The PSIM simulation is intended to show the different outcome of the converter by applying a constant solar irradiation and varied solar irradiation as a source of input. The third main discussion is all about the efficiency and performance of the converter. This is to determine the typical major loss factor for a converter which are switching losses and conduction losses. The losses measuring point are without question around the switching components in the circuit which are diode and MOSFET. The overall diode loss and MOSFET conduction loss are proven to be inversely proportional to the switching frequency. From the point of circuit efficiency calculation, it is without doubt that the two switching elements contribute to a major loss of overall circuit losses.

CHAPTER 5

CONCLUSIONS AND RECOMMENDATIONS

5.1 CONCLUSIONS

This study presents a simple Solar Charge Controller. The charge controller consists of two parts; controller and power. To conclude this study up, it is good to know whether the objectives of the study are successfully fulfilled or otherwise. The first objective is to develop a model of PV module in computer simulation based on varying solar irradiation at a specific geographical location. This objective is achieved as the PV module is developed using MATLAB and has been simulated by using a real time data that logged from Universiti Malaysia Pahang, Pekan weather station. From the simulation, it is obvious that the MPP tracking performance is better during sunny days and without doubt, the tracking algorithm works better above 400 W/m^2 intensity of solar irradiance.

The second objective is to realize a charge controller in computer simulation; consists of PV modules, DC/DC converter and control system. This objective also successfully achieved by realizing the charge controller and simulate it by using PSIM software. The set up of this part is described in sub-chapter 3.3.1 and 3.3.2. The simulation result concludes and proven that the P&O algorithm works fine under constant solar irradiation, but unable to track an MPP under rapidly changing solar irradiation below than 32 ms.

The last objective is to analyze the efficiency and the losses of a DC/DC converter via practical experiment where the circuit is analyzed through two different methods. One is using the calculation method as can be found in sub-chapter 3.4.1

while the other one is by measurement. This objective has been achieved by providing the circuit loss measurement and calculation results and also the circuit efficiency calculation. Under the loss measurement and calculation, it is proven that overall diode loss and MOSFET conduction loss is inversely proportional to the switching frequency based on the output illustrated in the Figure 4.16, Figure 4.17, Figure 4.18 and Figure 4.19. For the circuit efficiency calculation, it is without doubt that the two switching elements contribute to a major loss of overall circuit losses as illustrates in Figure 4.24. The experimental circuit works below par as its average efficiency is only 66.9 % and 77.3 % of the two frequencies tested. The two switching devices; MOSFET and diode, in total contribute to 77 % and 80 % of losses at both frequencies respectively. The experiment definitely shows that the conduction loss contributes much of the losses to the circuit compared to the switching loss even at higher frequency.

5.2 STATEMENT OF CONTRIBUTION

The main contribution of the study is the working model of a new solar charge controller, developed using P&O MPPT algorithm on SEPIC DC/DC converter. The system has been tested on real world data in computer simulation, and it is proven to give an adequate performance. The solar charge controller, a combination of P&O MPPT algorithm and SEPIC topology using in this research give an outstanding performance. The charge controller can well adapt with the changement of solar irradiation. It is however, the algorithm can track the rapid changing of solar irradiation which are not less than 32 ms. This charge controller can provide an efficiency of up to 98 % on constant solar irradiaton during the simulation. Meanwhile, under varying solar irradiation, the charge controller can give an efficiency of 93.6 % provided that the solar irradiation change from 200 W/m^2 to 1000 W/m^2 not less than 100 ms. If the time of changement of irradiation is not less than 20 ms, the efficiency is 77.7 %.

The contribution of the study is not only on the simulation part of the system, but also in real hardware. Since SEPIC can be considered as a new topology for DC/DC converter, a detail analysis of its efficiency and losses has also been conducted and presented. The hardware experiment is separated on two frequency setting of 7.8 kHz and 62.3 kHz. The experiment is focused on two main losses that contributes to less effectiveness of the DC/DC converter which are diode and MOSFET losses. The outcome of the experiment gives an efficiency of 66.9 % at lower frequency and 77.3 % at higher frequency. And as to strengthen the claim that the diode and the MOSFET are the two main losses contributer, both devices contributed about 77 % of losses at lower frequency and 80 % losses at higher frequency.

5.3 RECOMMENDATIONS FOR THE FUTURE RESEARCH

Correct modeling of the DC/DC converter is an important area of study and plays an integral part of overall Solar Charge Controller performance. There will be a need for a more realistic model of DC/DC converter where it consists of a loss calculation. This is where it exists SimPowerSystem, one of a tool in SIMULINK that provide components to create an electrical circuit. This will provide useful information such as the circuit losses and efficiency before going to hardware implementation.

The used of proper components in the hardware such as diode, MOSFET and capacitors will give better efficiency. The switching frequency selection also makes the MOSFET works at its optimum capability as the efficiency increased when the frequency increased.

The Arduino, use as a controller, where it can provide analog/digital (A/D) converters for the sensors, and also a driving circuit for power MOSFET. But as tested at the circuit, the Arduino UNO board can provide as maximum as 62.3 kHz frequency. There will be a need for an Arduino board with a higher frequency output to give a decent signal to power MOSFET.

REFERENCES

A. DOLARA, R. F., S. LEVA (September 2009). "Energy Comparison of Seven MPPT Techniques for PV Systems." Journal of Electromagnetic Analysis and Applications **1**(3): 11.

A.Pradeep Kumar Yadav, S. T., G.Haritha (2012). "Comparison of MPPT Algorithms for DC-DC Converters Based PV Systems " International Journal of Advanced Research in Electrical, Electronics and Instrumentation Engineering **1**(1): 6.

Abdelmoula, M., S. Moughamir and B. Robert (2014). Design and modeling of a stand-alone photovoltaic system. Sciences and Techniques of Automatic Control and Computer Engineering (STA), 2014 15th International Conference on.

Al-Saffar, M. A., E. H. Ismail, A. J. Sabzali and A. A. Fardoun (2008). "An Improved Topology of SEPIC Converter With Reduced Output Voltage Ripple." Power Electronics, IEEE Transactions on **23**(5): 2377-2386.

Alghuwainem, S. M. (1992). "Steady-state performance of DC motors supplied from photovoltaic generators with step-up converter." Energy Conversion, IEEE Transactions on **7**(2): 267-272.

Ali, M. K. M. (2013). Pinjaman pasang panel PV solar di bumbung. Utusan Malaysia Malaysia.

Articles, S. P. (2013) "Solar cell I-V characteristics and solar cell I-V curve." energy articles.

Bhatnagar, P. and R. K. Nema (2013). "Maximum power point tracking control techniques: State-of-the-art in photovoltaic applications." Renewable and Sustainable Energy Reviews **23**(0): 224-241.

Bhunia, M. and R. Gupta (2013). Voltage regulation of stand-alone photovoltaic system using boost SEPIC converter with battery storage system. Engineering and Systems (SCES), 2013 Students Conference on Engineering and Systems.

Bor-Ren, L., C. Po-Li and C. Jyun-Ji (2010). Interleaved sepic converter with low switching loss. TENCON 2010 - 2010 IEEE Region 10 Conference.

Bose, B. K. (2010). "Global Warming: Energy, Environmental Pollution, and the Impact of Power Electronics." Industrial Electronics Magazine, IEEE **4**(1): 6-17.

Burmester, D., R. Rayudu and T. Exley (2013). Single Ended Primary Inductor Converter reliance of efficiency on switching frequency for use in MPPT application. Power and Energy Engineering Conference (APPEEC), 2013 IEEE PES Asia-Pacific.

Byunggyu, Y., Y. Gwonjong and K. Youngroc (2011). Design and experimental results of improved dynamic MPPT performance by EN50530. Telecommunications Energy Conference (INTELEC), 2011 IEEE 33rd International.

Carrasco, J. M., L. G. Franquelo, J. T. Bialasiewicz, E. Galvan, R. C. P. Guisado, M. A. M. Prats, J. I. Leon and N. Moreno-Alfonso (2006). "Power-Electronic Systems for the Grid Integration of Renewable Energy Sources: A Survey." Industrial Electronics, IEEE Transactions on **53**(4): 1002-1016.

Chapin, D. M., C. S. Fuller and G. L. Pearson (1954). "A New Silicon p-n Junction Photocell for Converting Solar Radiation into Electrical Power." Journal of Applied Physics **25** (5): 676-677.

Charfi, S. and M. Chaabene (2014). A comparative study of MPPT techniques for PV systems. Renewable Energy Congress (IREC), 2014 5th International.

Chiang, S. J., S. Hsin-Jang and C. Ming-Chieh (2009). "Modeling and Control of PV Charger System With SEPIC Converter." Industrial Electronics, IEEE Transactions on **56**(11): 4344-4353.

Coelho, R. F., F. Concer and D. C. Martins (2009). A study of the basic DC-DC converters applied in maximum power point tracking. Power Electronics Conference, 2009. COBEP '09. Brazilian.

Coelho, R. F., F. M. Concer and D. C. Martins (2010). Analytical and experimental analysis of DC-DC converters in photovoltaic maximum Power Point Tracking applications. IECON 2010 - 36th Annual Conference on IEEE Industrial Electronics Society.

Coelho, R. F., F. M. Concer and D. C. Martins (2010). A simplified analysis of DC-DC converters applied as maximum power point tracker in photovoltaic systems. Power Electronics for Distributed Generation Systems (PEDG), 2010 2nd IEEE International Symposium on.

Coelho, R. F., W. M. dos Santos and D. C. Martins (2012). Influence of power converters on PV maximum power point tracking efficiency. Industry Applications (INDUSCON), 2012 10th IEEE/IAS International Conference on.

Dang, T. L. (1990). A Digitally-controlled Power Tracker. Master's, California Polytechnic State University.

Darla, R. B. (2007). Development of maximum power point tracker for PV panels using SEPIC converter. Telecommunications Energy Conference, 2007. INTELEC 2007. 29th International.

Das, M. and V. Agarwal (2012). A novel, high efficiency, high gain, front end DC-DC converter for low input voltage solar photovoltaic applications. IECON 2012 - 38th Annual Conference on IEEE Industrial Electronics Society.

Dhar, S., R. Sridhar and G. Mathew (2013). Implementation of PV cell based standalone solar power system employing incremental conductance MPPT algorithm. Circuits, Power and Computing Technologies (ICCPCT), 2013 International Conference on.

Durgadevi, A., S. Arulselvi and S. P. Natarajan (2011). Study and implementation of Maximum Power Point Tracking (MPPT) algorithm for Photovoltaic systems. Electrical Energy Systems (ICEES), 2011 1st International Conference on.

El Khateb, A., N. A. Rahim, J. Selvaraj and M. N. Uddin (2014). "Fuzzy Logic Controller Based SEPIC Converter for Maximum Power Point Tracking." Industry Applications, IEEE Transactions on **PP**(99): 1-1.

Elgendy, M. A., B. Zahawi and D. J. Atkinson (2012). Evaluation of perturb and observe MPPT algorithm implementation techniques. Power Electronics, Machines and Drives (PEMD 2012), 6th IET International Conference on.

Enrique, J. M., J. M. Andújar and M. A. Bohórquez (2010). "A reliable, fast and low cost maximum power point tracker for photovoltaic applications." Solar Energy **84**(1): 79-89.

Esram, T. and P. L. Chapman (2007). "Comparison of Photovoltaic Array Maximum Power Point Tracking Techniques." Energy Conversion, IEEE Transactions on **22**(2): 439-449.

EvoEnergy. (2012). "PV Cell Overview." from http://www.evoenergy.co.uk/

Falin, J. (2008). "Designing DC/DC converters based on SEPIC topology." Analog Applications Journal(High-Performance Analog Products).

Femia, N., G. Petrone, G. Spagnuolo and M. Vitelli (2004). Optimizing sampling rate of P&O MPPT technique. Power Electronics Specialists Conference, 2004. PESC 04. 2004 IEEE 35th Annual.

Femia, N., G. Petrone, G. Spagnuolo and M. Vitelli (2004). Perturb and observe MPPT technique robustness improved. Industrial Electronics, 2004 IEEE International Symposium on.

Geir Opdahl, A. B., Alex Youakim (2010). Photovoltaic Maximum Power Point Tracker, University of Victoria.

Graditi, G., G. Adinolfi, N. Femia and M. Vitelli (2011). Comparative analysis of Synchronous Rectification Boost and Diode Rectification Boost converter for DMPPT applications. Industrial Electronics (ISIE), 2011 IEEE International Symposium on.

Hemalatha, J. N., S. A. Hariprasad and G. S. Anitha (2014). Performance evaluation of single ended primary inductance converter for photo voltaic applications. Emerging Research Areas: Magnetics, Machines and Drives (AICERA/iCMMD), 2014 Annual International Conference on.

Hohm, D. P. and M. E. Ropp (2000). Comparative study of maximum power point tracking algorithms using an experimental, programmable, maximum power point tracking test bed. Photovoltaic Specialists Conference, 2000. Conference Record of the Twenty-Eighth IEEE.

Huimin, Y., Z. Zhizhi and L. Huayong (2009). Photovoltaic industry and market investigation. Sustainable Power Generation and Supply, 2009. SUPERGEN '09. International Conference on.

Hussein, K. H., I. Muta, T. Hoshino and M. Osakada (1995). "Maximum photovoltaic power tracking: an algorithm for rapidly changing atmospheric conditions." Generation, Transmission and Distribution, IEE Proceedings- **142**(1): 59-64.

J.M. Enrique, E. D. n., M. Sidrach-de-Cardona, J.M. Andu´jar (2006). "Theoretical assessment of the maximum power point tracking efficiency of photovoltaic facilities with different converter topologies." Solar Energy **81**: 8.

Jahanbakhsh, D. (2012). Implementation of DC-DC converter with maximum power point tracking control for thermoelectric generator applications. Master of Science Master Thesis, Royal Institute of Technology (KTH).

Jerin, G. K. (2014). Direct control method applied for improved incremental conductance mppt using SEPIC converter. Green Computing Communication and Electrical Engineering (ICGCCEE), 2014 International Conference on.

Junjian, Z., K. Yeates and H. Yehui (2013). Analysis of high efficiency DC/DC converter processing partial input/output power. Control and Modeling for Power Electronics (COMPEL), 2013 IEEE 14th Workshop on.

Kashyap, A. R., R. Ahmadi and J. W. Kimball (2013). Input voltage control of SEPIC for maximum power point tracking. Power and Energy Conference at Illinois (PECI), 2013 IEEE.

Kawaguchi, Y., Y. Yamaguchi, S. Kanie, A. Baba and A. Nakagawa (2008). Proposal of the method for high efficiency DC-DC converters and the efficiency limit restricted by silicon properties. Power Electronics Specialists Conference, 2008. PESC 2008. IEEE.

Kazmi, S., H. Goto, O. Ichinokura and G. Hai-Jiao (2009). An improved and very efficient MPPT controller for PV systems subjected to rapidly varying atmospheric conditions and partial shading. Power Engineering Conference, 2009. AUPEC 2009. Australasian Universities.

Kim, K., K. Lee, K. Lee, Y. Choi and G. Cho (2013). A study on the control of buck-boost converter using newton-method MPPT. Electrical Machines and Systems (ICEMS), 2013 International Conference on.

Kimball, J. W., T. L. Flowers and P. L. Chapman (2004). Issues with low-input-voltage boost converter design. Power Electronics Specialists Conference, 2004. PESC 04. 2004 IEEE 35th Annual.

Kollimalla, S. K. and M. K. Mishra (2014). "A Novel Adaptive P&O MPPT Algorithm Considering Sudden Changes in the Irradiance." Energy Conversion, IEEE Transactions on **29**(3): 602-610.

Kroposki, B., R. Margolis and D. Ton (2009). "Harnessing the sun." Power and Energy Magazine, IEEE **7**(3): 22-33.

KYOCERA (2011). KYOCERA KD Modules. K. S. Inc.

Lahyani, A., P. Venet, G. Grellet and P. J. Viverge (1998). "Failure prediction of electrolytic capacitors during operation of a switchmode power supply." Power Electronics, IEEE Transactions on **13**(6): 1199-1207.

Liu, X. and L. A. C. Lopes (2004). An improved perturbation and observation maximum power point tracking algorithm for PV arrays. Power Electronics Specialists Conference, 2004. PESC 04. 2004 IEEE 35th Annual.

Lohmeier, C. J. (2011). Highly Efficient Maximum Power Point Tracking Using a Quasi-Double-Boost DC/DC Converter for Photovoltaic Systems. Master of Science, University of Nebraska.

Martin A. Green, K. E., Yoshihiro Hishikawa, Wilhelm Warta, Ewan D. Dunlop (2013). "Solar cell efficiency tables (version 42)." Progress in Photovoltaics: Research and Applications **21**(1): 827-837.

Masters, G. M. (2004). Renewable and Efficient Electric Power Systems. Hoboken, New Jersey, John Wiley & Sons, Inc., Publication.

MITSUBISHI (2007). MITSUBISHI Electric Photovoltaic Module TE Series PV-TE125MF5N. M. E. Corporation.

Muoka, P. I., M. E. Haque, A. Gargoom and M. Negnevitsky (2012). Modeling and simulation of a SEPIC converter based photovoltaic system with battery energy storage. Universities Power Engineering Conference (AUPEC), 2012 22nd Australasian.

Oi, A. (2005). Design and Simulation of Photovoltaic Water Pumping System. Master of Science in Electrical Engineering, California Polytechnic State University.

Patarau, T., S. R. Daraban, D. Petreus and R. Etz (2011). A comparison between Sepic and Buck-Boost converters used in maximum power point trackers. Electronics Technology (ISSE), 2011 34th International Spring Seminar on.

Pittini, R., Z. Zhe and M. A. E. Andersen (2013). Analysis of DC/DC converter efficiency for energy storage system based on bidirectional fuel cells. Innovative Smart Grid Technologies Europe (ISGT EUROPE), 2013 4th IEEE/PES.

PowerSemiconductorDevice (2011). Lesson 6 Metal Oxide Semiconductor Field Effect Transistor. Department of Electrical Engineering, Indian Institute of Technology Kharagpur.

Prabhakar, A. J., J. D. Bollinger, M. Hong Tao, M. Ferdowsi and K. Corzine (2008). Efficiency analysis and comparative study of hard and soft switching DC-DC converters in a wind farm. Industrial Electronics, 2008. IECON 2008. 34th Annual Conference of IEEE.

Rebei, N., R. Gammoudi, A. Hmidet and O. Hasnaoui (2014). Experimental implementation techniques of P&O MPPT algorithm for PV pumping system. Multi-Conference on Systems, Signals & Devices (SSD), 2014 11th International.

Roshan, R., Y. Yadav, S. Umashankar, D. Vijayakumar and D. P. Kothari (2013). Modeling and simulation of Incremental conductance MPPT algorithm based solar Photo Voltaic system using CUK converter. Energy Efficient Technologies for Sustainability (ICEETS), 2013 International Conference on.

S.E.C.O (1997). Introduction to Photovoltaic Systems. S. E. C. O. Texas.

Salameh, Z. and D. Taylor (1990). "Step-up maximum power point tracker for photovoltaic arrays." Solar Energy **44**(1): 57-61.

Salas, V., E. Olías, A. Barrado and A. Lázaro (2006). "Review of the maximum power point tracking algorithms for stand-alone photovoltaic systems." Solar Energy Materials and Solar Cells **90**(11): 1555-1578.

Salim Abouda, F. N., Najib Essounbouli,Abdessattar Chaari,Yassine Koubaa (2013). " PID and Sliding Mode Control-SMC for a Motor-pump Voltage in a Photovoltaic- PV System based on MPPT Controller." International Journal of Computer Applications **73** (3): 6.

Sekiya, H. (2011) "Core Geometry Coefficient For Resonant Inductor." How2Power Newsletter, 4.

Sharma, D. K. and G. Purohit (2012). Advanced perturbation and observation (P&O) based maximum power point tracking (MPPT) of a solar photo-voltaic system. Power Electronics (IICPE), 2012 IEEE 5th India International Conference on.

Shreelakshmi, M. P., M. Das and V. Agarwal (2013). High gain, high efficiency bi-directional DC-DC converter for battery charging applications in stand-alone Photo-Voltaic systems. Photovoltaic Specialists Conference (PVSC), 2013 IEEE 39th.

Taghvaee, M. H., M. A. M. Radzi, S. M. Moosavain, H. Hizam and M. Hamiruce Marhaban (2013). "A current and future study on non-isolated DC–DC converters for photovoltaic applications." Renewable and Sustainable Energy Reviews **17**(0): 216-227.

Taherbaneh, M., A. H. Rezaie, H. Ghafoorifard, M. B. Menhaj and M. Mirsamadi (2011). "Power Loss Analysis for Efficiency Estimation of a DC-DC Converter." IEICE Transactions on Electronics **E94.C**(2): 220-230.

Taheri, H., Z. Salam, K. Ishaque and Syafaruddin (2010). A novel Maximum Power Point tracking control of photovoltaic system under partial and rapidly fluctuating shadow conditions using Differential Evolution. Industrial Electronics & Applications (ISIEA), 2010 IEEE Symposium on.

Volkan Kursun, S. G. N., Vivek K. De, Eby G. Friedman (2002). Efficiency Analysis of a High Frequency Buck Converter for On-Chip Integration with a Dual-VDD Microprocessor European Solid-State Circuits Conference. Firenze, Italy**:** 4.

Walker, G. R. (2000). Evaluating MPPT converter topologies using a MATLAB PV model. Australasian Universities Power Engineering Conference, AUPE. Brisbane.

Yingli (2013). YGE 60 cells series. Y. G. E. H. C. Ltd.

Zanotti, J. W., W. M. dos Santos and D. C. Martins (2013). The new MPPT method for PV systems employing input characteristic impedance. Power Electronics Conference (COBEP), 2013 Brazilian.

Zhang, D. (2013). AN-1484 Designing A SEPIC Converter, Texas Instruments Incorporated**:** 11.

Zhiguo, P., Z. Fan and F. Z. Peng (2005). Power losses and efficiency analysis of multilevel dc-dc converters. Applied Power Electronics Conference and Exposition, 2005. APEC 2005. Twentieth Annual IEEE.

APPENDIX A

MATLAB FUNCTIONS AND SCRIPTS

1. Function for Modeling Mitsubishi PVTE125_MF5N PV Module

```
function Ia =PVTE125_MF5N(Va,G,TaC)
% function PVTE125_MF5N.m models the PV-TE125MF5N PV module
% calculates module current under given voltage, irradiance and
temperature
% Ia = PVTE125_MF5N(Va,G,TaC)
%
% Out: Ia = Module operating current (A), vector or scalar
% In: Va = Module operating voltage (V), vector or scalar
% G = Irradiance (1G = 1000 W/m^2), scalar
% TaC = Module temperature in deg C, scalar
%
% Written by Akihiro Oi 01/07/2005
% Adapted by Wan Muhammad Firdaus 18/02/2012
%///////////////////////////////////////////////////////////////////////
% Define constants
k = 1.381e-23; % Boltzmann’s constant
q = 1.602e-19; % Electron charge
% Following constants are taken from the datasheet of PV module and
% curve fitting of I-V character (Use data for 1000W/m^2)
n = 1.62; % Diode ideality factor (n),
% 1 (ideal diode) < n < 2
Eg = 1.12; % Band gap energy; 1.12eV (Si), 1.42 (GaAs),
% 1.5 (CdTe), 1.75 (amorphous Si)
Ns = 36; % # of series connected cells (PVTE125_MF5N, 36 cells)
TrK = 298; % Reference temperature (25C) in Kelvin
Voc_TrK = 21.8 /Ns; % Voc (open circuit voltage per cell) @ temp TrK
Isc_TrK = 7.9; % Isc (short circuit current per cell) @ temp TrK
a = 0.54e-3; % Temperature coefficient of Isc (0.054%/C)
% Define variables
TaK = 273 + TaC; % Module temperature in Kelvin
Vc = Va / Ns; % Cell voltage
% Calculate short-circuit current for TaK
Isc = Isc_TrK * (1 + (a * (TaK - TrK)));
% Calculate photon generated current @ given irradiance
Iph = G * Isc;
% Define thermal potential (Vt) at temp TrK
Vt_TrK = n * k * TrK / q;
% Define b = Eg * q/(n*k);
b = Eg * q /(n * k);
% Calculate reverse saturation current for given temperature
Ir_TrK = Isc_TrK / (exp(Voc_TrK / Vt_TrK) -1);
Ir = Ir_TrK * (TaK / TrK)^(3/n) * exp(-b * (1 / TaK -1 / TrK));
% Calculate series resistance per cell (Rs = 5.1mOhm)
dVdI_Voc = -0.6/Ns/2; % Take dV/dI @ Voc from I-V curve of datasheet
Xv = Ir_TrK / Vt_TrK * exp(Voc_TrK / Vt_TrK);
Rs = - dVdI_Voc - 1/Xv;
% Define thermal potential (Vt) at temp Ta
Vt_Ta = n * k * TaK / q;
% Ia = Iph - Ir * (exp((Vc + Ia * Rs) / Vt_Ta) -1)
```

```
% f(Ia) = Iph - Ia - Ir * ( exp((Vc + Ia * Rs) / Vt_Ta) -1) = 0
% Solve for Ia by Newton's method: Ia2 = Ia1 - f(Ia1)/f'(Ia1)
Ia=zeros(size(Vc)); % Initialize Ia with zeros
% Perform 5 iterations
for j=1:5;
    Ia = Ia - (Iph - Ia - Ir .* ( exp((Vc + Ia .* Rs) ./ Vt_Ta) -
1))...
        ./ (-1 - Ir * (Rs ./ Vt_Ta) .* exp((Vc + Ia .* Rs) ./ Vt_Ta));
end
```

2. Script for P&O Algorithm

```
% Script file to test the P&O MPPT Algorithm
% Akihiro Oi 29/06/2005
% Adapted by Wan Muhammad Firdaus on 20/03/2012
%%%%%%%%%%%%%%%%%%%%%%%%%%%%%%%%%%%%%%%%%%%%%%%%%%%%%%%%%%%%%%%%%%%
clear;
% Define constants
TaC = 25; % Cell temperature (deg C)
C = 0.05; % Step size for ref voltage change (V)
% Define variables with initial conditions
G = 0.028; % Irradiance (1G = 1000W/m^2)
Va = 21.8; % PV voltage
Ia = PVTE125_MF5N(Va,G,TaC); % PV current
Pa = Va * Ia; % PV output power
Vref_new = Va + C; % New reference voltage
% Set up arrays storing data for plots
Va_array = [];
Pa_array = [];
% Load irradiance data
load data3.prn;    %  read data into PDXprecip matrix
x = data3(:,1);     %  copy first column of PDXprecip into time
y = data3(:,3);    %  and third column into irrad
plot(x,y,'');     %  plot precip vs. time with circles
xlabel('time');            % add axis labels and plot title
ylabel('irradiance (kW/m²)');
title('28/12/2011 irradiance @ Universiti Malaysia Pahang, Malaysia');
% Take 43200 samples (12 hours)
for Sample = 1:0.72e+3
% Read irradiance value
    G = y(Sample);
% Take new measurements
    Va_new = Vref_new;
    Ia_new = PVTE125_MF5N(Vref_new,G,TaC);
% Calculate new Pa
    Pa_new = Va_new * Ia_new;
    deltaPa = Pa_new - Pa;
% P&O Algorithm starts here
if deltaPa > 0
if Va_new > Va
            Vref_new = Va_new + C; % Increase Vref
else
            Vref_new = Va_new - C; % Decrease Vref
end
elseif deltaPa < 0
if Va_new > Va
            Vref_new = Va_new - C; % Decrease Vref
else
```

```
            Vref_new = Va_new + C; %Increase Vref
end
else
        Vref_new = Va_new; % No change
end
% Update history
    Va = Va_new;
    Pa = Pa_new;
% Store data in arrays for plot
Va_array = [Va_array Va];
Pa_array = [Pa_array Pa];
end
% Plot result
figure
plot (Va_array, Pa_array, 'g*')
% Overlay with P-I curves and MPP
Va = linspace (0, 25, 200);
hold on
for G=.2:.2:1
Ia = PVTE125_MF5N(Va, G, TaC);
    Pa = Ia.*Va;
    plot(Va, Pa)
[Pa_max, Imp, Vmp] = find_mpp(G, TaC);
    plot(Vmp, Pa_max, 'r*')
end
title('P&O Algorithm')
xlabel('Module Voltage (V)')
ylabel('Module Output Power (W)')
axis([0 25 0 130])
hold off
```

APPENDIX B

1. Photovoltaic History Timeline

U.S. Department of Energy
Energy Efficiency and Renewable Energy

The History of Solar

Byron Stafford NREL / PIX10730

Byron Stafford, NREL / PIX05370

Courtesy of New Vision Technologies, Inc./ Images ©2000 NVTech.com

Solar technology isn't new. Its history spans from the 7th Century B.C. to today. We started out concentrating the sun's heat with glass and mirrors to light fires. Today, we have everything from solar-powered buildings to solar-powered vehicles.

Here you can learn more about the milestones in the historical development of solar technology, century by century, and year by year. You can also glimpse the future.

This timeline lists the milestones in the historical development of solar technology from the 7th Century B.C. to the 1200s A.D.

7th Century B.C. — 1200s A.D.

7th Century B.C.

Magnifying glass used to concentrate sun's rays to make fire and to burn ants.

3rd Century B.C.

Greeks and Romans use burning mirrors to light torches for religious purposes.

2nd Century B.C.

As early as 212 BC, the Greek scientist, Archimedes, used the reflective properties of bronze shields to focus sunlight and to set fire to wooden ships from the Roman Empire which were besieging Syracuse. (Although no proof of such a feat exists, the Greek navy recreated the experiment in 1973 and successfully set fire to a wooden boat at a distance of 50 meters.)

20 A.D.

Chinese document use of burning mirrors to light torches for religious purposes.

1st to 4th Century A.D.

The famous Roman bathhouses in the first to fourth centuries A.D. had large south facing windows to let in the sun's warmth. For an example, see information on the http://www.hum.huji.ac.il/archaeology/zippori/RomanSeph.htm Zippori in the Roman Period from the Hebrew University of Jerusalem.

Courtesy of Susan Sczepanski, NREL

6th Century A.D.

Sunrooms on houses and public buildings were so common that the Justinian Code initiated "sun rights" to ensure individual access to the sun.

1200s A.D.

Ancestors of Pueblo people called Anasazi in North America live in south-facing cliff dwellings that capture the winter sun.

The Anasazi cliff dwellings demonstrate passive solar design. (John Thornton, NREL / PIX 03549)

1

This timeline lists the milestones in the historical development of solar technology from 1767 to 1891.

1767-1891

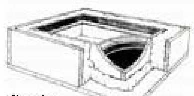

Illustration courtesy of Kevin Porter Solar Cookers, International

1767
Swiss scientist Horace de Saussure was credited with building the world's first solar collector, later used by Sir John Herschel to cook food during his South Africa expedition in the 1830s. See the Solar Cooking Archive for more information on http://solarcooking.org/saussure.htm Sassure and His Hot Boxes of the 1700s.

1816
On September 27, 1816, Robert Stirling applied for a patent for his economiser at the Chancery in Edinburgh, Scotland. By trade, Robert Stirling was actually a minister in the Church of Scotland and he continued to give services until he was eighty-six years old! But, in his spare time, he built heat engines in his home workshop. Lord Kelvin used one of the working models during some of his university classes. This engine was later used in the dish/Stirling system, a solar thermal electric technology that concentrates the sun's thermal energy in order to produce power.

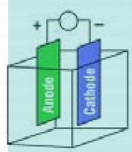

1839
French scientist Edmond Becquerel discovers the photovoltaic effect while experimenting with an electrolytic cell made up of two metal electrodes placed in an electricity-conducting solution—electricity-generation increased when exposed to light.

1860s
French mathematician August Mouchet proposed an idea for solar-powered steam engines. In the following two decades, he and his assistant, Abel Pifre, constructed the first solar powered engines and used them for a variety of applications. These engines became the predecessors of modern parabolic dish collectors.

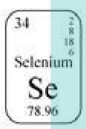

1873
Willoughby Smith discovered the photoconductivity of selenium.

William Grylls Adams, Courtesy of John Perlin 2002 From Space to Earth The Story of Solar Electricity

1876
1876 William Grylls Adams and Richard Evans Day discover that selenium produces electricity when exposed to light. Although selenium solar cells failed to convert enough sunlight to power electrical equipment, they proved that a solid material could change light into electricity without heat or moving parts.

Samuel P. Langley, Courtesy of NASA

Bolometer, Courtesy of NASA

1880
Samuel P. Langley, invents the bolometer, which is used to measure light from the faintest stars and the sun's heat rays. It consists of a fine wire connected to an electric circuit. When radiation falls on the wire, it becomes very slightly warmer. This increases the electrical resistance of the wire.

Heinrich Hertz, Courtesy of NASA/ Goddard Space Flight Center

1883
Charles Fritts, an American inventor, described the first solar cells made from selenium wafers.

1887
Heinrich Hertz discovered that ultraviolet light altered the lowest voltage capable of causing a spark to jump between two metal electrodes.

Solar Water Heater Courtesy of John Perlin/ Butti Solar Archives

1891
Baltimore inventor Clarence Kemp patented the first commercial solar water heater. For more information on the water heater, see the http://www.californiasolarcenter.org/history_solarthermal.html California Solar Center.

2

This timeline lists the milestones in the historical development of solar technology in the 1900s.

Early 1900s

Albert Einstein, courtesy of the Lotte Jacobi Archives, University of Hampshire

$$a = \frac{F}{M}\left(1 - \frac{v^2}{c^2}\right)^{3/2}$$

Theory of Relativity equation

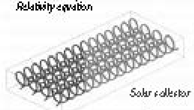

Solar collector

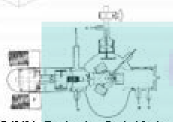

©1916 by The American Physical Society

Jan Czochralski, courtesy of Debra Kaiser, AACG newsletter

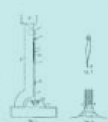

Single-crystal silicon

1904
Wilhelm Hallwachs discovered that a combination of copper and cuprous oxide is photosensitive.

1905
Albert Einstein published his paper on the photoelectric effect (along with a paper on his theory of relativity).

1908
1908 William J. Bailley of the Carnegie Steel Company invents a solar collector with copper coils and an insulated box—roughly, it's present design.

1914
The existence of a barrier layer in photovoltaic devices was noted.

1916
Robert Millikan provided experimental proof of the photoelectric effect.

1918
Polish scientist Jan Czochralski developed a way to grow single-crystal silicon. For more information on Czochralski, see the article http://rekt.pol.lublin.pl/users/ptwk/art2.htm Professor Jan Czolchralski (1885-1953) and His Contribution to the Art and Science of Crystal Growth.

1921
Albert Einstein wins the Nobel Prize for his theories (1904 research and technical paper) explaining the photoelectric effect.

1932
Audobert and Stora discover the photovoltaic effect in cadmium sulfide (CdS).

1947
1947 Passive solar buildings in the United States were in such demand, as a result of scarce energy during the prolonged W.W.II, that Libbey-Owens-Ford Glass Company published a book entitled Your Solar House, which profiled forty-nine of the nation's greatest solar architects. http://www.californiasolarcenter.org/history_solarthermal.html.

Mid 1950s

Bell Labs scientists, Daryl Chapin, Calvin Fuller, and Gerald Pearson, courtesy of John Perlin

Bell Labs silicon solar cell

1953
Dr. Dan Trivich, Wayne State University, makes the first theoretical calculations of the efficiencies of various materials of different band gap widths based on the spectrum of the sun.

1954
1954 Photovoltaic technology is born in the United States when Daryl Chapin, Calvin Fuller, and Gerald Pearson develop the silicon photovoltaic (PV) cell at Bell Labs—the first solar cell capable of converting enough of the sun's energy into power to run everyday electrical equipment. Bell Telephone Laboratories produced a silicon solar cell with 4% efficiency and later achieved 11% efficiency. See the http://www.californiasolarcenter.org/history_pv.html for more information.

1955
Western Electric began to sell commercial licenses for silicon photovoltaic (PV) technologies. Early successful products included PV-powered dollar bill changers and devices that decoded computer punch cards and tape.

Mid 1950s (cont.)

William Cherry, courtesy of Mark Fitzgerald

Mid-1950s

Architect Frank Bridgers designed the world's first commercial office building using solar water heating and passive design. This solar system has been continuously operating since that time and the Bridgers-Paxton Building, is now in the National Historic Register as the world's first solar heated office building.

1956

William Cherry, U.S. Signal Corps Laboratories, approaches RCA Labs' Paul Rappaport and Joseph Loferski about developing photovoltaic cells for proposed orbiting Earth satellites.

1957

Hoffman Electronics achieved 8% efficient photovoltaic cells.

1958

T. Mandelkorn, U.S. Signal Corps Laboratories, fabricates n-on-p silicon photovoltaic cells (critically important for space cells; more resistant to radiation).

1958

Hoffman Electronics achieves 9% efficient photovoltaic cells.

1958

The Vanguard I space satellite used a small (less than one watt) array to power its radios. Later that year, Explorer III, Vanguard II, and Sputnik-3 were launched with PV-powered systems on board. Despite faltering attempts to commercialize the silicon solar cell in the 1950s and 60s, it was used successfully in powering satellites. It became the accepted energy source for space applications and remains so today. For more information, see the Smithsonian National Air and Space Museum's information on http://www.nasm.si.edu/nasm/dsh/artifacts/SS-vanguard.htm "Vanguard 1".

1959

Hoffman Electronics achieves 10% efficient, commercially available photovoltaic cells. Hoffman also learns to use a grid contact, reducing the series resistance significantly.

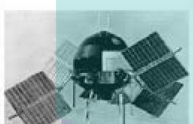

Courtesy of http://www.[illegible].com

1959

On August 7, the Explorer VI satellite is launched with a photovoltaic array of 9600 cells (1 cm x 2 cm each). Then, on October 13, the Explorer VII satellite is launched.

1960s

1960

Hoffman Electronics achieves 14% efficient photovoltaic cells.

1960

Silicon Sensors, Inc., of Dodgeville, Wisconsin, is founded. It starts producing selenium and silicon photovoltaic cells.

Bell Labs

1962

Bell Telephone Laboratories launches the first telecommunications satellite, the Telstar (initial power 14 watts).

SHARP

1963

Sharp Corporation succeeds in producing practical silicon photovoltaic modules.

1963

Japan installs a 242-watt, photovoltaic array on a lighthouse, the world's largest array at that time.

1960s (cont.)

1964
NASA launches the first Nimbus spacecraft—a satellite powered by a 470-watt photovoltaic array. See NASA's http://nssdc.gsfc.nasa.gov/earth/nimbus.html "Nimbus Program" for more information.

1965
Peter Glaser conceives the idea of the satellite solar power station. For more information, see DOE's reference brief, http://www.eere.energy.gov/consumerinfo/refbriefs/l123.html "Solar Power Satellites".

1966
NASA launches the first Orbiting Astronomical Observatory, powered by a 1-kilowatt photovoltaic array, to provide astronomical data in the ultraviolet and X-ray wavelengths filtered out by the earth's atmosphere.

1969
The Odeillo solar furnace, located in Odeillo, France was constructed. This featured an 8-story parabolic mirror.


Allan Lamandowski / PIX05409

1970s

1970s
Dr. Elliot Berman, with help from Exxon Corporation, designs a significantly less costly solar cell, bringing price down from $100 a watt to $20 a watt. Solar cells begin to power navigation warning lights and horns on many offshore gas and oil rigs, lighthouses, railroad crossings and domestic solar applications began to be viewed as sensible applications in remote locations where grid-connected utilities could not exist affordably.

1972
The French install a cadmium sulfide (CdS) photovoltaic system to operate an educational television at a village school in Niger.

1972
The Institute of Energy Conversion is established at the University of Delaware to perform research and development on thin-film photovoltaic (PV) and solar thermal systems, becoming the world's first laboratory dedicated to PV research and development.

1973
The University of Delaware builds "Solar One," one of the world's first photovoltaic (PV) powered residences. The system is a PV/thermal hybrid. The roof-integrated arrays fed surplus power through a special meter to the utility during the day and purchased power from the utility at night. In addition to electricity, the arrays acted as flat-plate thermal collectors, with fans blowing the warm air from over the array to phase-change heat-storage bins.

1976
The NASA Lewis Research Center starts installing 83 photovoltaic power systems on every continent except Australia. These systems provide such diverse applications as vaccine refrigeration, room lighting, medical clinic lighting, telecommunications, water pumping, grain milling, and classroom television. The Center completed the project in 1995, working on it from 1976-1985 and then again from 1992-1995.

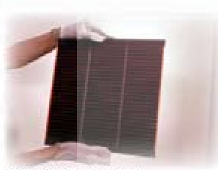
Warren Gretz, NREL / PIX01501

1976
David Carlson and Christopher Wronski, RCA Laboratories, fabricate first amorphous silicon photovoltaic cells.

1970s (cont.)

1977
The U.S. Department of Energy launches the Solar Energy Research Institute http://www.nrel.gov/ "National Renewable Energy Laboratory", a federal facility dedicated to harnessing power from the sun.

1977
Total photovoltaic manufacturing production exceeds 500 kilowatts.

1978
1978 NASA's Lewis Research Center dedicates a 3.5-kilowatt photovoltaic (PV) system it installed on the Papago Indian Reservation located in southern Arizona—the world's first village PV system. The system is used to provide for water pumping and residential electricity in 15 homes until 1983, when grid power reached the village. The PV system was then dedicated to pumping water from a community well.

1980s

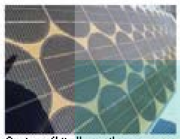
Courtesy of http://www.otherpower.com

1980
ARCO Solar becomes the first company to produce more than 1 megawatt of photovoltaic modules in one year.

1980
At the University of Delaware, the first thin-film solar cell exceeds 10% efficiency using copper sulfide/cadmium sulfide.


Courtesy of ©1988 National Air and Space Museum, Smithsonian Institution

1981
Paul MacCready builds the first solar-powered aircraft—the Solar Challenger—and flies it from France to England across the English Channel. The aircraft had over 16,000 solar cells mounted on its wings, which produced 3,000 watts of power. The Smithsonian Institute National Air and Space Museum has a photo of the http://www.nasm.edu/nasm/aero/aircraft/maccread.htm "Solar Challenger" in flight.

1982
The first, photovoltaic megawatt-scale power station goes on-line in Hisperia, California. It has a 1-megawatt capacity system, developed by ARCO Solar, with modules on 108 dual-axis trackers.


Courtesy of http://www.speedace.info/

1982
Australian Hans Tholstrup drives the first solar-powered car—the Quiet Achiever—almost 2,800 miles between Sydney and Perth in 20 days—10 days faster than the first gasoline-powered car to do so. Tholstrup is the founder of the http://www.wsc.org.au/2003/home.solar "World Solar Challenge" in Australia, considered the world championship of solar car racing.

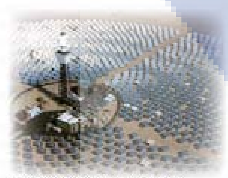
Sandia National Laboratories / PIX00036

1982
The U.S. Department of Energy, along with an industry consortium, begins operating Solar One, a 10-megawatt central-receiver demonstration project. The project established the feasibility of power-tower systems, a solar-thermal electric or concentrating solar power technology. In 1988, the final year of operation, the system could be dispatched 96% of the time. For more information, see www.eere.energy.gov/erec/factsheets/csp.html "Concentrating Solar Power: Energy From Mirrors" and http://www.energylan.sandia.gov/sunlab/Snapshot/STFUTURE.htm "Solar Two Demonstrates Clean Power for the Future".

– Photo caption: Solar One, a 10-megawatt central receiver power tower is located in Daggett, CA. (Sandia National Laboratories / PIX00036)

1980s (cont.)

1982

Volkswagen of Germany begins testing photovoltaic arrays mounted on the roofs of Dasher station wagons, generating 160 watts for the ignition system.

1982

The Florida Solar Energy Center's http://www.fsec.ucf.edu/About/quals/index.htm#recentcon "Southeast Residential Experiment Station" begins supporting the U.S. Department of Energy's photovoltaics program in the application of systems engineering.

1982

Worldwide photovoltaic production exceeds 9.3 megawatts.

1983

ARCO Solar dedicates a 6-megawatt photovoltaic substation in central California. The 120-acre, unmanned facility supplies the Pacific Gas & Electric Company's utility grid with enough power for 2,000-2,500 homes.

1983

Solar Design Associates completes a stand-alone, 4-kilowatt powered home in the Hudson River Valley.

1983

Worldwide photovoltaic production exceeds 21.3 megawatts, with sales of more than $250 million.

1984

The Sacramento Municipal Utility District commissions its first 1-megawatt photovoltaic electricity generating facility.

1985

The University of South Wales breaks the 20% efficiency barrier for silicon solar cells under 1-sun conditions.

1986

Warren Gretz, NREL / PIX01224

1986 The world's largest solar thermal facility, located in Kramer Junction, California, was commissioned. The solar field contained rows of mirrors that concentrated the sun's energy onto a system of pipes circulating a heat transfer fluid. The heat transfer fluid was used to produce steam, which powered a conventional turbine to generate electricity.

– Photo Caption: This solar power plant located in Kramer Junction, California, is the largest of nine such plants built in the 1980's. During operation, oil in the receiver tubes collects the concentrated solar energy as heat and is pumped to a power block located at the power plant for generating electricity. (Warren Gretz, NREL / PIX01224)

1986

ARCO Solar releases the G-4000—the world's first commercial thin-film power module.

1988

Dr. Alvin Marks receives patents for two solar power technologies he developed: Lepcon and Lumeloid. Lepcon consists of glass panels covered with a vast array of millions of aluminum or copper strips, each less than a micron or thousandth of a millimeter wide. As sunlight hits the metal strips, the energy in the light is transferred to electrons in the metal, which escape at one end in the form of electricity. Lumeloid uses a similar approach but substitutes cheaper, film-like sheets of plastic for the glass panels and covers the plastic with conductive polymers, long chains of molecular plastic units.

NREL

1990s

Warren Gretz, NREL / PIX03541

Sandia National Labs / PIX01728

Terry O'Rourke / PIX00253

Dave Parsons / PIX06995

Warren Gretz, NREL / PIX03302

Sandia National Laboratories / PIX01701

1991

President George Bush redesignates the U.S. Department of Energy's Solar Energy Research Institute as the National Renewable Energy Laboratory.

1992

1992 University of South Florida develops a 15.9% efficient thin-film photovoltaic cell made of cadmium telluride, breaking the 15% barrier for the first time for this technology.

– Photo caption: Thin-film modules, such as this one made with amorphous silicon, can be deposited on a variety of low-cost substrates, including glass and flexible plastic sheets. (Warren Gretz, NREL / PIX03541)

1992

A 7.5-kilowatt prototype dish system using an advanced stretched-membrane concentrator becomes operational.

1993

1993 Pacific Gas & Electric completes installation of the first grid-supported photovoltaic system in Kerman, California. The 500-kilowatt system was the first "distributed power" effort.

– Photo caption: Pacific Gas and Electric Company (PG&E) installed a 500-kilowatt photovoltaic system at its Kerman substation to reinforce a weak feeder. PG&E found that distributed systems like this have measurable benefits such as increased system reliability and peak-shaving capabilities. (Terry O'Rourke / PIX00253)

1994

The National Renewable Energy Laboratory (formerly the Solar Energy Research Institute) completes construction of its http://www.nrel.gov/buildings/highperformance/serf.html "Solar Energy Research Facility", which was recognized as the most energy-efficient of all U.S. government buildings worldwide. It features not only solar electric system, but also a passive solar design.

1994

First solar dish generator using a free-piston Stirling engine is tied to a utility grid.

1994

The National Renewable Energy Laboratory develops a solar cell—made from gallium indium phosphide and gallium arsenide—that becomes the first one to exceed 30% conversion efficiency.

1996

The world's most advanced solar-powered airplane, the Icare, flew over Germany. The wings and tail surfaces of the Icare are covered by 3,000 super-efficient solar cells, with a total area of 21 m2. See http://www.ifb.uni-stuttgart.de/icare/pictures/ica-fl2.jpg "Solar Aircraft of the University of Stuttgart" for more information about Icare.

1996

The U.S. Department of Energy, along with an industry consortium, begins operating Solar Two—an upgrade of its Solar One concentrating solar power tower project. Operated until 1999, Solar Two demonstrated how solar energy can be stored efficiently and economically so that power can be produced even when the sun isn't shining. It also fostered commercial interest in power towers. See http://www.energylan.sandia.gov/sunlab/Snapshot/STFUTURE.htm "Solar Two Demonstrates Clean Power for the Future" for more information.

– Photo Caption: The Solar Two project will improve the 10-megawatt Solar One central receiver plant in Daggett, CA. A field of mirrored heliostats focuses sunlight on a 300-foot (91 meter) tower, which will be filled with molten nitrate salt. The salt flows like water and can be heated to 1050 degrees F. The salt is pumped through a steam generator to produce the steam to power a conventional, high-efficiency steam turbine to produce electricity. (566 degrees C). (Sandia National Laboratories / PIX01701)

1990s

1998

The remote-controlled, solar-powered aircraft, "Pathfinder" sets an altitude record, 80,000 feet, on its 39th consecutive flight on August 6, in Monrovia, California. This altitude is higher than any prop-driven aircraft thus far.

United Solar Systems Corporation / PIX03636

1998

Subhendu Guha, a noted scientist for his pioneering work in amorphous silicon, led the invention of flexible solar shingles, a roofing material and state-of-the-art technology for converting sunlight to electricity.

– Photo caption: The PV shingles mount directly on to the roof and take the place of asphalt shingles. The system is connected to the utility grid through an inverter and produces electricity on customer's side of the meter. United Solar Systems Corporation / PIX03636)

Kiss + Cathcart - Architects / PIX06456

1999

1999 Construction was completed on 4 Times Square, the tallest skyscraper built in the 1990s in New York City. It incorporates more energy-efficient building techniques than any other commercial skyscraper and also includes building-integrated photovoltaic (BIPV) panels on the 37th through 43rd floors on the south- and west-facing facades that produce a portion of the buildings power.

– Photo Caption: 4 Times Squares most advanced feature is the photovoltaic skin, a system that uses thin-film PV panels to replace traditional glass cladding material. The PV curtain wall extends from the 35th to the 48th floor on the south and east walls of the building, making it a highly visible part of the midtown New York skyline. The developer, the Durst Organization, has implemented a wide variety of healthy building and energy efficiency strategies. Kiss + Cathcart Architects designed the building's PV system in collaboration with Fox and Fowle, the base building architects. Energy Photovoltaics of Princeton, NJ, developed the custom PV modules. (Kiss + Cathcon - Architects / PIX06456)

SPECTROLAB

A BOEING COMPANY

NREL

Warren Gretz, NREL / PIX00183

1999

Spectrolab, Inc. and the National Renewable Energy Laboratory develop a photovoltaic solar cell that converts 32.3 percent of the sunlight that hits it into electricity. The high conversion efficiency was achieved by combining three layers of photovoltaic materials into a single solar cell. The cell performed most efficiently when it received sunlight concentrated to 50 times normal. To use such cells in practical applications, the cell is mounted in a device that uses lenses or mirrors to concentrate sunlight onto the cell. Such "concentrator" systems are mounted on tracking systems that keep them pointed toward the sun.

1999

The National Renewable Energy Laboratory achieves a new efficiency record for thin-film photovoltaic solar cells. The measurement of 18.8 percent efficiency for the prototype solar cell topped the previous record by more than 1 percent.

1999

Cumulative worldwide installed photovoltaic capacity reaches 1000 megawatts.

This timeline lists the milestones in the historical development of solar technology in the 2000s.

2000s

Courtesy of NASA

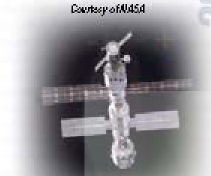

Sandia National Labs, PIX10809

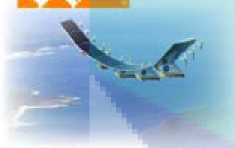

Courtesy of NASA Dryden Flight Research Center Photo Collection

2000

First Solar begins production in Perrysburg, Ohio, at the world's largest photovoltaic manufacturing plant with an estimated capacity of producing enough solar panels each year to generate 100 megawatts of power.

2000

At the International Space Station, astronauts begin installing solar panels on what will be the largest solar power array deployed in space. Each "wing" of the array consists of 32,800 solar cells.

2000

Sandia National Laboratories develops a new inverter for solar electric systems that will increase the safety of the systems during a power outage. Inverters convert the direct current (DC) electrical output from solar systems into alternating current (AC), which is the standard current for household wiring and for the power lines that supply electricity to homes.

2000

Two new thin-film solar modules, developed by BP Solarex, break previous performance records. The company's 0.5-square-meter module achieves 10.8 % conversion efficiency—the highest in the world for thin-film modules of its kind. And its 0.9-square-meter module achieved 10.6% conversion efficiency and a power output of 91.5 watts — the highest power output for any thin-film module in the world.

2000

A family in Morrison, Colorado, installs a 12-kilowatt solar electric system on its home—the largest residential installation in the United States to be registered with the U.S. Department of Energy's http://www.millionsolarroofs.com/ "Million Solar Roofs" program. The system provides most of the electricity for the 6,000-square-foot home and family of eight.

2001

Home Depot begins selling residential solar power systems in three of its stores in San Diego, California. A year later it expands sales to include 61 stores nationwide.

2001

NASA's solar-powered aircraft—Helios sets a new world record for non-rocket-powered aircraft: 96,863 feet, more than 18 miles high.

– Photo caption: The Helios Prototype flying wing is shown near the Hawaiian Islands during its first test flight on solar power. (Photo Courtesy of NASA, Dryden Flight Research Center Photo Collection)

2001

The National Space Development Agency of Japan, or NASDA, announces plans to develop a satellite-based solar power system that would beam energy back to Earth. A satellite carrying large solar panels would use a laser to transmit the power to an airship at an altitude of about 12 miles, which would then transmit the power to Earth.

2001

TerraSun LLC develops a unique method of using holographic films to concentrate sunlight onto a solar cell. Concentrating solar cells typically use Fresnel lenses or mirrors to concentrate sunlight. TerraSun claims that the use of holographic optics allows more selective use of the sunlight, allowing light not needed for power production to pass through the transparent modules. This capability allows the modules to be integrated into buildings as skylights.

10

2000s

PowerLight Corporation / PIX08431

2001

PowerLight Corporation places online in Hawaii the world's largest hybrid system that combines the power from both wind and solar energy. The grid-connected system is unusual in that its solar energy capacity—175 kilowatts—is actually larger than its wind energy capacity of 50 kilowatts. Such hybrid power systems combine the strengths of both energy systems to maximize the available power.

Warren Gretz NREL / PIX11979

2001

British Petroleum (BP) and BP Solar announce the opening of a service station in Indianapolis that features a solar-electric canopy. The Indianapolis station is the first U.S. "BP Connect" store, a model that BP intends to use for all new or significantly revamped BP service stations. The canopy is built using translucent photovoltaic modules made of thin films of silicon deposited onto glass.

– Photo Caption: The PowerView Semi-Transparent Photovoltaic Module, developed by NREL and BP Solar, is a novel system that serves as a roof or window while creating power for a building. BP has to date incorporated the system in more that 150 of its service stations and the panels are envisioned to become a functional replacement for conventional glass in walls, canopies, atriums, entrances and facades in commercial and residential architecture. (Warren Gretz, NREL / PIX 11979)

Courtesy of NASA Dryden Flight Research Center Photo Collection

2002

NASA successfully conducts two tests of a solar-powered, remote-controlled aircraft called Pathfinder Plus. In the first test in July, researchers demonstrated the aircraft's use as a high-altitude platform for tele-communications technologies. Then, in September, a test demonstrated its use as an aerial imaging system for coffee growers.

– Photo Caption: The Pathfinder Plus is a lightweight, solar-powered, remotely piloted flying wing aircraft that is demonstrating the technology of applying solar power for long-duration, high-altitude flight. This solar-powered aircraft could stay airborne for weeks or months on scientific sampling and imaging missions. Solar arrays covering most of the upper wing surface provide power for the aircraft's electric motors, avionics, communications and other electronic systems. It also has a backup battery system that can provide power for between two and five hours to allow limited-duration flight after dark. (Photo Courtesy of NASA, Dryden Flight Research Center Photo Collection)

2002

Union Pacific Railroad installs 350 blue-signal rail yard lanterns, which incorporate energy saving light-emitting diode (LED) technology with solar cells, at its North Platt, Nebraska, rail yard—the largest rail yard in the United States.

2002

ATS Automation Tooling Systems Inc. in Canada starts to commercialize an innovative method of producing solar cells, called Spheral Solar technology. The technology—based on tiny silicon beads bonded between two sheets of aluminum foil—promises lower costs due to its greatly reduced use of silicon relative to conventional multicrystalline silicon solar cells. The technology is not new. It was championed by Texas Instruments (TI) in the early 1990s. But despite U.S. Department of Energy (DOE) funding, TI dropped the initiative. See the DOE http://www.nrel.gov/pvmat/ti.html "Photovoltaic Manufacturing Technology" Web site.

Courtesy of www.atsautomation.com

2002

The largest solar power facility in the Northwest—the 38.7-kilowatt White Bluffs Solar Station—goes online in Richland, Washington.

2000s

Solar History: The Future

Courtesy of PowerLight Corporation / PIX12398

POWERLIGHT
SOLAR ELECTRIC SYSTEMS

2001

Powerlight Corporation installs the largest rooftop solar power system in the United States—a 1.18 megawatt system—at the Santa Rita Jail in Dublin, California.

– Photo Caption: In Spring 2002, Alameda County, CA successfully completed the fourth largest solar electric system in the world atop the Santa Rita Jail in Dublin, California. This solar installation, the United States' largest rooftop system, was commissioned to help Alameda County reduce and stabilize future energy costs. This smart energy project reduces the jail's use of utility-generated electricity by 30% through solar power generation and energy conservation. Clean energy is generated by a 1.18 Megawatt system consisting of three acres of solar electric or photovoltaic (PV) panels. (Courtesy of PowerLight Corporation / PIX12398)

Here's a look at the expected future direction of solar technology.

Chris Gunn Photography / PIX12165

All buildings will be built to combine energy-efficient design and construction practices and renewable energy technologies for a net-zero energy building. In effect, the building will conserve enough and produce its own energy supply to create a new generation of cost-effective buildings that have zero net annual need for non-renewable energy.

– Photo Caption: This home was built by students from the University of Colorado (CU) for the first Solar Decathlon, a competition sponsored by the U.S. Department of Energy (DOE). Student teams are challenged to integrate aesthetics and modern conveniences with maximum energy production and optimal efficiency. Each collegiate team will build a uniquely designed 500-ft2 -- 800-ft2 house. Decathletes will transported their houses to the National Mall in Washington D.C. for the competition in the fall of 2002. The CU team took first prize in the competition overall. (Chris Gunn Photography / PIX12165)

Photovoltaics research and development will continue intense interest in new materials, cell designs, and novel approaches to solar material and product development. It is a future where the clothes you wear and your mode of transportation can produce power that is clean and safe.

Technology roadmaps for the future outline the research and development path to full competitiveness of concentrating solar power (CSP) with conventional power generation technologies within a decade. The potential of solar power in the Southwest United States is comparable in scale to the hydropower resource of the Northwest. A desert area 10 miles by 15 miles could provide 20,000 megawatts of power, while the electricity needs of the entire United States could theoretically be met by a photovoltaic array within an area 100 miles on a side. Concentrating solar power, or solar thermal electricity, could harness the sun's heat energy to provide large-scale, domestically secure, and environmentally friendly electricity.

Kramer Junction Company / PIX11070

– Photo Caption: This is the world's largest solar power facility, located near Kramer Junction, CA. The facility consists of five Solar Electric Generating Stations (SEGS), with a combined capacity of 150 megawatts. At capacity, that is enough power for 150,000 homes. The facility covers more than 1000 acres, with over 1 million square meters of collector surface. (Kramer Junction Company / PIX11070)

The price of photovoltaic power will be competitive with traditional sources of electricity within 10 years.

Richard Parish / PIX10732

Solar electricity will be used to electrolyze water, producing hydrogen for fuel cells for transportation and buildings.

– Photo Caption: SunLine, a California transit agency, is being evaluated as they add state-of-the-art hydrogen fuel cell buses to their fleets and set up infrastructure facilities for fueling and maintenance. The hydrogen is produced at the site using solar-powered electrolysis and natural gas reforming. Because fuel cell buses aren't yet commercially available, these demonstration projects are used to better understand the technology and plan for the future. (Richard Parish / PIX10732)

2. Solar Irradiation Data on the Sunniest Day

Solar Irradiation Data on 19 March 2012

Time	Irradiation (W/m2)
7:00	0
7:01	0
7:02	0
7:03	0
7:04	0
7:05	0
7:06	0
7:07	0
7:08	0
7:09	0
7:10	0
7:11	0
7:12	0
7:13	0
7:14	0
7:15	0
7:16	0
7:17	0
7:18	0
7:19	0
7:20	0
7:21	0
7:22	0
7:23	5
7:24	0
7:25	8
7:26	11
7:27	11
7:28	12
7:29	12
7:30	15
7:31	16
7:32	16
7:33	16
7:34	16
7:35	16
7:36	17
7:37	19
7:38	21
7:39	21
7:40	21
7:41	21
7:42	21
7:43	21
7:44	21
7:45	21
7:46	16
7:47	14
7:48	19
7:49	18
7:50	18
7:51	19
7:52	19
7:53	21
7:54	20
7:55	21
7:56	21
7:57	11
7:58	23
7:59	25
8:00	27
8:01	30
8:02	33
8:03	39
8:04	42
8:05	44
8:06	45
8:07	46
8:08	47
8:09	49
8:10	53
8:11	53
8:12	51
8:13	53
8:14	54
8:15	58
8:16	54
8:17	54
8:18	56
8:19	60
8:20	62
8:21	65
8:22	69
8:23	74
8:24	77
8:25	81
8:26	81
8:27	69
8:28	79
8:29	79
8:30	98
8:31	113
8:32	127
8:33	135
8:34	144
8:35	193
8:36	197
8:37	197
8:38	213
8:39	234
8:40	311
8:41	341
8:42	278
8:43	258
8:44	350
8:45	403
8:46	401
8:47	274
8:48	281
8:49	190
8:50	146
8:51	114
8:52	101
8:53	100
8:54	102
8:55	105
8:56	109
8:57	111
8:58	111
8:59	109
9:00	128
9:01	139
9:02	144
9:03	156
9:04	158
9:05	139
9:06	121
9:07	111
9:08	104
9:09	95
9:10	101
9:11	97

Time	Irradiation (W/m2)
9:12	97
9:13	97
9:14	98
9:15	104
9:16	117
9:17	121
9:18	120
9:19	132
9:20	193
9:21	162
9:22	193
9:23	185
9:24	227
9:25	227
9:26	454
9:27	454
9:28	95
9:29	392
9:30	457
9:31	457
9:32	239
9:33	466
9:34	422
9:35	446
9:36	485
9:37	483
9:38	461
9:39	456
9:40	446
9:41	439
9:42	452
9:43	485
9:44	517
9:45	463
9:46	466
9:47	469
9:48	469
9:49	468
9:50	469
9:51	456
9:52	438
9:53	415
9:54	415
9:55	552
9:56	571
9:57	553

Time	Irradiation (W/m2)
9:58	552
9:59	561
10:00	559
10:01	564
10:02	547
10:03	547
10:04	554
10:05	531
10:06	443
10:07	422
10:08	457
10:09	503
10:10	476
10:11	445
10:12	380
10:13	380
10:14	547
10:15	207
10:16	213
10:17	292
10:18	292
10:19	292
10:20	241
10:21	250
10:22	250
10:23	341
10:24	367
10:25	367
10:26	761
10:27	738
10:28	738
10:29	169
10:30	158
10:31	156
10:32	191
10:33	172
10:34	171
10:35	174
10:36	186
10:37	193
10:38	181
10:39	165
10:40	193
10:41	193
10:42	784
10:43	773

Time	Irradiation (W/m2)
10:44	752
10:45	754
10:46	761
10:47	754
10:48	765
10:49	773
10:50	752
10:51	738
10:52	731
10:53	731
10:54	728
10:55	730
10:56	737
10:57	735
10:58	735
10:59	733
11:00	728
11:01	740
11:02	731
11:03	737
11:04	752
11:05	749
11:06	765
11:07	783
11:08	780
11:09	770
11:10	775
11:11	775
11:12	775
11:13	777
11:14	786
11:15	780
11:16	779
11:17	780
11:18	780
11:19	791
11:20	780
11:21	772
11:22	800
11:23	782
11:24	779
11:25	777
11:26	782
11:27	777
11:28	777
11:29	773

Time	Irradiation (W/m2)
11:30	779
11:31	778
11:32	791
11:33	796
11:34	810
11:35	805
11:36	805
11:37	809
11:38	810
11:39	835
11:40	817
11:41	828
11:42	820
11:43	830
11:44	831
11:45	831
11:46	830
11:47	821
11:48	825
11:49	816
11:50	835
11:51	838
11:52	840
11:53	838
11:54	847
11:55	858
11:56	867
11:57	789
11:58	881
11:59	872
12:00	880
12:01	874
12:02	874
12:03	882
12:04	898
12:05	909
12:06	896
12:07	884
12:08	881
12:09	881
12:10	858
12:11	863
12:12	872
12:13	833
12:14	861
12:15	893

Time	Irradiation (W/m2)
12:16	886
12:17	880
12:18	896
12:19	888
12:20	896
12:21	909
12:22	907
12:23	897
12:24	895
12:25	896
12:26	896
12:27	900
12:28	904
12:29	905
12:30	902
12:31	904
12:32	912
12:33	911
12:34	909
12:35	913
12:36	919
12:37	918
12:38	921
12:39	904
12:40	904
12:41	909
12:42	912
12:43	891
12:44	858
12:45	865
12:46	842
12:47	816
12:48	775
12:49	823
12:50	823
12:51	784
12:52	788
12:53	728
12:54	657
12:55	657
12:56	552
12:57	552
12:58	747
12:59	817
13:00	817
13:01	881

Time	Irradiation (W/m2)
13:02	838
13:03	833
13:04	829
13:05	888
13:06	853
13:07	812
13:08	846
13:09	870
13:10	907
13:11	921
13:12	914
13:13	942
13:14	918
13:15	875
13:16	866
13:17	884
13:18	895
13:19	877
13:20	840
13:21	840
13:22	818
13:23	816
13:24	830
13:25	798
13:26	819
13:27	824
13:28	806
13:29	805
13:30	765
13:31	742
13:32	749
13:33	701
13:34	696
13:35	682
13:36	708
13:37	700
13:38	715
13:39	719
13:40	777
13:41	763
13:42	724
13:43	802
13:44	765
13:45	687
13:46	650
13:47	592

Time	Irradiation (W/m2)
13:48	578
13:49	649
13:50	596
13:51	531
13:52	570
13:53	578
13:54	594
13:55	628
13:56	587
13:57	569
13:58	545
13:59	636
14:00	680
14:01	664
14:02	670
14:03	660
14:04	650
14:05	679
14:06	617
14:07	578
14:08	580
14:09	570
14:10	563
14:11	598
14:12	592
14:13	503
14:14	438
14:15	504
14:16	642
14:17	673
14:18	684
14:19	668
14:20	663
14:21	722
14:22	722
14:23	791
14:24	809
14:25	837
14:26	822
14:27	754
14:28	689
14:29	621
14:30	652
14:31	671
14:32	738
14:33	752

Time	Irradiation (W/m2)
14:34	714
14:35	712
14:36	710
14:37	708
14:38	654
14:39	654
14:40	635
14:41	610
14:42	682
14:43	670
14:44	686
14:45	708
14:46	617
14:47	687
14:48	684
14:49	691
14:50	698
14:51	656
14:52	661
14:53	654
14:54	656
14:55	656
14:56	631
14:57	575
14:58	550
14:59	510
15:00	506
15:01	525
15:02	512
15:03	540
15:04	541
15:05	527
15:06	524
15:07	521
15:08	510
15:09	510
15:10	744
15:11	773
15:12	779
15:13	800
15:14	812
15:15	812
15:16	802
15:17	786
15:18	772
15:19	769

Time	Irradiation (W/m2)
15:20	751
15:21	738
15:22	694
15:23	693
15:24	729
15:25	754
15:26	724
15:27	626
15:28	610
15:29	540
15:30	503
15:31	592
15:32	571
15:33	536
15:34	610
15:35	657
15:36	687
15:37	680
15:38	554
15:39	554
15:40	742
15:41	717
15:42	715
15:43	705
15:44	666
15:45	661
15:46	647
15:47	629
15:48	655
15:49	643
15:50	649
15:51	661
15:52	654
15:53	654
15:54	674
15:55	680
15:56	691
15:57	691
15:58	680
15:59	680
16:00	686
16:01	664
16:02	659
16:03	631
16:04	580
16:05	527

Time	Irradiation (W/m2)
16:06	496
16:07	508
16:08	517
16:09	454
16:10	471
16:11	476
16:12	405
16:13	371
16:14	396
16:15	429
16:16	380
16:17	322
16:18	243
16:19	269
16:20	267
16:21	283
16:22	258
16:23	255
16:24	239
16:25	232
16:26	236
16:27	251
16:28	244
16:29	244
16:30	255
16:31	262
16:32	283
16:33	258
16:34	243
16:35	236
16:36	225
16:37	223
16:38	220
16:39	216
16:40	218
16:41	219
16:42	221
16:43	225
16:44	229
16:45	230
16:46	230
16:47	224
16:48	220
16:49	214
16:50	207
16:51	200

Time	Irradiation (W/m2)
16:52	197
16:53	193
16:54	186
16:55	185
16:56	181
16:57	179
16:58	178
16:59	175
17:00	172
17:01	171
17:02	127
17:03	127
17:04	167
17:05	167
17:06	167
17:07	167
17:08	167
17:09	169
17:10	173
17:11	176
17:12	178
17:13	185
17:14	190
17:15	190
17:16	190
17:17	197
17:18	197
17:19	197
17:20	202
17:21	206
17:22	204
17:23	197
17:24	181
17:25	169
17:26	160
17:27	155
17:28	147
17:29	139
17:30	134
17:31	130
17:32	127
17:33	125
17:34	120
17:35	114
17:36	113
17:37	109

Time	Irradiation (W/m2)
17:38	107
17:39	105
17:40	103
17:41	98
17:42	97
17:43	95
17:44	93
17:45	90
17:46	86
17:47	84
17:48	83
17:49	81
17:50	79
17:51	77
17:52	76
17:53	76
17:54	74
17:55	72
17:56	72
17:57	70
17:58	67
17:59	65
18:00	65
18:01	63
18:02	62
18:03	60
18:04	58
18:05	56
18:06	54
18:07	54
18:08	54
18:09	54
18:10	54
18:11	54
18:12	54
18:13	54
18:14	53
18:15	53
18:16	51
18:17	51
18:18	51
18:19	49
18:20	49
18:21	49
18:22	47
18:23	26

Time	Irradiation (W/m2)
18:24	47
18:25	47
18:26	47
18:27	47
18:28	46
18:29	46
18:30	46
18:31	46
18:32	46
18:33	46
18:34	46
18:35	46
18:36	47
18:37	47
18:38	47
18:39	49
18:40	51
18:41	56
18:42	58
18:43	54
18:44	50
18:45	49
18:46	49
18:47	53
18:48	53
18:49	51
18:50	50
18:51	46
18:52	44
18:53	42
18:54	42
18:55	40
18:56	40
18:57	39
18:58	39
18:59	37
19:00	35

3. Solar Irradiation Data on the Cloudiest Day

Solar Irradiation Data on 28 December 2011

Time	Irradiation (W/m2)	Time	Irradiation (W/m2)	Time	Irradiation (W/m2)
7:00	0	7:44	19	8:28	25
7:01	0	7:45	24	8:29	25
7:02	0	7:46	28	8:30	25
7:03	0	7:47	30	8:31	25
7:04	0	7:48	32	8:32	25
7:05	0	7:49	32	8:33	28
7:06	0	7:50	32	8:34	32
7:07	0	7:51	35	8:35	35
7:08	0	7:52	33	8:36	40
7:09	0	7:53	33	8:37	41
7:10	0	7:54	35	8:38	37
7:11	0	7:55	35	8:39	35
7:12	0	7:56	27	8:40	39
7:13	0	7:57	19	8:41	37
7:14	0	7:58	18	8:42	26
7:15	0	7:59	18	8:43	24
7:16	0	8:00	16	8:44	19
7:17	0	8:01	12	8:45	16
7:18	0	8:02	13	8:46	21
7:19	0	8:03	19	8:47	30
7:20	0	8:04	21	8:48	42
7:21	0	8:05	23	8:49	55
7:22	0	8:06	21	8:50	72
7:23	5	8:07	19	8:51	81
7:24	5	8:08	17	8:52	70
7:25	5	8:09	14	8:53	56
7:26	5	8:10	16	8:54	51
7:27	5	8:11	19	8:55	62
7:28	5	8:12	21	8:56	76
7:29	7	8:13	18	8:57	74
7:30	7	8:14	28	8:58	81
7:31	9	8:15	30	8:59	90
7:32	9	8:16	32	9:00	98
7:33	8	8:17	35	9:01	104
7:34	7	8:18	37	9:02	90
7:35	7	8:19	39	9:03	84
7:36	5	8:20	33	9:04	88
7:37	7	8:21	30	9:05	83
7:38	9	8:22	30	9:06	74
7:39	10	8:23	28	9:07	57
7:40	12	8:24	28	9:08	35
7:41	12	8:25	28	9:09	16
7:42	14	8:26	26	9:10	12
7:43	18	8:27	25	9:11	16

Time	Irradiation (W/m2)
9:12	19
9:13	23
9:14	25
9:15	25
9:16	26
9:17	26
9:18	24
9:19	25
9:20	25
9:21	26
9:22	11
9:23	11
9:24	10
9:25	12
9:26	11
9:27	9
9:28	9
9:29	9
9:30	7
9:31	7
9:32	7
9:33	11
9:34	14
9:35	16
9:36	17
9:37	14
9:38	14
9:39	12
9:40	12
9:41	12
9:42	14
9:43	16
9:44	16
9:45	16
9:46	18
9:47	18
9:48	23
9:49	28
9:50	32
9:51	37
9:52	42
9:53	57
9:54	70
9:55	77
9:56	79
9:57	79

Time	Irradiation (W/m2)
9:58	79
9:59	76
10:00	70
10:01	70
10:02	81
10:03	93
10:04	81
10:05	96
10:06	113
10:07	120
10:08	118
10:09	120
10:10	121
10:11	131
10:12	148
10:13	155
10:14	151
10:15	144
10:16	144
10:17	139
10:18	149
10:19	163
10:20	178
10:21	188
10:22	192
10:23	185
10:24	178
10:25	176
10:26	179
10:27	186
10:28	195
10:29	216
10:30	236
10:31	241
10:32	243
10:33	250
10:34	257
10:35	248
10:36	237
10:37	225
10:38	211
10:39	199
10:40	197
10:41	218
10:42	236
10:43	248

Time	Irradiation (W/m2)
10:44	258
10:45	265
10:46	277
10:47	287
10:48	294
10:49	304
10:50	320
10:51	332
10:52	352
10:53	380
10:54	401
10:55	401
10:56	396
10:57	380
10:58	318
10:59	306
11:00	306
11:01	306
11:02	325
11:03	258
11:04	185
11:05	158
11:06	160
11:07	169
11:08	171
11:09	148
11:10	121
11:11	125
11:12	137
11:13	156
11:14	179
11:15	222
11:16	234
11:17	255
11:18	253
11:19	269
11:20	274
11:21	264
11:22	272
11:23	278
11:24	292
11:25	295
11:26	308
11:27	310
11:28	306
11:29	311

Time	Irradiation (W/m2)
11:30	320
11:31	316
11:32	274
11:33	250
11:34	258
11:35	234
11:36	190
11:37	155
11:38	165
11:39	195
11:40	234
11:41	257
11:42	271
11:43	250
11:44	227
11:45	146
11:46	86
11:47	95
11:48	91
11:49	102
11:50	100
11:51	106
11:52	121
11:53	146
11:54	151
11:55	156
11:56	165
11:57	199
11:58	209
11:59	229
12:00	255
12:01	283
12:02	311
12:03	313
12:04	295
12:05	290
12:06	234
12:07	287
12:08	265
12:09	274
12:10	301
12:11	318
12:12	322
12:13	320
12:14	322
12:15	287

Time	Irradiation (W/m2)
12:16	271
12:17	260
12:18	262
12:19	267
12:20	276
12:21	229
12:22	186
12:23	160
12:24	146
12:25	139
12:26	130
12:27	125
12:28	118
12:29	120
12:30	123
12:31	130
12:32	143
12:33	158
12:34	176
12:35	190
12:36	207
12:37	210
12:38	206
12:39	229
12:40	246
12:41	255
12:42	251
12:43	258
12:44	265
12:45	269
12:46	269
12:47	269
12:48	265
12:49	261
12:50	248
12:51	241
12:52	234
12:53	223
12:54	216
12:55	213
12:56	216
12:57	225
12:58	239
12:59	258
13:00	274
13:01	291

Time	Irradiation (W/m2)
13:02	309
13:03	315
13:04	304
13:05	287
13:06	262
13:07	248
13:08	239
13:09	218
13:10	132
13:11	97
13:12	111
13:13	126
13:14	132
13:15	169
13:16	195
13:17	232
13:18	263
13:19	232
13:20	232
13:21	234
13:22	216
13:23	165
13:24	118
13:25	141
13:26	148
13:27	139
13:28	111
13:29	100
13:30	106
13:31	125
13:32	141
13:33	137
13:34	135
13:35	135
13:36	125
13:37	118
13:38	118
13:39	116
13:40	120
13:41	146
13:42	180
13:43	209
13:44	220
13:45	220
13:46	227
13:47	223

Time	Irradiation (W/m2)
13:48	191
13:49	169
13:50	160
13:51	153
13:52	153
13:53	153
13:54	123
13:55	107
13:56	111
13:57	120
13:58	137
13:59	189
14:00	172
14:01	130
14:02	100
14:03	70
14:04	67
14:05	88
14:06	111
14:07	127
14:08	141
14:09	156
14:10	167
14:11	176
14:12	162
14:13	127
14:14	98
14:15	88
14:16	77
14:17	58
14:18	72
14:19	86
14:20	98
14:21	97
14:22	88
14:23	76
14:24	70
14:25	69
14:26	62
14:27	53
14:28	46
14:29	47
14:30	56
14:31	69
14:32	63
14:33	65

Time	Irradiation (W/m2)
14:34	79
14:35	79
14:36	67
14:37	67
14:38	86
14:39	128
14:40	169
14:41	167
14:42	144
14:43	125
14:44	139
14:45	146
14:46	141
14:47	130
14:48	137
14:49	163
14:50	176
14:51	171
14:52	164
14:53	162
14:54	165
14:55	169
14:56	178
14:57	181
14:58	182
14:59	185
15:00	178
15:01	169
15:02	148
15:03	127
15:04	99
15:05	81
15:06	93
15:07	107
15:08	127
15:09	144
15:10	147
15:11	134
15:12	114
15:13	125
15:14	123
15:15	100
15:16	99
15:17	116
15:18	116
15:19	100

Time	Irradiation (W/m2)
15:20	130
15:21	160
15:22	151
15:23	93
15:24	83
15:25	134
15:26	151
15:27	191
15:28	169
15:29	153
15:30	135
15:31	120
15:32	111
15:33	111
15:34	116
15:35	125
15:36	135
15:37	135
15:38	105
15:39	75
15:40	62
15:41	40
15:42	39
15:43	51
15:44	65
15:45	62
15:46	67
15:47	79
15:48	93
15:49	102
15:50	109
15:51	119
15:52	109
15:53	91
15:54	83
15:55	79
15:56	77
15:57	73
15:58	69
15:59	72
16:00	77
16:01	83
16:02	92
16:03	98
16:04	100
16:05	100

Time	Irradiation (W/m2)
16:06	91
16:07	91
16:08	90
16:09	72
16:10	91
16:11	93
16:12	130
16:13	132
16:14	152
16:15	153
16:16	139
16:17	111
16:18	77
16:19	83
16:20	133
16:21	167
16:22	178
16:23	186
16:24	211
16:25	207
16:26	170
16:27	158
16:28	111
16:29	130
16:30	120
16:31	105
16:32	130
16:33	160
16:34	200
16:35	211
16:36	213
16:37	207
16:38	185
16:39	171
16:40	144
16:41	142
16:42	132
16:43	116
16:44	100
16:45	88
16:46	72
16:47	51
16:48	44
16:49	59
16:50	54
16:51	51

Time	Irradiation (W/m2)
16:52	51
16:53	65
16:54	79
16:55	98
16:56	81
16:57	62
16:58	56
16:59	65
17:00	63
17:01	70
17:02	102
17:03	102
17:04	97
17:05	79
17:06	65
17:07	47
17:08	37
17:09	44
17:10	53
17:11	65
17:12	70
17:13	70
17:14	86
17:15	95
17:16	111
17:17	114
17:18	102
17:19	87
17:20	51
17:21	56
17:22	86
17:23	97
17:24	116
17:25	130
17:26	142
17:27	141
17:28	97
17:29	58
17:30	67
17:31	51
17:32	53
17:33	63
17:34	72
17:35	79
17:36	93
17:37	105

Time	Irradiation (W/m2)
17:38	114
17:39	113
17:40	84
17:41	65
17:42	79
17:43	88
17:44	79
17:45	69
17:46	74
17:47	77
17:48	75
17:49	79
17:50	81
17:51	77
17:52	72
17:53	69
17:54	74
17:55	76
17:56	77
17:57	77
17:58	76
17:59	74
18:00	66
18:01	51
18:02	44
18:03	42
18:04	40
18:05	43
18:06	51
18:07	54
18:08	54
18:09	44
18:10	47
18:11	49
18:12	54
18:13	54
18:14	54
18:15	54
18:16	51
18:17	43
18:18	30
18:19	25
18:20	28
18:21	35
18:22	39
18:23	43

Time	Irradiation (W/m2)
18:24	40
18:25	37
18:26	32
18:27	25
18:28	19
18:29	15
18:30	12
18:31	12
18:32	12
18:33	11
18:34	11
18:35	12
18:36	12
18:37	11
18:38	9
18:39	9
18:40	9
18:41	7
18:42	7
18:43	7
18:44	7
18:45	5
18:46	5
18:47	5
18:48	5
18:49	5
18:50	0
18:51	0
18:52	0
18:53	0
18:54	0
18:55	0
18:56	0
18:57	0
18:58	0
18:59	0
19:00	0

Changes for the Better

MITSUBISHI ELECTRIC

PHOTOVOLTAIC MODULE

TE series

PV-TE130MF5N 130Wp
PV-TE125MF5N 125Wp
PV-TE120MF5N 120Wp
PV-TE115MF5N 115Wp

Top in Quality

High Efficiency
- Solder-coatingless cells
- Fine Grid Electrodes
- BSF (Back Surface Field) Structure
- Anti-Reflective Coating
- Back Film Reflected Light
- High Reflectance Back Film
- Celium-Free/High-Transmittance Glass
- High Power in Actual Use

High Reliability
- Original derating designing concept
- Straight Tabs
- Double-Sided Independent Tabs
- Lower slope of module frame
- Higher Tensile Strength Structure
- Better Water Drainage Structure
- High-Corrosion Resistant Frame
- Max. System Voltage 1000V with Four-Layer Structure Back Film

High Safety
- Triple-Layer Structure Junction Box
- Highly Reliable Bypass Diode
- Lock Mechanism Equipped Connectors
- Lighter Weight 13.5kg per module
- Conformity with IEC61215 2nd edition, TUV Safety Class II, EN61730

Eco-Friendly
- Lead-free solder PV module
- Manufactured in the plant certified ISO 14001
- Recyclable steel pallets

SPECIFICATION SHEET

Mamufacturer	MITSUBISHI ELECTRIC			
Model name	PV-TE130MF5N	PV-TE125MF5N	PV-TE120MF5N	PV-TE115MF5N
Cell type	Polycrystalline Silicon, 156mm x 156mm			
Number of cells	36 cells in a series			
Maximum power rating(Pmax)	130W	125W	120W	115W
Warranted minimum Pmax	123.5W	118.8W	114.0W	109.3W
Tolerance of maximum power rating	+10/-5%			
Open circuit voltage (Voc)	21.9V	21.8V	21.6V	21.5V
Short circuit current (Isc)	8.05A	7.90A	7.75A	7.60A
Maximum power voltage (Vmp)	17.4V	17.3V	17.2V	17.1V
Maximum power current (Imp)	7.47A	7.23A	6.99A	6.75A
Normal operating cell temperature(NOCT)	47.5 degree C			
Maximum system voltage	DC 1000V			
Fuse rating	15A			
Dimensions	1495x674x46mm (58.9x26.5x1.81inch)			
Weight	13.5kg (29.8lbs.)			
Output terminal	(+) 800mm/(-) 1250mm with MC connector (PV-KBT4/6Ⅱ-UR, PV-KST4/6Ⅱ-UR)			
Module efficiency	12.9%	12.4%	11.9%	11.4%
Packing condition	2 pcs - 1 carton			
Certificate	IEC 61215 edition 2(static load test 2400Pa passed), EN 61730, TUV Safety Class Ⅱ			

DRAWINGS AND DIMENSIONS

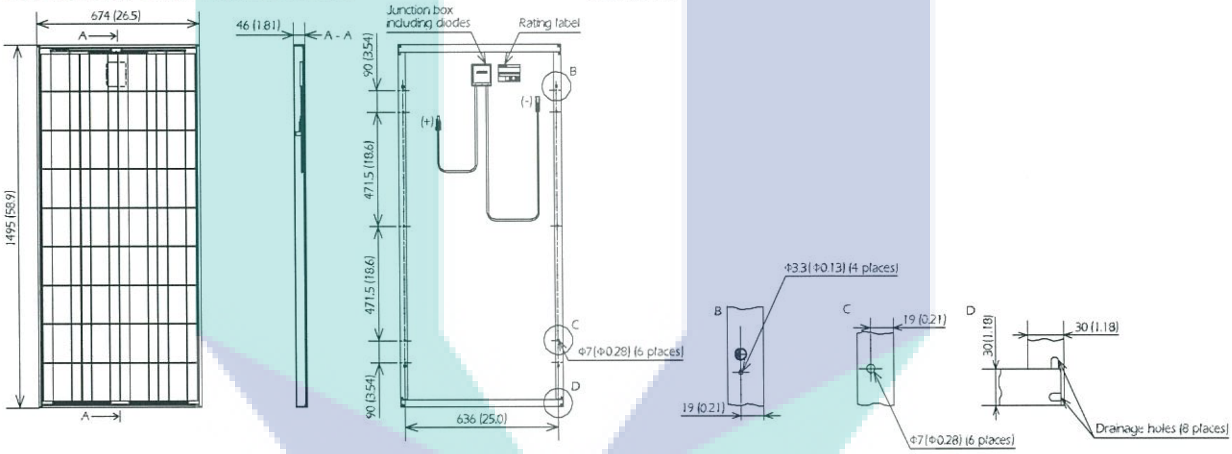

ELECTRICAL CHARACTERISTICS

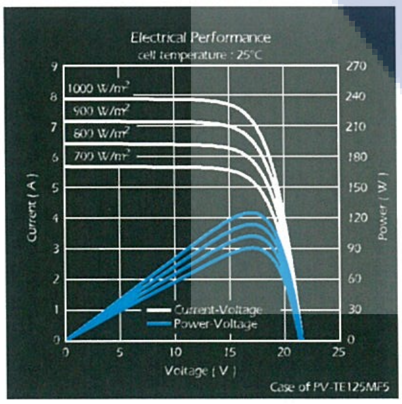

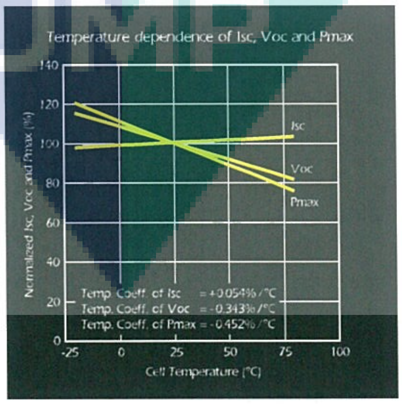

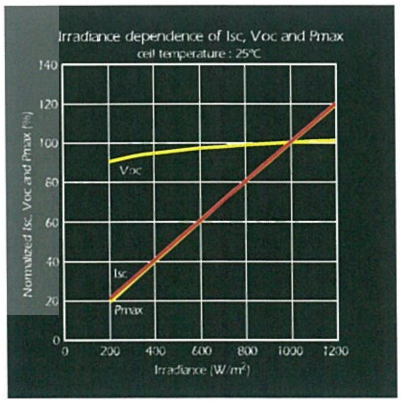

MITSUBISHI ELECTRIC CORPORATION

HEAD OFFICE: TOKYO BLDG., 2-7-3, MARUNOUCHI, CHIYODA-KU,TOKYO 100-8310, JAPAN
http://Global.MitsubishiElectric.com/solar

L-175-6-B7539-B NK0706 Printed in Japan(MDOC)

Revised Publication, effective Jun. 2007.
Superseding Publication, L-175-6-B7539-B of Sep. 2006.
Specifications subject to change without notice.